ELSEVIER
Physics Reports 303 (1998) 1–80
PHYSICS REPORTS

The physics of trapped dilute-gas Bose–Einstein condensates

A.S. Parkins*, D.F. Walls

Department of Physics, University of Auckland, Private Bag 92019, Auckland, New Zealand

Received December 1997; editor: I. Proccacia

Contents

1. Introduction 4
   1.1. The experiments 4
   1.2. The theory 7
   1.3. Outline 7
2. Ground state properties of dilute-gas Bose–Einstein condensates in traps 8
   2.1. Hamiltonian: binary collision model 8
   2.2. Mean-field theory 9
   2.3. Ground state properties of a condensate with repulsive interactions 10
   2.4. Ground state properties of a condensate with attractive interactions 14
   2.5. Vortex states 16
   2.6. Condensate lifetime 18
   2.7. Binary mixtures of Bose–Einstein condensates 19
   2.8. Beyond mean-field theory: quantum properties of trapped condensates 20
3. Elementary excitations of a trapped Bose–Einstein condensate 29
   3.1. Collective excitations of a trapped Bose–Einstein condensate (at $T = 0$) 30
   3.2. Propagation of sound in a Bose–Einstein condensate 34
   3.3. Decay of collective excitations 35
   3.4. Collective excitations of trapped double condensates 36
   3.5. Finite temperature excitations 37
4. Light scattering from a Bose–Einstein condensate 40
   4.1. Coherent light scattering 40
   4.2. Incoherent light scattering 42
   4.3. Manipulation of the scattering length via light scattering 47
   4.4. Nonlinear atom optics 47
   4.5. Interaction with quantised cavity radiation fields 48
5. Broken gauge symmetry in pairs of condensates 48
   5.1. Interference of two Bose–Einstein condensates and measurement-induced phase 48
   5.2. Collapses and revivals of the interference pattern visibility 54
   5.3. Pumping of twin-trap condensates 55
   5.4. Detection of broken gauge symmetry via light scattering 56
   5.5. Pumping of double condensates via light scattering 58
   5.6. Establishment of relative phase via light scattering 59
6. Quantum dynamics of a Bose–Einstein condensate in a double-well potential 60
   6.1. Coherent quantum tunnelling 60
   6.2. Quantum phase between tunnelling Bose–Einstein condensates 62
7. The atom laser 63
   7.1. What is an “atom laser”? 63
   7.2. Proposed models 64
   7.3. An atom laser based on evaporative cooling 65
   7.4. An atom laser based on optical cooling 68
   7.5. Output couplers for Bose–Einstein condensates 70
   7.6. Higher-order coherence of Bose–Einstein condensates 71
8. Conclusions 72
Appendix A. Bose–Einstein condensation in a weakly interacting gas: Bogoliubov theory 73
   A.1. Elimination of the condensate mode 74
   A.2. Bogoliubov transformation 74
References 76

* Corresponding author. E-mail: s.parkins@auckland.ac.nz.

PII S0370-1573(98)00014-3

THE PHYSICS OF TRAPPED DILUTE-GAS BOSE–EINSTEIN CONDENSATES

A.S. PARKINS, D.F. WALLS

Department of Physics, University of Auckland, Private Bag 92019, Auckland, New Zealand

ELSEVIER

AMSTERDAM – LAUSANNE – NEW YORK – OXFORD – SHANNON – TOKYO

Abstract

The experimental realisation of Bose–Einstein condensates of dilute atomic vapours has generated immense interest and activity in this field. Here, we present a review of recent theoretical research into the properties of trapped dilute-gas Bose–Einstein condensates. Topics covered include ground-state properties of trapped condensates, elementary excitations, light scattering properties, tests of broken gauge symmetry, and the atom laser.

PACS: 03.75.Fi

1. Introduction

One of the most fascinating predictions of quantum statistical mechanics is that of a phase transition in an ideal gas of identical bosons (particles with integral total angular momentum) when the thermal de Broglie wavelength exceeds the mean spacing between particles. Under such conditions, bosons are stimulated by the presence of other bosons in the lowest energy state to occupy that state as well, resulting in a macroscopic occupation of a single quantum state (Bose, 1924; Einstein, 1925). This transition is termed *Bose–Einstein condensation* (BEC) and the condensate that forms constitutes a macroscopic quantum-mechanical object.

This condensation provides a basis for the theoretical understanding of, e.g., superfluidity in liquid helium. However, in this system, strong interactions exist between the constituent particles, making a simple interpretation in terms of quantum statistical mechanics impossible. Hence, there has been growing interest in the past couple of decades in finding a system that could provide a weakly interacting condensate, for which a more rigorous and detailed comparison between theory and experiment would be possible. Such a system was supplied in spectacular fashion in 1995 by the atomic physics community in the form of ultracold, trapped atomic vapours. Specifically, in a landmark experiment, Anderson et al. (1995) at JILA[1] produced a condensate of spin-polarised ^{87}Rb atoms confined in a magnetic trap. Similarly significant experiments demonstrating BEC with trapped vapours of ^{23}Na and ^{7}Li were also performed by Davis et al. (1995) at MIT[2] and Bradley, Sackett and Hulet (1997a, 1997b) at Rice University, respectively.

1.1. The experiments

In the JILA experiment a condensate of approximately 2000 spin-polarised ^{87}Rb atoms was produced in a cylindrically symmetric magnetic trap (for a general review of this experiment, see Cornell, 1996). A finite condensate fraction first appeared at a temperature of 170 nK and a density of $2.6\times 10^{12}\,\mathrm{cm}^{-3}$. To reach these regimes of temperature and density with alkali gas samples required state-of-the-art cooling and trapping techniques. In particular, the gas sample was first optically trapped and cooled using laser light in a magneto-optical trap, as depicted and described in Fig. 1. Densities and temperatures of the order of $10^{11}\,\mathrm{cm}^{-3}$ and tens of micro-Kelvin, respectively, are routinely achieved in such configurations (for more detailed descriptions of laser cooling and trapping techniques, see, e.g., the articles in Arimondo et al., 1991).

After being optically pumped into a suitable magnetic sublevel (the $F=2$, $m_F=2$ angular momentum state of ^{87}Rb), the atoms were then loaded into a purely magnetic trap,[3] providing an essentially harmonic confining potential with axial and radial oscillation frequencies of approximately 120 and 42 Hz, respectively. At this point, the technique of evaporative cooling was employed to achieve a further reduction in the temperature of the gas. Briefly, this cooling technique is based on the preferential removal of atoms with an energy higher than the average energy (in practice, via

[1] Joint Institute for Laboratory Astrophysics, University of Colorado at Boulder.

[2] Massachusetts Institute of Technology.

[3] Here, the interaction between the magnetic field and the magnetic moment of the unpaired electron in ^{87}Rb is sufficient to trap an atom.

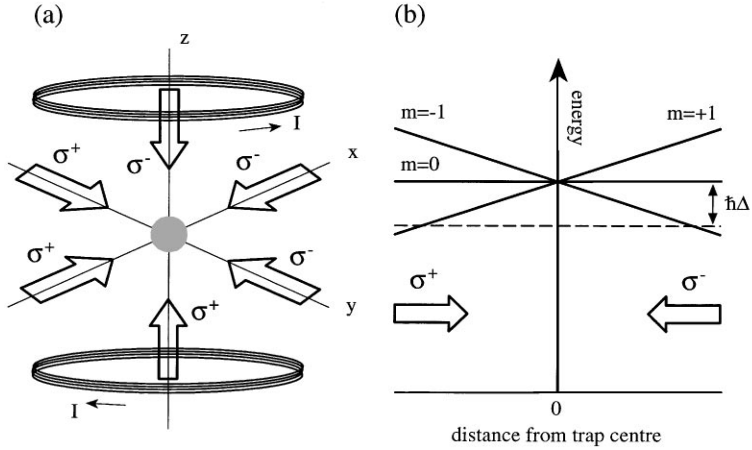

Fig. 1. (a) A typical magneto-optical trap configuration. Three pairs of counter-propagating laser beams with opposite circular polarisations (σ^+ and σ^-) and a frequency tuned slightly below the atomic resonance (by an amount Δ) are superimposed on a magnetic quadrupole field produced by a pair of anti-Helmholtz coils. As shown in (b) (in one dimension), the Zeeman sublevels of an atom are shifted by the local magnetic field in such a way that (due to selection rules) the atom tunes into resonance with the laser field propagating in the opposite direction to the atom's displacement from the origin; hence, the net force on the atom is always towards the origin. In practice, additional repumping laser beams are required to maintain the atoms in the correct hyperfine levels and these beams are spatially distributed so as to create a "dark spot" in the centre of the cloud where atoms are "hidden" from the trapping beams in an uncoupled hyperfine level; this reduces trap loss and heating due to light scattering, allowing higher densities to be attained before transfer to a purely magnetic trap.

spin-flip-inducing radiofrequency excitation, tuned to excite only the most energetic atoms, i.e., those in the outermost regions of the trap). Subsequent rethermalisation of the gas by elastic collisions produces an equilibrium state at a lower temperature (for a review of evaporative cooling methods, see Ketterle and van Druten, 1996a). A particular magnetic trap configuration and a depiction of the evaporative cooling process is shown in Fig. 2.

This final step of cooling enabled Anderson et al. to attain temperatures in the nano-Kelvin regime, well below the critical temperature for BEC of the gas sample, which, for an ideal gas of N atoms in a harmonic potential, is given by (de Groot et al., 1950; Bagnato et al., 1987)

$$T_c = (\hbar\bar{\omega}/k_B)(N/1.202)^{1/3}\,, \tag{1}$$

where $\bar{\omega} = (\omega_x\omega_y\omega_z)^{1/3}$ is the geometric mean of the harmonic trap frequencies. Below this critical temperature, the condensate fraction varies as (de Groot et al., 1950)

$$N_0/N = 1 - (T/T_c)^3\,. \tag{2}$$

As mentioned above, the ^{87}Rb experiment of Anderson et al. was complimented by demonstrations of BEC in trapped vapours of ^{23}Na (Davis et al., 1995) and ^{7}Li (Bradley et al., 1995, 1997a). These experiments employed somewhat different physical configurations, but followed the same basic

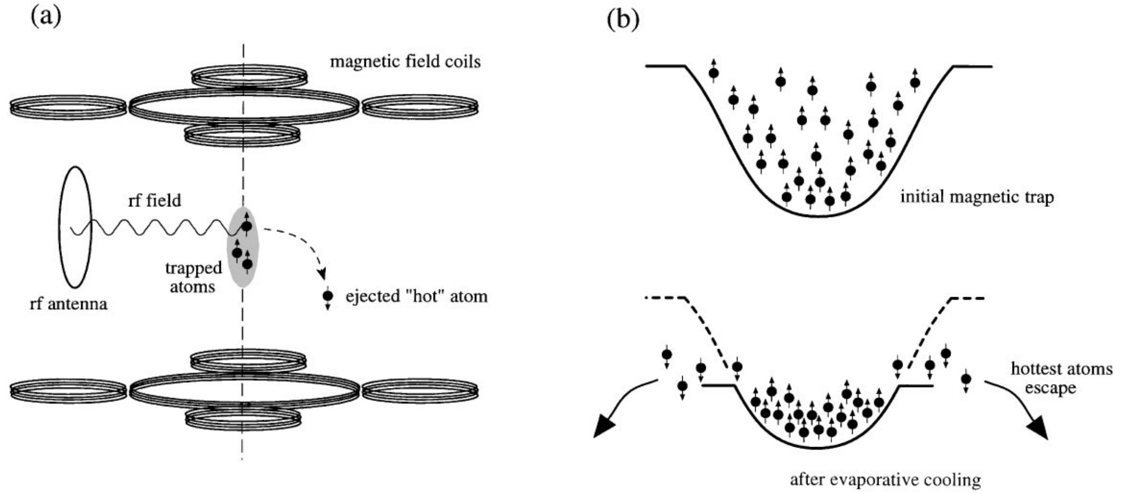

Fig. 2. Schematics of the evaporative cooling process in a magnetic trap configuration. (a) Cloverleaf configuration of trapping coils used by Mewes et al. (1996a). The central (outer) coils provide axial (radial) confinement. The rf field induces spinflips of hot atoms. By adjusting the frequency of the rf field, the effective depth of the trap is altered, facilitating evaporative cooling as depicted in (b).

approach to obtaining the necessary densities and temperatures, i.e., an initial stage of laser cooling followed by evaporative cooling in a magnetic trap. In the MIT experiment with ^{23}Na the critical temperature for condensation was 2 μK and condensates of approximately 5×10^5 atoms were created at densities of the order of $10^{14}\,\mathrm{cm}^{-3}$. The ^{7}Li experiment at Rice University was somewhat distinct from the other experiments in that the *s*-wave scattering length for ^{7}Li is *negative*, meaning that the interatomic interactions are effectively attractive (as opposed to the positive scattering length for ^{87}Rb and ^{23}Na, corresponding to repulsive interactions). This puts limits on the maximum size and stability of the condensate, which was observed by Bradley et al., below a critical temperature of around 400 nK, to contain approximately 10^3 atoms at a density of the order of $10^{12}\,\mathrm{cm}^{-3}$.

The ensuing months have seen the rapid development of refined and improved experimental configurations, together with more detailed quantitative measurements and studies of fundamental condensate properties, such as the condensate fraction and the interaction energy (Ensher et al., 1996; Jin et al., 1996b; Mewes et al., 1996a; Andrews et al., 1996). Collective excitations have also been examined by slightly perturbing the trap potential and then observing the response of the condensate (Jin et al., 1996a,b, 1997; Mewes et al., 1996b). Other significant advances include the production of *binary* condensates, i.e., of two co-existing condensates corresponding to two different spin states of ^{87}Rb ($|F=1,m=-1\rangle$ and $|F=2,m=2\rangle$) (Myatt et al., 1997), and the demonstration of a pulsed coherent output coupler for a trapped condensate (Mewes et al., 1997), realising what can be regarded as a pulsed "atom laser." That the output pulses of atoms are indeed coherent has been beautifully confirmed in a further experiment by Andrews et al. (1997b), who observe high-contrast matter-wave interference fringes when two condensates (formed by "slicing" the original condensate in half with a thin laser beam) are made to overlap.

1.2. The theory

Preceding and parallel to this dramatic experimental progress, a large body of theoretical work has accumulated relating specifically to trapped dilute-gas Bose–Einstein condensates. Careful comparisons of theory with experiment are indeed now being performed, with impressive levels of agreement already achieved for such things as condensate size and shape, interaction energy, and excitation frequencies. As well as modelling present experiments, theorists are now also exploring the plethora of new possibilities offered by the alkali-gas condensates (in comparison to more traditional systems such as liquid helium). In this category are, for example, light scattering as a probe of condensate properties, effects due to quantum fluctuations in small ($N \sim 10^3$) condensates, and the interference of pairs of condensates. These and other effects also touch upon long-standing issues of broken gauge symmetry and the condensate phase, and how best to describe the actual state of the condensate.

The purpose of the present work is to provide a description and overview of theoretical research that has been done in recent times pertaining to the properties of dilute-gas Bose–Einstein condensates (see also the recent summary of BEC research by Burnett, 1996). For the most part, we concentrate on the physics of essentially pure condensates and neglect issues of condensate formation. The experiments have clearly demonstrated that pure condensates are both obtainable and amenable to further experimentation. However, while we choose not to discuss it in this review, it is important to note the recent development of (quantum) kinetic theories for the description of the formation of the condensate in weakly-interacting dilute-gas systems (see, e.g., Griffin et al., 1995; Stoof, 1997b; Gardiner and Zoller, 1997; Jaksch et al., 1997; Holland et al., 1997; Anglin, 1997; Gardiner et al., 1997;Kagan and Svistunov, 1997). Notably, predictions for the time scale for the growth of the condensate are now being made and appear to be consistent with the experiments (Gardiner et al., 1997).

1.3. Outline

Our review begins in Section 2 with the ground state properties of dilute-gas condensates, for which research has, in the main, been based upon mean-field theory, specifically in the form of the so-called Gross–Pitaevskii equation. This theory is strictly only valid in the thermodynamic limit, and, as alluded to above, the finite size of actual condensates may lead to noticeable deviations from the mean-field behaviour. This aspect is covered in the final part of Section 2. The mean-field theory and slight variations thereof have also provided the basis for the majority of investigations into the elementary excitations of trapped condensates and we review this work in Section 3. Light scattering properties are discussed in Section 4 for various regimes of laser excitation; unlike the subject matter of Sections 2 and 3, the theoretical predictions of this section still await corresponding experimental results, although progress along these lines is likely to occur soon. In Section 5 we turn to some fascinating future possibilities offered by systems comprising a pair of condensates, upon which measurements (e.g., atom detections) can be made in the manner of interference experiments and information about the relative phase between the condensates established. Section 6 deals with the behaviour of a condensate subject to a double-well trapping potential and, in particular, the possibility of coherent quantum tunnelling, in direct analogy with the Josephson effect. Finally, in Section 7 we discuss some of the issues and models associated with atom lasers, or coherent atomic beam generators, which represent a natural progression from Bose–Einstein condensates, but also constitute an interesting challenge for experimentalists.

2. Ground state properties of dilute-gas Bose–Einstein condensates in traps

2.1. Hamiltonian: binary collision model

The effects of interparticle interactions are of fundamental importance in the study of dilute-gas Bose–Einstein condensates. Although the actual interaction potential between atoms is typically very complex (see, e.g., Julienne et al., 1993), the regime of operation of current experiments is such that interactions can in fact be treated very accurately with a much-simplified model. In particular, at very low temperature the de Broglie wavelengths of the atoms are very large compared to the range of the interatomic potential. This, together with the fact that the density and energy of the atoms are so low that they rarely approach each other very closely, means that atom–atom interactions are effectively *weak* and dominated by (elastic) s-wave scattering (see, e.g., Walraven, 1996). It follows also that to a good approximation one need only consider *binary* collisions (i.e., three-body processes can be neglected) in the theoretical model.

The s-wave scattering is characterised by the s-wave scattering length, a, the sign of which depends sensitively on the precise details of the interatomic potential (see, e.g., Verhaar, 1995) [$a > 0$ ($a < 0$) for repulsive (attractive) interactions]. Given the conditions described above, the interaction potential can be approximated by

$$U(\boldsymbol{r} - \boldsymbol{r}') = U_0 \delta(\boldsymbol{r} - \boldsymbol{r}') \,, \tag{3}$$

(i.e., a hard sphere potential) with U_0 the interaction "strength", given by

$$U_0 = 4\pi\hbar^2 a/m \,, \tag{4}$$

and the Hamiltonian for the system of weakly interacting bosons in an external potential, $V_{\mathrm{trap}}(\boldsymbol{r})$, can be written in the second quantised form as

$$\hat{H} = \int \mathrm{d}^3 r \, \hat{\Psi}^\dagger(\boldsymbol{r}) \left[-\frac{\hbar^2}{2m} \nabla^2 + V_{\mathrm{trap}}(\boldsymbol{r}) \right] \hat{\Psi}(\boldsymbol{r}) + \frac{1}{2} \int \mathrm{d}^3 r \int \mathrm{d}^3 r' \, \hat{\Psi}^\dagger(\boldsymbol{r}) \, \hat{\Psi}^\dagger(\boldsymbol{r}') U(\boldsymbol{r} - \boldsymbol{r}') \hat{\Psi}(\boldsymbol{r}') \hat{\Psi}(\boldsymbol{r}) \,, \tag{5}$$

where $\hat{\Psi}(\boldsymbol{r})$ and $\hat{\Psi}^\dagger(\boldsymbol{r})$ are the boson field operators that annihilate or create a particle at the position $\boldsymbol{r}$, respectively.

To put a quantitative estimate on the applicability of the model, if ρ is the density of bosons, then a necessary condition is that $a^3\rho \ll 1$ (for $a > 0$). This condition is indeed satisfied in the alkali gas BEC experiments (Anderson et al., 1995; Davis et al., 1995), where achieved densities of the order of 10^{12}–10^{13} cm^{-3} correspond to $a^3\rho \simeq 10^{-5}$–10^{-6}. The model is also suitable for dilute systems of bosons having *negative* scattering lengths ($a < 0$) (Bradley et al., 1995, 1997a), although, as we shall see later in this section, the attractive interaction ultimately leads to instability and collapse of the condensate when the number of atoms exceeds a critical value.

2.2. Mean-field theory

The Heisenberg equation of motion for $\hat{\Psi}(\boldsymbol{r})$ is derived as

$$i\hbar\frac{\partial\hat{\Psi}(\boldsymbol{r},t)}{\partial t}=\left[-\frac{\hbar^2}{2m}\nabla^2+V_{\text{trap}}(\boldsymbol{r})\right]\hat{\Psi}(\boldsymbol{r},t)+U_0\hat{\Psi}^{\dagger}(\boldsymbol{r},t)\hat{\Psi}(\boldsymbol{r},t)\hat{\Psi}(\boldsymbol{r},t)\,, \tag{6}$$

which cannot in general be solved. In the mean-field approach, however, the expectation value of Eq. (6) is taken and the field operator decomposed as

$$\hat{\Psi}(\boldsymbol{r},t)=\Psi(\boldsymbol{r},t)+\tilde{\Psi}(\boldsymbol{r},t)\,, \tag{7}$$

where $\Psi(\boldsymbol{r},t)=\langle\hat{\Psi}(\boldsymbol{r},t)\rangle$ is the "condensate wave function" and $\tilde{\Psi}(\boldsymbol{r})$ describes quantum and thermal fluctuations around this mean value. The quantity $\Psi(\boldsymbol{r},t)$ is in fact a classical field possessing a well-defined phase, reflecting a broken gauge symmetry associated with the condensation process. The expectation value of $\tilde{\Psi}(\boldsymbol{r},t)$ is zero and in the mean-field theory its effects are assumed to be small, amounting to the assumption of the thermodynamic limit, where the number of particles tends to infinity while the density is held fixed (Lifshitz and Pitaevskii, 1980). For the effects of $\tilde{\Psi}(\boldsymbol{r})$ to be *negligibly small* in the equation for $\Psi(\boldsymbol{r})$ also amounts to an assumption of zero temperature (i.e., pure condensate). Given that this is so, and using the normalisation

$$\int d^3r|\Psi(\boldsymbol{r},t)|^2=1\,, \tag{8}$$

one is lead to the nonlinear Schrödinger equation, or "Gross–Pitaevskii equation" (GP equation), for the condensate wave function $\Psi(\boldsymbol{r},t)$ (Lifshitz and Pitaevskii, 1980),

$$i\hbar\frac{\partial\Psi(\boldsymbol{r},t)}{\partial t}=\left[-\frac{\hbar^2}{2m}\nabla^2+V_{\text{trap}}(\boldsymbol{r})+NU_0|\Psi(\boldsymbol{r},t)|^2\right]\Psi(\boldsymbol{r},t)\,, \tag{9}$$

where N is the mean number of particles in the condensate. The nonlinear interaction term (or mean-field pseudo-potential) is proportional to the number of atoms in the condensate and to the s-wave scattering length through the parameter U_0.

The influence of quantum fluctuations through the term $\tilde{\Psi}(\boldsymbol{r})$ and the appropriateness of the decomposition (7) (with concomitant relevance to the concept of broken symmetry) are of importance when it comes to the study of the effects of a finite temperature and of a finite number of condensate particles (i.e., finite N). These issues are considered later in this review.

To find a stationary solution for the condensate wave function in the mean-field theory, one can substitute the form $\Psi(\boldsymbol{r},t)=\exp(-i\mu t/\hbar)\psi(\boldsymbol{r})$ into Eq. (9) (where μ is the chemical potential of the condensate) to give the time-independent equation

$$(-(\hbar^2/2m)\nabla^2+V_{\text{trap}}(\boldsymbol{r})+NU_0|\psi(\boldsymbol{r})|^2)\psi(\boldsymbol{r})=\mu\psi(\boldsymbol{r})\,. \tag{10}$$

For a condensate of neutral atoms confined by a harmonic potential, $V_{\text{trap}}(\boldsymbol{r})$ can be written in the general form (allowing for different oscillation frequencies along each of the three axes, i.e., for an "anisotropic" trap),

$$V_{\text{trap}}(\boldsymbol{r})=\tfrac{1}{2}m(\omega_x^2x^2+\omega_y^2y^2+\omega_z^2z^2)\,, \tag{11}$$

so that $\boldsymbol{r}=(x,y,z)$ represents the displacement from the centre of the trap.

Solutions of Eq. (10), and of the time-dependent Eq. (9), have been computed numerically by a number of authors using a variety of techniques. In cases where the trap potential is isotropic ($\omega_x = \omega_y = \omega_z$) or cylindrically symmetric ($\omega_x = \omega_y \neq \omega_z$) the problem becomes effectively one- or two-dimensional respectively, allowing some simplification. As we will see, in certain limits approximate analytical solutions can also be calculated and relatively simple expressions derived for basic properties of the condensate.

2.3. Ground state properties of a condensate with repulsive interactions

2.3.1. Numerical results

Numerical solutions of the GP equation for the ground state wave functions of a harmonically trapped weakly interacting condensate with repulsive interactions have been obtained by a variety of groups for both the isotropic case ($\omega_x = \omega_y = \omega_z$) (Edwards and Burnett, 1995; Ruprecht et al., 1995; You et al., 1996; Kagan et al., 1996) and the anisotropic case ($\omega_x = \omega_y \neq \omega_z$, i.e., matching current experimental configurations) (Edwards et al., 1996a; Holland and Cooper, 1996; Dalfovo and Stringari, 1996). Compared to the bare harmonic oscillator ground state wave function, the wave function of the condensate is broadened in space as a result of the repulsive interactions and its shape deviates markedly from a Gaussian, with a much flatter density profile in the central region for sufficiently large N. The broadening increases as N increases, and for an anisotropic trapping potential, the extent of broadening is greatest in directions where the restoring forces are weakest. Fig. 3 illustrates these features for a ^{87}Rb condensate.

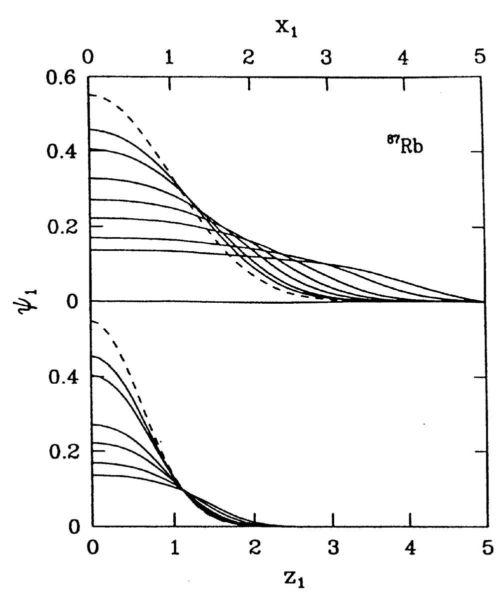

Fig. 3. Ground-state wave function for ^{87}Rb along the x axis (upper part) and z axis (lower part). Distances are in units of $d_\perp = (\hbar/m\omega_\perp)^{1/2}$, with $\omega_x = \omega_y = \omega_\perp$ and $\omega_z = \sqrt{8}\omega_\perp$. The dashed line is for noninteracting atoms; the solid lines correspond to $N = 100, 200, 500, 1000, 2000, 5000, 10^4$, in descending order of central density. From Dalfovo and Stringari (1996).

The energy per particle has three contributions: the kinetic energy, the harmonic oscillator potential energy, and the internal potential energy arising from the interactions. Applying the virial theorem to the trap leads to the rigorous relation

$$\langle p_x^2 \rangle/2m - (m/2)\omega_x \langle x^2 \rangle + \tfrac{1}{2}E_{\text{pot}} = 0\,, \tag{12}$$

and similarly for y and z. Summing over the three dimensions yields

$$2E_{\text{kin}} - 2E_{\text{HO}} + 3E_{\text{pot}} = 0\,. \tag{13}$$

As N increases, E_{pot} increases and the repulsive interaction expands the cloud to regions where the trapping potential is higher, thus increasing E_{HO}. Conversely, the kinetic energy, E_{kin}, decreases. Dalfovo and Stringari (1996) have explicitly demonstrated this aspect in their numerical computations.

Having computed the ground state wave function, Holland and Cooper (1996) also considered the ballistic expansion of the condensate, given that the trapping potential is suddenly reduced. This modelled the experimental procedure used by Anderson et al. (1995) to increase the size of the atom cloud before imaging it via light scattering. The numerical results for $N = 2000$ atoms show good agreement with the experiment and demonstrate the significance of interactions in determining the structure of the condensate. Along similar lines, Holland et al. (1997) have also carefully modelled more recent experiments at JILA, obtaining very nice agreement between the mean-field theory and experiment for the release energy from ballistic expansion and the density profile of the atom cloud. Significantly, the comparison between theory and experiment required essentially no fitting parameters.

2.3.2. Analytical results

The trap potentials in BEC experiments to date have typically been cylindrically symmetric and so we shall concentrate on such a configuration, i.e., we set $\omega_x = \omega_y = \omega_\perp$ and $\omega_z = \lambda\omega_\perp$. Introducing the standard length

$$d_\perp = (\hbar/m\omega_\perp)^{1/2}\,, \tag{14}$$

we follow Dalfovo and Stringari (1996) and define rescaled variables through

$$\boldsymbol{r} = d_\perp \bar{\boldsymbol{r}}, \qquad \psi(\boldsymbol{r}) = d_\perp^{-3/2}\bar{\psi}(\bar{\boldsymbol{r}}), \qquad \bar{u}_0 = 8\pi a N/d_\perp, \qquad \mu = \hbar\omega_\perp\bar{\mu}\,. \tag{15}$$

The time-independent GP equation (10) can then be rewritten

$$[-\bar{\nabla}^2 + (\bar{x}^2 + \bar{y}^2 + \lambda^2\bar{z}^2) + \bar{u}_0|\bar{\psi}(\bar{\boldsymbol{r}})|^2]\bar{\psi}(\bar{\boldsymbol{r}}) = 2\bar{\mu}\bar{\psi}(\bar{\boldsymbol{r}})\,. \tag{16}$$

The dimensionless parameter $\bar{u}_0$ characterises the effect of the interactions on the condensate. Note that, for the trap of Anderson et al. (1995), $d_\perp \simeq 1.2\,\mu\text{m}$, so taking $a \simeq 5\,\text{nm}$ gives $\bar{u}_0 \simeq 0.1N$, and hence values of $\bar{u}_0$ much greater than one are to be expected for condensates comprised of thousands of atoms.

2.3.2.1. Non-interacting limit. First, however, we consider the case in which $\bar{u}_0 = 0$, corresponding simply to a non-interacting anisotropic harmonic oscillator. The ground state wave function is the Gaussian

$$\bar{\psi}(\bar{\boldsymbol{r}}) = \lambda^{1/4}\pi^{-3/4}\exp[-\tfrac{1}{2}(\bar{x}^2 + \bar{y}^2 + \lambda\bar{z}^2)]\,. \tag{17}$$

The chemical potential, obtained from the normalisation of the wave function, is

$$\bar{\mu} = 1 + \tfrac{1}{2}\lambda\,, \tag{18}$$

(equal to the energy per particle, E/N) and the position and momentum variances for this ground state are given by

$$\langle \bar{x}^2 \rangle = \langle \bar{y}^2 \rangle = \tfrac{1}{2}, \qquad \langle \bar{z}^2 \rangle = 1/2\lambda\,, \tag{19}$$

$$\langle \bar{p}_x^2 \rangle = \langle \bar{p}_y^2 \rangle = \tfrac{1}{2}, \qquad \langle \bar{p}_z^2 \rangle = \tfrac{1}{2}\lambda\,, \tag{20}$$

respectively, where we have defined $\boldsymbol{p} = (\hbar m\omega_\perp)^{1/2}\bar{\boldsymbol{p}}$. Quantities of considerable interest in the interpretation of experiments are the *aspect ratios*

$$\sqrt{\frac{\langle \bar{x}^2 \rangle}{\langle \bar{z}^2 \rangle}} = \sqrt{\frac{\langle \bar{p}_z^2 \rangle}{\langle \bar{p}_x^2 \rangle}} = \sqrt{\lambda}\,. \tag{21}$$

Observed values of λ different from one indicate the macroscopic occupation of the anisotropic ground state of the potential.

2.3.2.2. Strongly repulsive limit: Thomas–Fermi approximation. The opposite limit is when $\bar{u}_0 \gg 1$, corresponding to a large number of particles. In this limit, it is possible to neglect the kinetic energy term in the GP equation (Thomas–Fermi model) and to derive the approximate solution (Edwards and Burnett, 1995; Kagan et al., 1996; Dalfovo and Stringari, 1996; Baym and Pethick, 1996)

$$|\bar{\psi}(\bar{\boldsymbol{r}})|^2 = (1/\bar{u}_0)(2\bar{\mu} - \bar{x}^2 - \bar{y}^2 - \lambda^2\bar{z}^2) \tag{22}$$

in the region where the right-hand side is positive and $|\bar{\psi}(\bar{\boldsymbol{r}})|^2 = 0$ outside this region. The chemical potential follows as

$$\bar{\mu} = \tfrac{1}{2}((15/8\pi)\lambda\bar{u}_0)^{2/5} = \tfrac{1}{2}(15\lambda N\, a/d_\perp)^{2/5}\,, \tag{23}$$

and using the relation $\mu = (\mathrm{d}E/\mathrm{d}N)$, one finds that the energy per particle is now $E/N = (5/7)\mu$. For sufficiently large N (typically of the order of a few thousand or greater), the wave function (22) provides a reasonably good approximation to the "exact" numerical solution, except in regions where the density is small, i.e., at the surface of the condensate, where the sharp cut-off of Eq. (22) is artificial, as shown in Fig. 4, where the numerical and analytical solutions are compared. In reality, the kinetic energy causes the wave function to vanish smoothly (Baym and Pethick, 1996; Dalfovo et al., 1996; Lundh et al., 1997; Timmermans et al., 1997). Note that recent BEC experiments with condensates of $N \sim 10^4$–10^6 atoms have indeed confirmed the $N^{2/5}$ dependence of the mean-field energy per atom (Mewes et al., 1996a; Jin et al., 1996a). Fig. 5 shows a fit of this form to data from the ^{23}Na experiment of Mewes et al., 1996a.

One deduces from the wave function (22) that the condensate extends over a radius $\bar{R} = \sqrt{2\bar{\mu}}$ and a vertical distance $\bar{Z} = \lambda\bar{R}$. One also derives the results

$$\langle \bar{x}^2 \rangle = \langle \bar{y}^2 \rangle = 2\bar{\mu}/7, \qquad \langle \bar{z}^2 \rangle = 2\bar{\mu}/7\lambda^2\,, \tag{24}$$

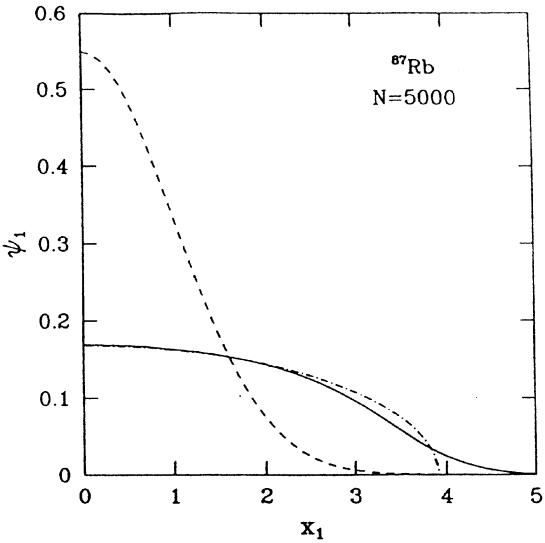

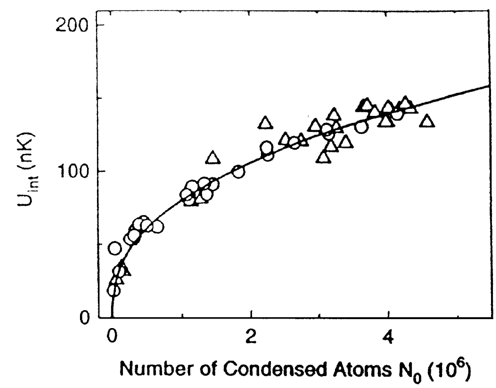

Fig. 4. Ground-state wave function for 5000 ^{87}Rb atoms. Dashed line, noninteracting gas; dot-dashed line, strongly repulsive limit (Thomas–Fermi model); solid line, numerical solution of GP equation. From Dalfovo and Stringari (1996).

Fig. 5. Mean-field energy per condensed atom versus the number of atoms in the condensate. $\triangle$: clouds with no visible normal (noncondensed) fraction. $\bigcirc$: clouds with both normal and condensed fractions visible. The solid line is a fit proportional to $N^{2/5}$. From Mewes et al. (1996a).

and the aspect ratios

$$\sqrt{\frac{\langle \bar{x}^2\rangle}{\langle \bar{z}^2\rangle}} = \sqrt{\frac{\langle \bar{p}_z^2\rangle}{\langle \bar{p}_x^2\rangle}} = \lambda \,. \tag{25}$$

That is, the aspect ratios are now equal to λ, in contrast to $\sqrt{\lambda}$ for the non-interacting case (Dalfovo and Stringari, 1996; Baym and Pethick, 1996). This change in aspect ratios is borne out by numerical solutions in the limit of large N (Edwards et al., 1996a; Holland and Cooper, 1996, Dalfovo and Stringari, 1996) and is consistent with experiments (Anderson et al., 1995; Mewes et al., 1996a).

The expansion of the condensate with increasing N is illustrated by the result $\bar{R} = \sqrt{2\bar{\mu}} \propto N^{1/5}$. Note that for the values of a and $d_\perp$ quoted earlier, and for $\lambda = \sqrt{8}$ (as in the experiment of Anderson et al., 1995), one finds $\bar{\mu} \simeq 0.25N^{2/5}$ and $\langle \bar{x}^2\rangle \simeq 0.07N^{2/5} \simeq 1.1$ for $N = 1000$.

The behaviour of the various contributions to the particle energy as a function of the particle number can also be put on a slightly more quantitative basis. The harmonic oscillator potential energy per particle is $E_{\mathrm{HO}} \sim m\omega_\perp^2 R^2/2 \propto N^{2/5}$, while, assuming a particle density $\rho \sim N/R^3$, the interaction energy is $E_{\mathrm{pot}} \sim (4\pi\hbar^2 a/m)N/R^3 \propto N^{2/5}$. In contrast, the kinetic energy per particle, E_{kin}, is of order $\hbar^2/(2mR^2) \propto N^{-2/5}$.

2.4. Ground state properties of a condensate with attractive interactions

2.4.1. Numerical results

A homogeneous condensate with negative scattering length, corresponding to an attractive interaction between particles, is predicted to be unstable (Lifshitz and Pitaevskii, 1980). If, however, the condensate is confined by a potential and the number of particles is not too large, then it is possible for the zero-point energy to exceed the attractive interaction energy and to stabilise the condensate against collapse. Confirmation of this effect has, of course, come from the experiments of Bradley et al. (1995, 1997a), in which evidence for BEC of a trapped atomic vapour of ^{7}Li (for which $a<0$) has been found.

Numerical studies of the GP equation with a confining potential have also shown that stable condensates can exist for $a<0$, provided N is not too large (Ruprecht et al., 1995; Dalfovo and Stringari, 1996; Dodd et al., 1996; Bergeman, 1997). Example wave functions are shown in Fig. 6 for ^{7}Li in an anisotropic potential. In general, the central density of the condensate *increases* with N and the atom cloud contracts under the increasing influence of the attractive potential. Noticeably also, the cloud approaches spherical symmetry, in spite of the anisotropy of the potential. Dalfovo and Stringari (1996), Dodd et al. (1996), and Bergeman (1997) have concentrated specifically on the experimental configuration and parameters of Bradley et al., 1995 and have determined a critical number, $N_c \simeq 1400$, above which stable solutions of the GP equation no longer exist. This is *not* consistent with the original experiment of Bradley et al., 1995, in which the number of atoms was estimated to be an order of magnitude larger. However, following improvements to their experiment and data analysis, the group at Rice University have subsequently

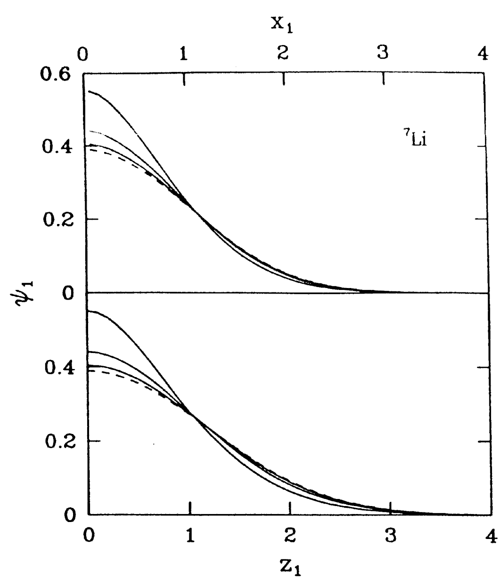

Fig. 6. Ground-state wave function for ^{7}Li along the x axis (upper part) and z axis (lower part). Distances are in units of $d_\perp = (\hbar/m\omega_\perp)^{1/2}$, with $\omega_x=\omega_y=\omega_\perp$ and $\omega_z=0.72\omega_\perp$. The dashed line is for noninteracting atoms; the solid lines correspond to $N=200, 500, 1000$, in ascending order of central density. From Dalfovo and Stringari (1996).

revised their estimates of the number of condensate atoms to between 650 and 1300 (Bradley et al., 1997a,b).

It is interesting to note at this point that experimental efforts to observe Bose–Einstein condensation in a trapped dilute gas of cesium atoms have thusfar proved unsuccessful. The sign and magnitude of the scattering length for cesium are not accurately known, but some evidence (see, e.g., Arndt et al., 1997) does point to it being large and negative, which, following from above, would preclude the formation of a stable condensate of reasonable size.

2.4.2. Analytical results

Following Baym and Pethick (1996) and Stoof (1997a) (see also Shuryak, 1996; Shi and Zheng, 1997), it is possible to obtain a useful analytical estimate of the critical atom number at which the condensate is expected to become unstable by performing a variational calculation of the ground state energy. In the Gross–Pitaevskii theory, this energy is given by the energy functional

$$E[\psi(\boldsymbol{r})] = \int \mathrm{d}^3 r \left[\frac{\hbar^2}{2m} |\nabla\psi(\boldsymbol{r})|^2 + \frac{1}{2} m\omega^2 r^2 |\psi(\boldsymbol{r})|^2 + \frac{2\pi a \hbar^2}{m} |\psi(\boldsymbol{r})|^4 \right] , \tag{26}$$

where $\psi(\boldsymbol{r})$ is the condensate wave function, or order parameter (normalised in this case to N), and, for simplicity, we have assumed an isotropic harmonic trapping potential with angular frequency ω. The shape of the condensate mode is given by the function that minimises the energy functional. As a reasonable first approximation, consider a Gaussian wave function of the form

$$\psi(\boldsymbol{r}) = (N/d^3\pi^{3/2})^{1/2} \exp(-r^2/2d^2) , \tag{27}$$

with d an effective width, treated as a variational parameter. Substituting this wave function into Eq. (26) and performing the integration, one obtains

$$E(d) = \frac{3\hbar^2 N}{4md^2} + \frac{3}{4} N m\omega^2 d^2 + \frac{\hbar^2 a N^2}{\sqrt{2\pi} m d^3} . \tag{28}$$

If E is plotted as a function of d for parameters appropriate to the ^{7}Li experiment of Bradley et al., 1995 ($\omega = 2\pi \times 160$ Hz, $a = -27.3 a_0$, with a_0 the Bohr radius), one sees (Fig. 7) that a stable local minimum exists only up to a certain maximum number of atoms; above this number, the zero-point kinetic energy is unable to stabilise the condensate against collapse. The critical point occurs where

$$\left.\frac{\partial E}{\partial d}\right|_{\{d_c,\, N_c\}} = 0 \quad \text{and} \quad \left.\frac{\partial^2 E}{\partial d^2}\right|_{\{d_c,\, N_c\}} = 0 , \tag{29}$$

and one finds

$$d_c = \frac{5}{8}\left(\frac{4}{5}\right)^{5/4} \sqrt{2} (\hbar/m\omega)^{1/2} \approx 0.67 (\hbar/m\omega)^{1/2} , \tag{30}$$

$$N_c = -\frac{1}{2}\left(\frac{4}{5}\right)^{5/4} (\sqrt{\pi}/a)(\hbar/m\omega)^{1/2} \approx 1400 . \tag{31}$$

This value for N_c is in good agreement with the result from a full numerical treatment.

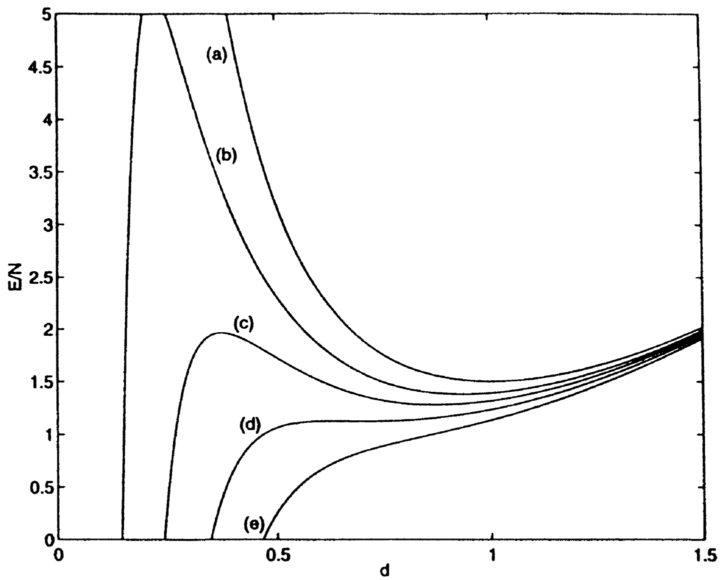

Fig. 7. Energy per particle (in units of $\hbar\omega$) as a function of the variational parameter d (in units of $(\hbar/m\omega)^{1/2}$) for $\omega/2\pi = 160\,\mathrm{Hz}$ and $a = -27.3a_0$ (^{7}Li). Curves are shown for (a) the noninteracting case, (b) $N = 600$, (c) $N = 1000$, (d) $N = 1450$, and (e) $N = 2000$. From Dunningham (1997).

Houbiers and Stoof (1996) have also presented calculations (for ^{7}Li) for nonzero temperatures which show that the critical number of condensate atoms decreases with increasing temperature. This occurs because the noncondensate part of the gas effectively increases the strength of the trap potential (from the point of view of the condensate part) as the temperature increases, limiting the maximum size of the condensate.

2.5. Vortex states

It is also possible to consider a system that is *rotating* about the z-axis, giving rise to so-called "vortex states" (Lifshitz and Pitaevskii, 1980). In such states, atoms flow around a vortex line (the z-axis) with quantised circulation.

2.5.1. Description and properties

The appropriate axially symmetric condensate wave function for a vortex state can be written in the form

$$\Psi(\boldsymbol{r}) = \psi(\boldsymbol{r})\exp[\mathrm{i}S(\boldsymbol{r})]\,, \tag{32}$$

where $\psi(\boldsymbol{r}) = \sqrt{\rho(\boldsymbol{r})}$ is the modulus and S is chosen as $S = \kappa\phi$, where ϕ is the angle around the z-axis and κ is an integer (the *quantum of circulation*). The tangential velocity is then

$$v = (\hbar/mr_\perp)\kappa\,, \tag{33}$$

with $r_\perp^2 = x^2 + y^2$, and the angular momentum along z is $L_z = N\kappa\hbar$.

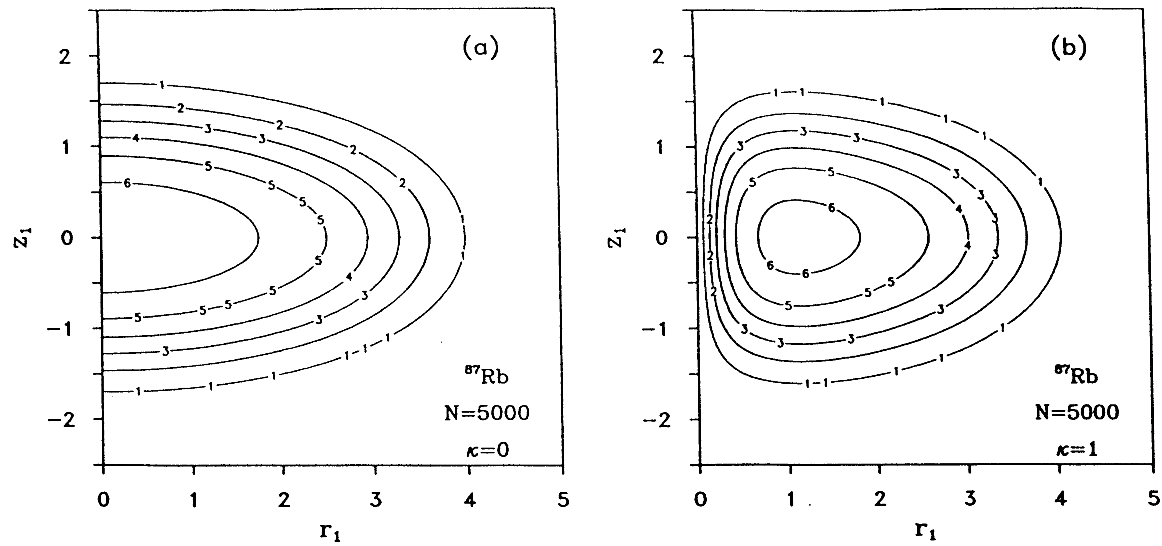

Fig. 8. Wave function for a trapped condensate of 5000 ^{87}Rb atoms ($\lambda = \sqrt{8}$): (a) Ground state ($\kappa = 0$). (b) Vortex state ($\kappa = 1$). From Dalfovo and Stringari (1996).

Using the form (32) in the GP equation, one derives the modified nonlinear Schrödinger equation (in dimensionless form)

$$[-\bar{\nabla}^2 + \kappa^2(\bar{r}_\perp)^{-2} + (\bar{r}_\perp^2 + \lambda^2\bar{z}^2) + \bar{u}_0|\bar{\psi}(\bar{\boldsymbol{r}})|^2]\bar{\psi}(\bar{\boldsymbol{r}}) = 2\bar{\mu}\bar{\psi}(\bar{\boldsymbol{r}})\,. \tag{34}$$

Note that due to the centrifugal term, the solution of this equation for $\kappa \neq 0$ has to vanish on the z-axis. That is, atoms are pushed away from the axis forming a toroidal cloud.

The critical frequency, $\Omega_{\rm cr}$, at which the formation of a vortex line becomes energetically favourable is determined from the condition $E - L_z\Omega_{\rm cr} = 0$, where E is the energy difference between the ground state and the vortex state. For the condensate of Anderson et al. (1995) with approximately 2000 atoms, the critical frequency for $\kappa = 1$ is found (numerically) to be $\Omega_{\rm cr}/2\pi = 37$ Hz (Edwards et al., 1996a). An approximate analytical expression for $\Omega_{\rm cr}$ giving reasonable agreement with numerical results is (Lundh et al., 1997)

$$\Omega_{\rm cr} = \tfrac{5}{2}(\hbar/mR^2)\ln(0.671R/\xi_0)\,, \tag{35}$$

where $R/d_\perp = (15N\lambda a/d_\perp)^{1/5}$ and $\xi_0 = [8\pi\rho(0)a]^{-1/2}$ (the "healing" or "coherence" length), with $\rho(0)$ the central density of the condensate in the absence of a vortex.

Vortex solutions of Eq. (34) have been computed numerically by Edwards et al. (1996a) (for $a > 0$) and by Dalfovo and Stringari (1996) (for $a > 0$ and $a < 0$). A comparison of the ground state ($\kappa = 0$) with the $\kappa = 1$ vortex state is shown in Fig. 8 for the ^{87}Rb trap with 5000 atoms. Interestingly, for the case of attractive interactions, it is found that the vortex state can support a larger number of condensate atoms than the $\kappa = 0$ ground state, i.e., more atoms can be put in the rotating cloud before reaching the critical density for collapse. For example, Dalfovo and Stringari find a critical value $N_{\rm c} \simeq 4000$ for the $\kappa = 1$ state in the ^{7}Li trap (as opposed to 1400 for the $\kappa = 0$

ground state). Shi and Zheng (1997) have found similar results for the critical value in this particular vortex state using a variational approach.

2.5.2. Generation and stability of vortex states

Straightforward rotation of the confining trap at the critical frequency Ω_{cr} should promote the condensate into the vortex state. However, alternative schemes for preparing vortex states have been proposed based on laser-light-induced Raman transitions between different internal atomic states (Bolda and Walls, 1997; Marzlin et al., 1997; Dum et al., 1997). In these schemes, which can involve laser beams with Laguerre–Gaussian mode profiles,[4] angular momentum is transferred from the laser photons to the condensed atoms.

Given that a vortex state has been prepared in a harmonically confined Bose gas, the question of stability of the state arises, particularly in the case where the imposed rotation is removed; superfluidity is associated with the persistence of the circulating flow in the absence of a rotating drive. Rokhsar (1997) has recently examined the issue of stability, finding that vortex states are in fact *unstable* in the absence of driving and consequently that harmonically confined Bose gases are not superfluid. This is a result of collision-induced excitations occurring preferentially near the centre of the trap, which has the effect of destabilising the vortex, at least in the limit of weak interactions. In the limit of strong interactions (i.e., large N) the azimuthal symmetry of the rotating condensate is broken, giving rise to a precession about the axis of the trap which, in the presence of a normal component (i.e., at a finite temperature), causes dissipation of energy and angular momentum.

2.6. Condensate lifetime

In practice, inelastic two- and three-body collisions cause atoms to be lost from the condensate, ultimately limiting its lifetime. In particular, collisions producing changes in the internal hyperfine state of the atoms ("spin exchange") or leading to molecule formation ("recombination") give rise to loss from the trap and a reduction in density. These processes have been studied in some detail and estimates of the rates calculated for various species of atom. These rates depend, naturally, on the density distribution of atoms in the trap; the total loss rate for two- and three-body collisions is given by (Edwards et al., 1996a; Hijmans et al., 1993; Moerdijk et al., 1996)

$$R(N) = \alpha N^2 \int d^3r \; |\psi(\boldsymbol{r})|^4 + L N^3 \int d^3r \; |\psi(\boldsymbol{r})|^6 \,, \tag{36}$$

where α is the two-body dipolar loss rate coefficient and L is the three-body recombination loss rate coefficient. For the experiment of Anderson et al. (1995), $1/e$ lifetimes for the condensate population of the order of tens of seconds are predicted, roughly consistent with the experimental result.

Loss rates for condensates with attractive interactions ($a < 0$) will in general be more significant than with repulsive interactions, due to the contraction of the ground state and enhancement of the density. Kagan et al. (1996) have also identified another intrinsic loss mechanism for the case of

[4] Such laser modes possess orbital angular momentum in addition to the angular momentum contributed by the polarisation of the light.

attractive interactions that arises from the fact that it is possible to form a much denser state of the system that still has the same total energy as the "standard" ground state. This state consists of dense clusters of atoms, within which *elastic* pair collisions can transfer atoms to excited trap states (as a result of the interaction energy per atom exceeding the trap level spacing). Transitions of the system to the much denser state are, however, not expected to figure significantly until the system approaches the boundary for stability of the condensate.

2.7. Binary mixtures of Bose–Einstein condensates

As we shall see throughout the course of this review, very interesting physics and applications can arise when one considers the dynamics of a *pair* of Bose–Einstein condensates consisting of two distinct "species" of atoms (e.g., two different spin states of a particular atom) that are possibly overlapping in space. In a spectacular recent experiment, such a situation has indeed been realised by Myatt et al. (1997) with the two condensates corresponding to two different spin states of ^{87}Rb ($|F=1, m=-1\rangle$ and $|F=2, m=2\rangle$). Evaporative cooling of the $|F=1, m=-1\rangle$ state combined with sympathetic cooling of the state $|F=2, m=2\rangle$ (resulting from elastic collisions with the $|F=1, m=-1\rangle$ atoms) is used to produce the double condensate in a single magnetic trap. Because of their different magnetic moments, the two states experience different magnetic forces; this, combined with the force of gravity, leads to different equilibrium positions of the condensates, although with modifications to the magnetic field strength and/or the axis of the trap, the degree of overlap between the two condensates can be controlled.

Amongst many interesting effects, Myatt et al. (1997) observed a repulsive interaction between the two condensates, tending to push them apart and, for a sufficient separation, to reduce inelastic spin exchange collisions between the two species that would otherwise significantly reduce the condensate lifetimes. A detailed theoretical analysis of the double condensate experiment has been performed by Esry et al. (1997), based upon numerical solutions of the Hartree–Fock equations for the condensate wave functions $\psi_1(\boldsymbol{r})$ and $\psi_2(\boldsymbol{r})$ [with normalisation $\int d^3r\, |\psi_1(\boldsymbol{r})|^2 = \int d^3r\, |\psi_2(\boldsymbol{r})|^2 = 1$]:

$$\left[-\frac{\hbar^2}{2m}\nabla^2 + V_1^{\mathrm{trap}}(\boldsymbol{r}) + (N_1-1)U_{11}|\psi_1(\boldsymbol{r})|^2 + N_2U_{12}|\psi_2(\boldsymbol{r})|^2\right]\psi_1(\boldsymbol{r}) = \varepsilon_1\psi_1(\boldsymbol{r})\,, \tag{37}$$

$$\left[-\frac{\hbar^2}{2m}\nabla^2 + V_2^{\mathrm{trap}}(\boldsymbol{r}) + N_1U_{12}|\psi_1(\boldsymbol{r})|^2 + (N_2-1)U_{22}|\psi_2(\boldsymbol{r})|^2\right]\psi_2(\boldsymbol{r}) = \varepsilon_2\psi_2(\boldsymbol{r})\,. \tag{38}$$

Here, $U_{ij} = 4\pi\hbar^2 a_{ij}/m$, with a_{ij} the s-wave scattering length between an i species atom and a j species atom, and

$$V_i^{\mathrm{trap}}(\boldsymbol{r}) = \tfrac{1}{2}m[\omega_{ix}^2x^2 + \omega_{iy}^2y^2 + \omega_{iz}^2(z-z_{i0})^2]\,, \tag{39}$$

with $z_{i0} = -g/\omega_{iz}^2$ the displacement of the i-th trap centre due to the gravitational acceleration g. Using the (positive) scattering length values $a_{11} = 108.8$ a.u., $a_{12} = 108.0$ a.u., and $a_{22} = 109.1$ a.u., and choosing other parameters to match the experimental configuration, the single particle probability densities $|\psi_i(\boldsymbol{r})|^2$ take the form shown in Fig. 9 (where the z axis is parallel to gravity). The separation between the centers of the condensates is due (i) to the differing gravitational "sag" experienced by each species and (ii) to the repulsive interaction U_{12} between the two species. Loss

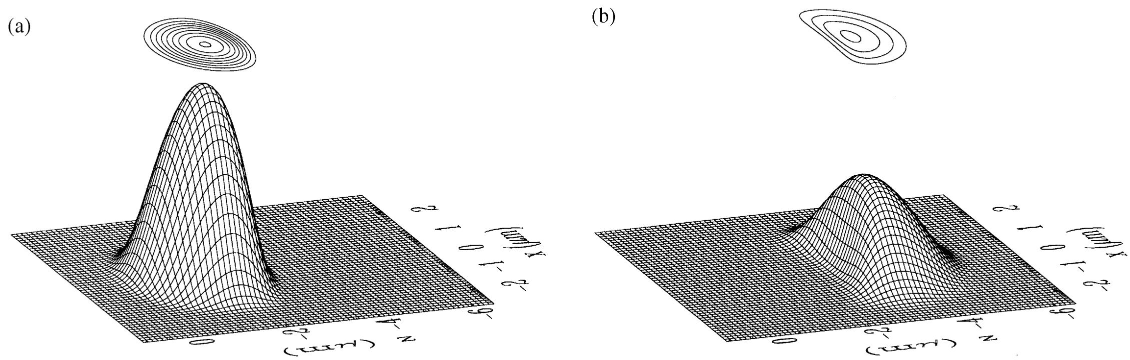

Fig. 9. Single particle densities $|\psi_i(\boldsymbol{r})|^2$ in the $y=0$ plane for parameters corresponding to the double-condensate experiment of Myatt et al. (1997): (a) $|2,2\rangle$ and (b) $|1,-1\rangle$ internal atomic state. From Esry et al. (1997).

rates due to spin exchange collisions and dipolar relaxation, proportional to $\int d^3r\ |\psi_1|^2|\psi_2|^2$ (i.e., the overlap between the two condensates) and $\int d^3r\ |\psi_1|^4$ or $\int d^3r\ |\psi_2|^4$, respectively, can be estimated and give results consistent with the experimental findings. Interestingly, the spin-exchange inelastic collision rate is found to be unusually small for ^{87}Rb. Recent theoretical calculations explain this somewhat fortuitous result as a consequence of interference between singlet and triplet collision channels, made possible by a special coincidence of the singlet and triplet scattering lengths for ^{87}Rb (Kokkelmans et al., 1997; Julienne et al., 1997; Burke et al., 1997). For ^{23}Na, such a coincidence does not occur and spin-exchange collisions are predicted to preclude the formation of a double condensate of the form produced with ^{87}Rb.

Beyond the first experiment of Myatt et al., and within the limitations set by loss rates due to "undesirable" collisions, it is possible to consider other species of atoms and, in particular, the effect of differing values of the respective scattering lengths. As shown by Esry et al. (1997), varying the value of the scattering length a_{12} (including negative values) has important consequences for the stability and lifetimes of the condensates. For example, a sufficiently strong attractive interaction between the different species (i.e., $a_{12}<0$) can overwhelm repulsive interactions within each condensate ($a_{11}, a_{22}>0$), leading to their collapse. Busch et al. (1997) have also demonstrated this by solving the coupled Gross–Pitaevskii equations for the two components using a Gaussian ansatz for the condensate wave functions and variational techniques.

Further along these lines, using a Thomas–Fermi approximation Ho and Shenoy (1996) have studied the stability and ground state structures of binary mixtures of condensates with positive values of the scattering lengths and varying numbers of atoms in each condensate (but neglecting gravity and assuming concentric condensates). In analogy with superfluid phenomena, they find regimes, dependent on the numbers of atoms and on the magnitudes of interaction parameters, of both coexisting and separated phases.

2.8. *Beyond mean-field theory: quantum properties of trapped condensates*

In some of the recent alkali-gas BEC experiments, the number of condensate atoms has only been in the range $N\approx 10^3$–10^5, which is very small in comparison with, for example, liquid helium experiments, where $N\approx 10^{20}$. It is therefore necessary to consider the possibility of deviations from the mean-field behavior and, in particular, what effect quantum fluctuations [as represented by the second term in Eq. (7)] may have on the system. In fact, it is necessary to address the very validity of the general mean-field decomposition,

$$\hat{\Psi}(\boldsymbol{r},t) = \langle \hat{\Psi}(\boldsymbol{r},t) \rangle + \tilde{\Psi}(\boldsymbol{r},t)\,, \tag{40}$$

which also touches upon the role and suitability of the wave function $\langle \hat{\Psi}(\boldsymbol{r},t) \rangle$ as the so-called "order parameter" for the system.

This issue of associating $\langle \hat{\Psi}(\boldsymbol{r},t) \rangle$ with the order parameter is very interesting in itself; as a brief overview, let us begin with the standard formal condition for BEC in an interacting Bose gas (see, e.g., Anderson, 1984; Griffin, 1993). In particular, the criterion for BEC is that the one-particle reduced density matrix $\rho_1(\boldsymbol{r},\boldsymbol{r}',t) = \langle \hat{\Psi}^\dagger(\boldsymbol{r},t)\hat{\Psi}(\boldsymbol{r}',t) \rangle$ (here $\langle \cdots \rangle$ denotes the restricted ensemble average over all atoms but one) does not vanish for large values of the separation, $|\boldsymbol{r}-\boldsymbol{r}'|$, and can be factorised into the form

$$\rho_1(\boldsymbol{r},\boldsymbol{r}',t) = \Phi^*(\boldsymbol{r},t)\Phi(\boldsymbol{r}',t) \quad (+\text{ small terms})\,, \tag{41}$$

where $\Phi(\boldsymbol{r},t)$ characterises the spatial distribution of the condensate and is referred to as the "order parameter." The non-vanishing of $\rho_1(\boldsymbol{r},\boldsymbol{r}',t)$ as $|\boldsymbol{r}-\boldsymbol{r}'| \to \infty$ represents an "off-diagonal long-range order" (ODLRO), absent from ordinary non-condensed systems.

Assuming the decomposition (40) to be valid, one can make the explicit identification $\Phi(\boldsymbol{r},t) = \langle \hat{\Psi}(\boldsymbol{r},t) \rangle$. A non-zero expectation value of the field annihilation operator, $\langle \hat{\Psi}(\boldsymbol{r},t) \rangle$, is referred to as a "broken symmetry," since the Hamiltonian describing the system is invariant under the transformation $\hat{\Psi}^\dagger(\boldsymbol{r}) \to \hat{\Psi}^\dagger(\boldsymbol{r})\mathrm{e}^{-\mathrm{i}\theta}$, $\hat{\Psi}(\boldsymbol{r}) \to \hat{\Psi}(\boldsymbol{r})\mathrm{e}^{\mathrm{i}\theta}$, whereas the expectation values $\langle \hat{\Psi}(\boldsymbol{r},t) \rangle$ and $\langle \hat{\Psi}^\dagger(\boldsymbol{r},t) \rangle$ *are not*. However, as we shall see below, the identification of $\langle \hat{\Psi}(\boldsymbol{r},t) \rangle$ with the order parameter $\Phi(\boldsymbol{r},t)$ is not always suitable; with a finite number of condensate atoms, $\langle \hat{\Psi}(\boldsymbol{r},t) \rangle$ may in fact vanish, yielding the operator decomposition above invalid.

2.8.1. Single mode approximation

The study of the quantum statistical properties of the condensate (at $T=0$) can be reduced to a relatively simple model by using a mode expansion and subsequent truncation to just a single mode (the "condensate mode"). In particular, one writes the Heisenberg atomic field annihilation operator as a mode expansion over single-particle states,

$$\hat{\Psi}(\boldsymbol{r},t) = \sum_\alpha \hat{a}_\alpha(t)\psi_\alpha(\boldsymbol{r})\mathrm{e}^{-\mathrm{i}\mu_\alpha t/\hbar} = \hat{a}_0(t)\psi_0(\boldsymbol{r})\mathrm{e}^{-\mathrm{i}\mu_0 t/\hbar} + \tilde{\Psi}(\boldsymbol{r},t)\,, \tag{42}$$

where $\{\psi_\alpha(\boldsymbol{r})\}$ are a complete orthonormal basis set and $\{\mu_\alpha\}$ the corresponding eigenvalues. The first term in the second line of Eq. (42) acts only on the condensate state vector, with $\psi_0(\boldsymbol{r})$ chosen as a solution of the stationary GP equation (10) (with chemical potential μ_0 and mean number of condensate atoms N). The second term, $\tilde{\Psi}(\boldsymbol{r},t)$, accounts for non-condensate atoms. Substituting this mode expansion into the Hamiltonian

$$\hat{H} = \int \mathrm{d}^3r\, \hat{\Psi}^\dagger(\boldsymbol{r})\left[-\frac{\hbar^2}{2m}\nabla^2 + V_{\mathrm{trap}}(\boldsymbol{r})\right]\hat{\Psi}(\boldsymbol{r}) + \tfrac{1}{2}U_0\int \mathrm{d}^3r\, \hat{\Psi}^\dagger(\boldsymbol{r})\hat{\Psi}^\dagger(\boldsymbol{r})\hat{\Psi}(\boldsymbol{r})\hat{\Psi}(\boldsymbol{r})\,, \tag{43}$$

and retaining only condensate terms, one arrives at the single-mode effective Hamiltonian

$$\hat{H} = \hbar\tilde{\omega}_0 \hat{a}_0^\dagger \hat{a}_0 + \hbar\kappa \hat{a}_0^\dagger \hat{a}_0^\dagger \hat{a}_0 \hat{a}_0 , \tag{44}$$

where

$$\hbar\tilde{\omega}_0 = \int d^3 r\, \psi_0^*(\boldsymbol{r}) \left[-\frac{\hbar^2}{2m}\nabla^2 + V_{\mathrm{trap}}(\boldsymbol{r}) \right] \psi_0(\boldsymbol{r}) , \tag{45}$$

$$\hbar\kappa = \frac{U_0}{2} \int d^3 r\, |\psi_0(\boldsymbol{r})|^4 . \tag{46}$$

2.8.2. Quantum state of the condensate

In this section, we summarise the results of Dunningham (1997) (see also Dunningham et al., 1997), who has considered in detail the quantum state of a condensate which, importantly, is assumed to possess broken symmetry.[5] The assumption is also made that the state is prepared slowly, with damping and pumping rates vanishingly small compared to the trap frequencies and collision rates. This means that the condensate remains in thermodynamic equilibrium throughout its preparation. Finally, the atom number distribution is assumed to be sufficiently narrow that the parameters $\tilde{\omega}_0$ and κ, which of course depend on the atom number, can be regarded as constants (evaluated at the mean atom number); in practice, this proves in general to be a very good approximation.

The state of the condensate is then the lowest energy eigenstate of the free energy, defined by

$$\hat{F} = (\hbar\tilde{\omega}_0 - \mu)\hat{a}_0^\dagger \hat{a}_0 + \hbar\kappa \hat{a}_0^\dagger \hat{a}_0^\dagger \hat{a}_0 \hat{a}_0 . \tag{47}$$

Writing the operator $\hat{a}_0$ as the sum of a coherent amplitude and a fluctuation, i.e., setting $\hat{a}_0 = \alpha + \delta\hat{a}_0$ (with α taken for convenience to be real), choosing $\mu = \hbar\tilde{\omega}_0 + 2\hbar\kappa\alpha^2$ (so that the driving term vanishes), and retaining terms up to quadratic order in $\delta\hat{a}_0$, one finds

$$\hat{F} = -\hbar\kappa\alpha^2(\alpha^2 + 1) + \hbar\kappa\alpha^2 \hat{X}^2 , \tag{48}$$

where we have introduced the quadrature operators,

$$\hat{X} = \delta\hat{a}_0 + \delta\hat{a}_0^\dagger, \qquad \hat{Y} = -\mathrm{i}(\delta\hat{a}_0 - \delta\hat{a}_0^\dagger) . \tag{49}$$

This expression suggests that the condensate is in an $\hat{X}$-quadrature eigenstate (Lewenstein and You, 1996b) corresponding to infinite fluctuations in the $\hat{Y}$ quadrature; this plainly unphysical result arises because the chemical potential precisely cancels the $\hat{Y}$-dependence of the free energy. One must, therefore, include terms of higher than quadratic order in $\delta\hat{a}_0$ in order to incorporate at least the leading $\hat{Y}$-dependence in the free energy.

Doing this, and assuming Gaussian statistics, the mean value of the free energy takes the form

$$\begin{aligned} \langle \hat{F} \rangle = {} & (\hbar\tilde{\omega}_0 - \mu)(\alpha^2 + \langle \delta\hat{a}_0^\dagger \delta\hat{a}_0 \rangle) + \hbar\kappa[\alpha^4 + \alpha^2(\langle \delta\hat{a}_0 \delta\hat{a}_0 \rangle + 4\langle \delta\hat{a}_0^\dagger \delta\hat{a}_0 \rangle + \langle \delta\hat{a}_0 \delta\hat{a}_0 \rangle^*) \\ & + \langle \delta\hat{a}_0 \delta\hat{a}_0 \rangle^* \langle \delta\hat{a}_0 \delta\hat{a}_0 \rangle + 2\langle \delta\hat{a}_0^\dagger \delta\hat{a}_0 \rangle^2] . \end{aligned} \tag{50}$$

[5] The phase of the condensate may be defined relative to a much larger "reference condensate." Then, the quantum properties of this relative phase are effectively those of the smaller condensate of interest.

Note that with the assumption of Gaussian statistics, cubic terms of the form $\langle(\delta\hat{a}_0^\dagger)^2\delta\hat{a}_0\rangle$ and $\langle\delta\hat{a}_0^\dagger(\delta\hat{a}_0)^2\rangle$ vanish.

To find values of μ, α, and $\langle\hat{X}^2\rangle$ that minimise the free energy for a fixed mean number of atoms, N, one solves the equations

$$\partial\langle\hat{F}\rangle/\partial\langle\hat{X}^2\rangle = 0, \qquad \partial\langle\hat{F}\rangle/\partial\alpha = 0\,, \tag{51}$$

subject to the constraint

$$\alpha^2 + \langle\delta\hat{a}_0^\dagger\delta\hat{a}_0\rangle \equiv \alpha^2 + \tfrac{1}{4}(\langle\hat{X}^2\rangle + \langle\hat{X}^2\rangle^{-1} - 2) = N\,. \tag{52}$$

Given that $\alpha^2 \gg 1$, one finds

$$\mu = \hbar\tilde{\omega}_0 + \hbar\kappa(2\alpha^2 + \tfrac{3}{2}\langle\hat{X}^2\rangle + \tfrac{1}{2}\langle\hat{X}^2\rangle^{-1} - 2)\,, \tag{53}$$

$$\langle\hat{X}^2\rangle \simeq (1/4\alpha^2)^{1/3} - 1/12\alpha^2 \simeq (1/4\alpha^2)^{1/3}\,. \tag{54}$$

Hence, the inclusion of higher-order terms leads to a finite width of the $\hat{X}$-quadrature distribution. The actual condensate state predicted by this calculation is a strongly *amplitude-squeezed state*,

$$|\alpha, r\rangle = D(\alpha)S(r)|0\rangle\,, \tag{55}$$

where $D(\alpha) = \exp(\alpha\hat{a}_0^\dagger - \alpha^*\hat{a}_0)$ is the coherent displacement operator and $S(r) = \exp\{(r/2)[(\hat{a}_0)^2 - (\hat{a}_0^\dagger)^2]\}$ is the squeezing operator (see, e.g., Walls and Milburn, 1994). In Fig. 10, the Wigner function for this state is compared with a coherent state of the same amplitude and with an $\hat{X}$-quadrature eigenstate.

The number variance for this state is straightforwardly calculated as

$$(\Delta n)^2 = \langle(\hat{a}_0^\dagger\hat{a}_0)^2\rangle - \langle\hat{a}_0^\dagger\hat{a}_0\rangle^2 \simeq \tfrac{3}{2}(\tfrac{1}{4})^{1/3}\alpha^{4/3}\,, \tag{56}$$

and corresponds to an amplitude-squeezed state with the *minimum possible particle number fluctuations*, i.e., to the state (55) with $r \simeq (1/6)\ln(4\alpha^2)$.

In the model outlined above, only the condensate mode is taken into account. Dunningham (1997) has also considered corrections to the above results due to the inclusion of noncondensate modes, but finds these to be negligible for physically reasonable situations (e.g., for the experimental conditions of Anderson et al., 1995). More important, however, are corrections to the state of the condensate produced by a more careful treatment of the condensate-mode cubic terms in the free energy [i.e., terms of the form $(\delta\hat{a}_0^\dagger)^2\delta\hat{a}_0$ and $\delta\hat{a}_0^\dagger(\delta\hat{a}_0)^2$]; that is, by going beyond the Gaussian approximation. Using perturbation theory, Dunningham (1997) shows that, in terms of Wigner function contours, the effect of these terms is a “bending” of the amplitude-squeezed state derived above along the contour of the number state with the same mean number of atoms. This effect is illustrated in Fig. 11, and the state so-produced is referred to as a number-squeezed state.

2.8.3. *Quantum phase diffusion: collapses and revivals of Bose–Einstein condensates*

In a study of the macroscopic wave function for relatively small samples of atoms (i.e., a few thousand atoms), Wright et al. (1996, 1997) find that the wave function actually exhibits the phenomena of *collapses* and *revivals* (see also Lewenstein and You, 1996b; Castin and Dalibard,

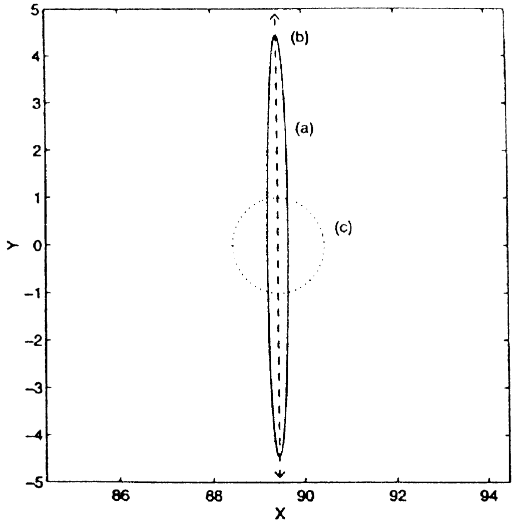

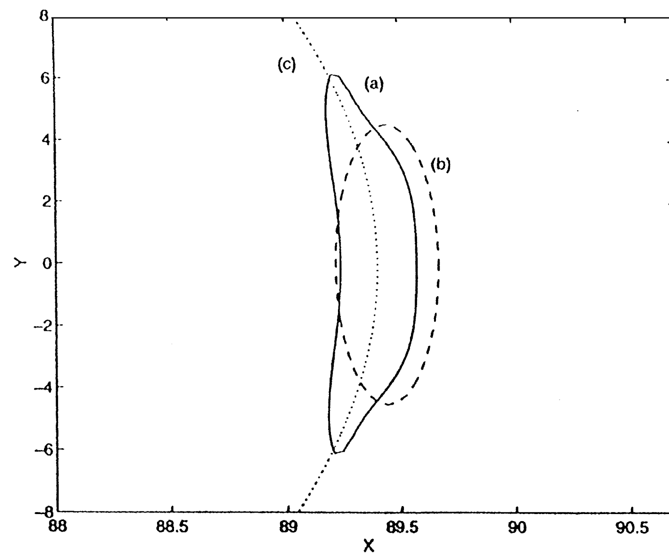

Fig. 10. Wigner function contours (one standard deviation) for a condensate of 2000 atoms: (a) Gaussian-approximation amplitude-squeezed state. (b) X-quadrature eigenstate (neglecting terms of higher of quadratic order). (c) Coherent state of same amplitude. From Dunningham (1997).

Fig. 11. Comparison of Wigner function contours for a condensate of 2000 atoms: (a) Second-order perturbation result (i.e., including effect of cubic terms in the free energy) – number-squeezed state. (b) Amplitude-squeezed state (Gaussian approximation). (c) Number state $|n = 2000\rangle$. From Dunningham (1997).

1997), i.e. $\langle \hat{\Psi}(\boldsymbol{r}, t) \rangle$ (periodically) reduces to zero and then at a later time returns to some finite amplitude. They consider the state vector of the system to be a wavepacket of states of fixed atom number n, with expansion coefficients c_n such that the probability distribution $|c_n|^2$ is sharply peaked around a mean number N. Assuming, in particular, a coherent state description (i.e., a Poissonian distribution) (Barnett et al., 1996), for which the variance $\Delta n = N^{1/2}$, they find the period for the revivals to be

$$T_N \simeq (5/\omega_\perp)(d_\perp/\lambda a)^{2/5} N^{3/5} , \tag{57}$$

while the collapse time depends on the variance of the initial distribution and is approximated by

$$t_{\mathrm{coll}} \simeq T_N/\Delta n . \tag{58}$$

These collapses and revivals follow straightforwardly from the single-mode model, as we now show. From the Hamiltonian

$$\hat{H} = \hbar\tilde{\omega}_0 \hat{a}_0^\dagger \hat{a}_0 + \hbar\kappa \hat{a}_0^\dagger \hat{a}_0^\dagger \hat{a}_0 \hat{a}_0 , \tag{59}$$

the Heisenberg equation of motion for the condensate mode operator follows as

$$\dot{\hat{a}}_0(t) = -\frac{\mathrm{i}}{\hbar}[\hat{a}_0, \hat{H}] = -\mathrm{i}(\tilde{\omega}_0 \hat{a}_0 + 2\kappa \hat{a}_0^\dagger \hat{a}_0 \hat{a}_0) , \tag{60}$$

for which a solution can be written in the form

$$\hat{a}_0(t) = \exp[-\mathrm{i}(\tilde{\omega}_0 + 2\kappa \hat{a}_0^\dagger \hat{a}_0)t]\hat{a}_0(0) . \tag{61}$$

Writing the initial state of the condensate, $|i\rangle$, as a superposition of number states,

$$|i\rangle = \sum_n c_n |n\rangle , \tag{62}$$

the expectation value $\langle i|\hat{a}_0(t)|i\rangle$ is given by

$$\begin{aligned}\langle i|\hat{a}_0(t)|i\rangle &= \sum_n c_{n-1}^* c_n \sqrt{n} \exp\{-\mathrm{i}[\tilde{\omega}_0 + 2\kappa(n-1)]t\} \\ &= \sum_n c_{n-1}^* c_n \sqrt{n} \exp\left(-\frac{\mathrm{i}\mu t}{\hbar}\right) \exp\{-\mathrm{i}[2\kappa(n-N)t]\} ,\end{aligned} \tag{63}$$

where the relationship

$$\mu = \hbar\tilde{\omega}_0 + 2\hbar\kappa(N-1) , \tag{64}$$

has been used [this expression for μ uses the approximation $\langle n^2\rangle = N^2 + (\Delta n)^2 \approx N^2$]. The factor $\exp(-\mathrm{i}\mu t/\hbar)$ describes the deterministic motion of the condensate mode in phase space and can be removed by transforming to a rotating frame of reference, allowing one to write

$$\langle i|\hat{a}_0(t)|i\rangle = \sum_n c_{n-1}^* c_n \sqrt{n} \{\cos[2\kappa(n-N)t] - \mathrm{i}\sin[2\kappa(n-N)t]\} . \tag{65}$$

This expression consists of a weighted sum of trigonometric functions with different frequencies. With time, these functions alternately "dephase" and "rephase," giving rise to collapses and revivals, respectively, in analogy with the behaviour of the Jaynes–Cummings Model of the interaction of a two-level atom with a single electromagnetic field mode (Eberly et al., 1980). The period of the revivals follows directly from (65) as $T = \pi/\kappa$; evaluating κ explicitly yields a result for T in close agreement with Eq. (57) (a small difference arises from the single-mode approximation). The collapse time can be derived by considering the spread of frequencies for particle numbers between $n = N + (\Delta n)$ and $n = N - (\Delta n)$, which yields $(\Delta\Omega) = 2\kappa(\Delta n)$; from this one estimates $t_{\mathrm{coll}} \simeq 2\pi/(\Delta\Omega) = T/(\Delta n)$, as before.

During the collapse, it is clear that $\langle\hat{\Psi}(\boldsymbol{r},t)\rangle \to 0$, and hence the condensate wave function cannot be identified with the order parameter at that time [note that in the thermodynamic limit, collapses and revivals become irrelevant and $\Phi(\boldsymbol{r},t) = \langle\hat{\Psi}(\boldsymbol{r},t)\rangle$ is a suitable identification (Wright et al., 1996, 1997)]. ODLRO, and hence BEC, does however persist, as the one-particle reduced density operator is given by

$$\rho_1(\boldsymbol{r},\boldsymbol{r}',t) = \langle\hat{\Psi}^\dagger(\boldsymbol{r},t)\hat{\Psi}(\boldsymbol{r}',t)\rangle = N\psi_0^*(\boldsymbol{r})\psi_0(\boldsymbol{r}') , \tag{66}$$

which is of the form (41) with $\Phi(\boldsymbol{r},t) = N^{1/2}\psi_0(\boldsymbol{r})$.[6]

---

[6] An interesting comparison can be made with the properties of a two-dimensional Bose gas below the critical temperature for the so-called Kosterlitz–Thouless transition (to two-dimensional superfluidity) (see, e.g., Griffin et al., 1995); phase fluctuations preclude the existence of a global order parameter although (short range) algebraic off-diagonal order occurs.

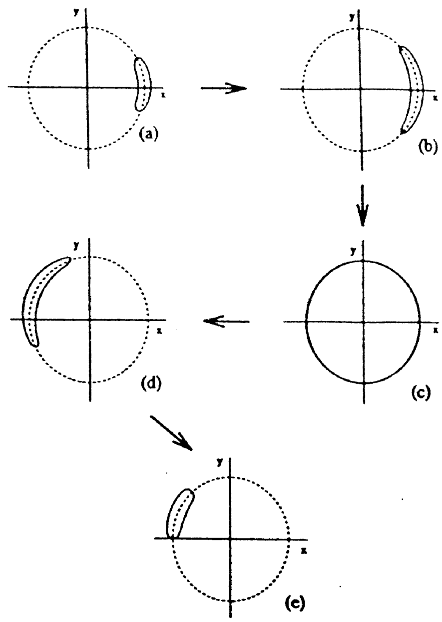

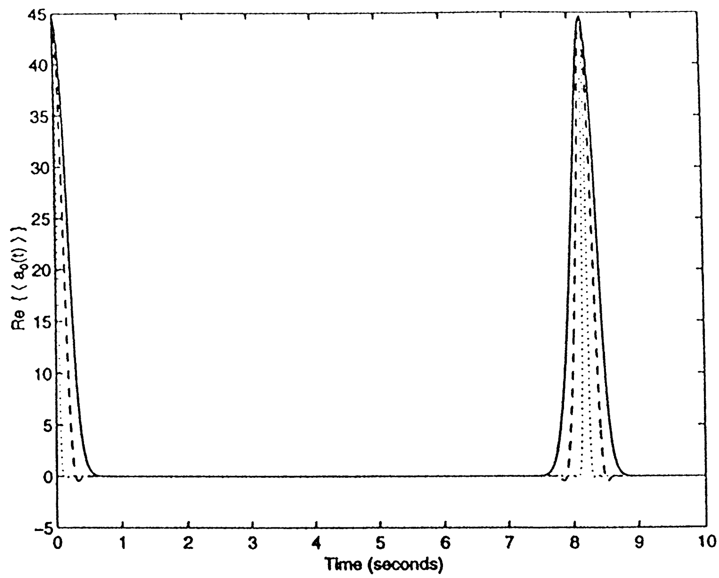

Fig. 12. Schematic representation of collapses and revivals of the condensate wave function. As time proceeds, the phase of the initial state shown in (a) begins to diffuse until, at time $t_{\rm coll}$, shown in (c), the phase is completely smeared out. After a further period of time, different components of the state come back into phase with one another, producing a revival, as in (e). Note that the mean phase of the revived state need not be the same as that of the initial state. From Dunningham (1997).

Fig. 13. Diagram of collapses and revivals of $\mathrm{Re}\{\langle \hat{a}_0(t)\rangle\}$ for a number-squeezed state (solid line), an amplitude-squeezed state (Gaussian approximation) (dashed line), and a coherent state (dotted line) with the same mean number of atoms, $N = 2000$. From Dunningham (1997).

The mechanism of collapse and revival is depicted in a phase-space representation in Fig. 12. From the expression $t_{\rm coll} \simeq T/(\Delta n)$, it follows that the time taken for collapse is vitally dependent on the statistics of the condensate; in particular, on the "width" of the initial distribution. This dependence is illustrated in Fig. 13, where the real part of $\langle \hat{a}_0(t)\rangle$ is plotted as a function of time for three different initial states: (i) a coherent state, (ii) an amplitude-squeezed state (as derived in the previous section under the assumption of Gaussian statistics), and (iii) a number-squeezed state (of the sort shown in Fig. 11). The mean number of atoms is chosen in each case to be $N = 2000$, and the calculations assume a condensate of rubidium atoms in an isotropic harmonic trap of frequency $\omega/2\pi = 60$ Hz.

The timescales of the collapses show clear differences; the more strongly number-squeezed the state is, the longer its collapse time. The revival times, however, are independent of the degree of number squeezing and depend only on the interaction parameter, κ. For the example shown, the revival time is approximately 8 s, which, significantly, lies within the typical lifetime of the experimental condensate (10–20 s).

A likely scheme for the experimental detection of collapses and revivals would actually involve a pair of condensates between which a relative phase is first established via a suitable preparation/measurement process. After a period of free evolution, the re-measured relative phase should reveal the effects of wave function collapse or revival. Such a configuration and measurements are discussed in detail in Section 5 in the context of broken gauge symmetry.

Finally, Imamoḡlu et al. (1997) have recently considered the dependence of the collapse and revival effect on the nature of the trap potential, the dimensionality of the condensate, and the atom number fluctuations. In particular, given a trap potential of the form $V_{\mathrm{trap}}(r) = ar^{\eta}$, a dimensionality D of the condensate, and an initial dispersion $\sigma(N)$ of the atom number N, they find that if $\eta > D$ and the dispersion $\sigma(N) \propto N^{1/2}$, then the collapse time goes to *zero* in the limit $N \to \infty$ and revivals *do not occur*. This finding evidently sets a fundamental limit on the existence of a well-defined condensate phase.

2.8.4. Localised fluctuations: a stochastic nonlinear Schrödinger equation

The works described above were concerned with phase diffusion arising from fluctuations in the number of atoms and the action of the mean-field nonlinearity. Using a generalisation of the phase-space methods of quantum optics (see, e.g., Gardiner, 1991), Olsen et al. (1997) have derived a pair of equations[7] that incorporate, in addition to the mean-field nonlinearity, *stochastic* terms that model *localised* density and phase fluctuations. These stochastic nonlinear Schrödinger equations take the form (for one spatial dimension)

$$i\hbar\frac{\partial \Psi_1(x,t)}{\partial t} = \mathscr{L}\Psi_1(x,t) + NU_0\Psi_2^*(x,t)\Psi_1(x,t)^2 + (iU_0)^{1/2}\eta_1(x,t)\Psi_1(x,t)\,, \tag{67}$$

$$i\hbar\frac{\partial \Psi_2(x,t)}{\partial t} = \mathscr{L}\Psi_2(x,t) + NU_0\Psi_1^*(x,t)\Psi_2(x,t)^2 + (iU_0)^{1/2}\eta_2(x,t)\Psi_2(x,t)\,, \tag{68}$$

where Ψ_1 and Ψ_2 are conjugate *in the mean*, $\mathscr{L} \equiv -(\hbar^2/2m)\partial^2/\partial x^2 + V_{\mathrm{trap}}(x)$, and the noise sources $\eta_{1,2}(x,t)$ are real, Gaussian (with zero mean), and delta-correlated in space and time, $\overline{\eta_i(x,t)\eta_j(x',t')} = \delta_{ij}\delta(x-x')\delta(t-t')$.

Using these equations, Olsen et al. (1997) are able to compute correlation functions such as

$$\langle \hat{\Psi}^\dagger(x,t)\hat{\Psi}(x',t')\rangle = \overline{\Psi_2^*(x,t)\Psi_1(x',t')}\,. \tag{69}$$

More particularly, computing the quantity

$$\overline{\int dx\, \Psi_2^*(x,t)\Psi_1(x,0)} \tag{70}$$

in the stationary limit provides Olsen et al. (1997) with the coherence time of the condensate. For an initial Poissonian number distribution they find, at least for relatively short times (of the order of a trap period), a correlation function and decoherence rate very similar to that computed, for example, by Lewenstein and You (1996b) (who take into account only the fluctuations in the initial atom number).

[7] This pair of equations characterises a so-called *positive-P* distribution (see Gardiner, 1991), in which the number of variables is doubled in order to yield a Fokker–Planck equation for the distribution that has a positive-definite diffusion matrix.

2.8.5. Tomography of atom fields: reconstruction of the quantum state of a condensate

Given that the true quantum state of a Bose–Einstein condensate constitutes an open and very interesting subject, it is natural to consider ways in which one might reconstruct this state via measurements of some sort. Following the approach of optical homodyne tomography (for a review and references, see Leonhardt and Paul, 1995), employed for the measurement of the state of a mode of the electromagnetic field, Bolda et al. (1997) (see also Walser, 1997; Mancini and Tombesi, 1997) have proposed a scheme for the tomographic reconstruction of the quantum state of a condensate using an arrangement composed of an atomic beam splitter and an ideal atom counter.[8]

Specifically, they assume that a condensate with a fixed number of atoms is first prepared in the *two-mode* quantum state

$$\rho = \sum_a p_a |\psi_a\rangle\langle\psi_a| , \tag{71}$$

where

$$|\psi_a\rangle = \sum_{n=0}^{N} c_{n,a} |N-n\rangle_1 \otimes |n\rangle_2 . \tag{72}$$

These modes could, for example, correspond simply to two different hyperfine states. A phase shift ϕ is applied to one of the modes, after which the two modes are recombined at a lossless atomic beam splitter of transmission $\cos^2(\theta)$. As a result of these actions, the density matrix is transformed to ρ_{out}, given by

$$\rho_{\mathrm{out}} = U(\theta,\phi)^\dagger \rho U(\theta,\phi) , \tag{73}$$

with

$$U(\theta,\phi) = \exp[\mathrm{i}\theta(\hat{a}_1^\dagger \hat{a}_2 \mathrm{e}^{\mathrm{i}\phi} + \hat{a}_2^\dagger \hat{a}_1 \mathrm{e}^{-\mathrm{i}\phi})] \tag{74}$$

(note that atom interactions are neglected – these would result in a mixing of the modes). Finally, the number of atoms in one of the output modes of the beamsplitter is counted with a detector. The probability of m counts at the detector, for the phase shift ϕ, is

$$P_m(\phi) = \langle m|U(\theta,\phi)^\dagger \rho U(\theta,\phi)|m\rangle . \tag{75}$$

Repeating this process for many different phase shifts, a sequence of probability distributions $P_m(\phi)$ can be accumulated from which a tomographic reconstruction of the density matrix ρ is possible (provided the beamsplitter is *not* balanced, i.e., $\theta \neq \pi/4$). Bolda et al. (1997) have numerically simulated such a procedure for a small number of atoms, showing that the technique can successfully reconstruct a sample state. An example is shown in Fig. 14, where original and reconstructed density matrix elements are compared for a state corresponding to a projection of coherent states for modes 1 and 2 onto the subspace with fixed total number $N = 49$ (Mølmer, 1997). The reconstruction is most accurate, in both magnitude and phase, for elements close to the

[8] Note that the scheme of Bolda et al. (1997) does not involve mixing of the condensate with an independent "local oscillator" field as is the case in optical homodyne tomography.

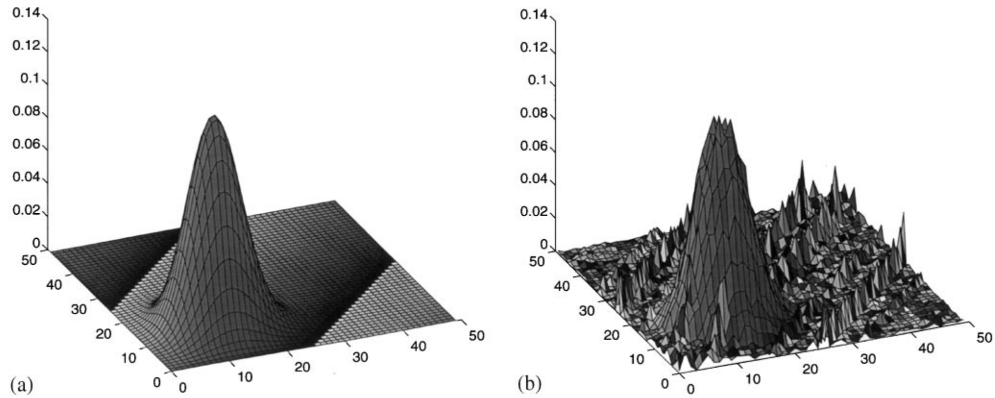

Fig. 14. Density matrix elements of (a) the original state and (b) the reconstructed state, in the number-state basis. Magnitude is height and phase is represented by the shading. From Bolda et al. (1997).

diagonal. Bolda et al. (1997) also show that errors can be estimated before data collection and minimised by choosing an appropriate beamsplitter transmission if some qualitative features are known about the initial state.

In practice, such a scheme might be realised as a variation of the output-coupling experiment of Mewes et al., 1997; two radiofrequency fields coupling to two different (untrapped) hyperfine states could produce the two-mode state from an initial condensate. A relative phase shift between the two modes could be produced with a magnetic field, after which a second set of radiofrequency pulses would recombine the modes in the manner of a beamsplitter.

3. Elementary excitations of a trapped Bose–Einstein condensate

The Bogoliubov theory for the elementary excitations of a dilute Bose gas, described in Appendix A, was derived for the case of a homogeneous system. However, in the recent experiments demonstrating Bose–Einstein condensation, trapping potentials have played an integral part and so the earlier theory of the elementary excitations has had to be revised in order to correspond more directly to the experimental situation. Jin et al. (1996a) at JILA and Mewes et al. (1996b) at MIT have now observed collective excitations of a confined Bose–Einstein condensate by applying small time-dependent perturbations to the trapping potential.[9] For an ideal gas the frequencies of the excitations induced are simply multiples of the trap frequencies; for an interacting condensate, however, deviations from these frequencies are expected and were indeed observed in these experiments.

[9] Walsworth and You (1997) have also proposed an interesting scheme for the selective generation of excitations in which auxiliary magnetic fields are tailored (spatially and temporally) to excite the condensate into quasiparticle (excited) states with the desired symmetry.

3.1. Collective excitations of a trapped Bose–Einstein condensate (at $T = 0$)

A large number of theoretical analyses of the elementary excitations of a confined interacting condensate have recently appeared; these have, in large part, been based on zero-temperature mean-field theory, in the form of the GP equation. For the case $T = 0$, we divide these analyses into two categories based on direct numerical simulation and approximate analytical solutions, respectively.

3.1.1. Numerical results

3.1.1.1. Linear response regime. We begin with the work of Edwards et al. (1996b) and Ruprecht et al. (1996), who have applied linear response theory (solving the response equations numerically), as well as direct numerical integration, to the modified GP equation,

$$i\hbar\frac{\partial\Psi(\mathbf{r},t)}{\partial t} = \left[-\frac{\hbar^2}{2m}\nabla^2 + V_{\rm trap}(\mathbf{r}) + NU_0|\Psi(\mathbf{r},t)|^2\right]\Psi(\mathbf{r},t) + [f_+(\mathbf{r})e^{-i\omega_p t} + f_-(\mathbf{r})e^{i\omega_p t}]\Psi(\mathbf{r},t)\,. \tag{76}$$

Here, $f_\pm(\mathbf{r})$ are the spatially dependent amplitudes of the perturbation at the angular frequency ω_p. In the linear-response approach, a trial function of the form

$$\Psi(\mathbf{r},t) = e^{-i\mu t/\hbar}[\psi_g(\mathbf{r}) + u(\mathbf{r})e^{-i\omega_p t} + v(\mathbf{r})e^{i\omega_p t}] \tag{77}$$

is substituted into the above equation. Retaining only terms to first-order in $u(\mathbf{r})$, $v(\mathbf{r})$, and $f_\pm(\mathbf{r})$, and equating like powers of $e^{\pm i\omega_p t}$ yields the linear response equations

$$[\mathscr{L} - (\mu + \hbar\omega_p) + 2NU_0|\psi_g(\mathbf{r})|^2]u(\mathbf{r}) + NU_0\psi_g(\mathbf{r})^2 v(\mathbf{r}) = -f_+(\mathbf{r})\psi_g(\mathbf{r})\,, \tag{78}$$

$$[\mathscr{L} - (\mu - \hbar\omega_p) + 2NU_0|\psi_g(\mathbf{r})|^2]v(\mathbf{r}) + NU_0\psi_g^*(\mathbf{r})^2 u(\mathbf{r}) = -f_-(\mathbf{r})\psi_g(\mathbf{r})\,, \tag{79}$$

where $\mathscr{L} \equiv [-(\hbar^2/2m)\nabla^2 + V_{\rm trap}(\mathbf{r})]$ and $\psi_g(\mathbf{r})$ is determined from

$$[\mathscr{L} + NU_0|\psi_g(\mathbf{r})|^2]\psi_g(\mathbf{r}) = \mu\psi_g(\mathbf{r})\,. \tag{80}$$

The linear response equations are solved using an expansion in the condensate normal modes, determined from

$$[\mathscr{L} - (\mu + \hbar\omega_\lambda) + 2NU_0|\psi_g(\mathbf{r})|^2]u_\lambda(\mathbf{r}) + NU_0\psi_g(\mathbf{r})^2 v_\lambda(\mathbf{r}) = 0\,, \tag{81}$$

$$[\mathscr{L} - (\mu - \hbar\omega_\lambda) + 2NU_0|\psi_g(\mathbf{r})|^2]v_\lambda(\mathbf{r}) + NU_0\psi_g^*(\mathbf{r})^2 u_\lambda(\mathbf{r}) = 0\,, \tag{82}$$

which simply define the quasi-particle modes and frequencies of a trapped (non-uniform) condensate in the Bogoliubov approximation (Fetter, 1972). For the case of a homogeneous condensate [i.e., $V_{\rm trap}(\mathbf{r}) = 0$], $u(\mathbf{r})$ and $v(\mathbf{r})$ are plane waves and the quasiparticle excitation frequency ω_λ has the continuous Bogoliubov spectrum derived in the appendix. For a trapped condensate, however, the excitations are confined and ω_λ has a discrete spectrum. A transient disturbance [i.e., $f_\pm(\mathbf{r})$] at a frequency close to one of the resonances ω_λ will produce a response (in free oscillation after the disturbance) predominantly at the frequency ω_λ.

Numerically solving Eqs. (80)–(82) for the experimental configuration of Jin et al. (1996a), Edwards et al. (1996b) (see also the work of You et al., 1997) have obtained frequencies for the elementary excitations in very good agreement with the experimental observations. Further details are given in the following section in a comparison with approximate analytical analyses of condensate excitations. We note that other numerically based studies of condensate excitations have been performed by Singh and Rokhsar (1996), who also used a generalised (i.e., nonuniform condensate) Bogoliubov approach but employed variationally determined condensate wave functions [for $\psi_g(\boldsymbol{r})$], and by Esry (1997), who has followed techniques familiar in atomic-structure calculations (e.g., Hartree–Fock and random-phase approximations) to obtain the elementary excitation energies for the experimentally realised condensates.

Also using the linear response approach outlined above, Dodd et al. (1997) have calculated the excitation spectrum of *vortex states* of trapped Bose–Einstein condensates. The spectra obtained can differ significantly from those of the ground state, suggesting a useful technique for the detection and study of vortex states.

3.1.1.2. Nonlinear regime. To go beyond the linear response regime, Ruprecht et al. (1996) have solved the time-dependent, driven GP equation (76) by direct numerical integration. With increasing strength of the perturbation, the nonlinear response of the condensate gives rise to the generation of harmonics of the driving frequency and frequency mixing between the normal modes. The origin of this nonlinear response is of course the nonlinear mean-field potential; a perturbation of the overall potential causes a time-dependent change in the wave function, which in turn causes a change in the nonlinear potential, and so on. The nonlinear phenomena that result are matter–wave analogs of the corresponding effects arising in conventional nonlinear optics. Further numerical investigations along these lines have been performed by Smerzi and Fantoni (1997), who also use the time-dependent GP equation, and by Dalfovo et al. (1997a, 1997b), who use hydrodynamic equations [derived from the GP equation – see below and Stringari (1996)] in the Thomas–Fermi approximation. Some experimental results relevant to this regime have been obtained (Jin et al., 1996a; Mewes et al., 1996b) and Dalfovo et al. (1997b) and Smerzi and Fantoni (1997) find some agreement with these results (in particular, with the mode frequencies), although more detailed comparison will evidently be necessary.

3.1.2. Analytical results

To obtain some approximate analytical results for the properties of the elementary excitations of an inhomogeneous condensate, Stringari (1996) has recently developed a relatively simple approach based on solutions to the linearised GP equation in the Thomas–Fermi approximation. In this approach, one begins with equations of motion for the density,

$$\rho(\boldsymbol{r},t) = N|\Psi(\boldsymbol{r},t)|^2 \tag{83}$$

and velocity field,

$$\boldsymbol{v}(\boldsymbol{r},t) = N\frac{\Psi^*(\boldsymbol{r},t)\nabla\Psi(\boldsymbol{r},t) - \nabla\Psi^*(\boldsymbol{r},t)\Psi(\boldsymbol{r},t)}{2\mathrm{i}m\rho(\boldsymbol{r},t)}, \tag{84}$$

which are derived from the time-dependent GP equation (9) and take the forms

$$\frac{\partial}{\partial t}\rho + \nabla\cdot(\boldsymbol{v}\rho) = 0\,, \tag{85}$$

$$m(\partial/\partial t)\boldsymbol{v} + \nabla[\delta\mu + \tfrac{1}{2}m\boldsymbol{v}^2] = 0\,, \tag{86}$$

respectively, where

$$\delta\mu = V_{\mathrm{ext}} + (4\pi\hbar^2 a/m)\rho - (\hbar^2/2m\sqrt{\rho})\nabla^2\sqrt{\rho} - \mu \tag{87}$$

is the change in chemical potential with respect to its ground state value, μ. Note that these equations have the general structure of the dynamic equations of superfluids at zero temperature.

The chemical potential μ is fixed by the normalisation of the ground state density, $\rho_0(\boldsymbol{r})$, which can be approximated by the Thomas–Fermi form

$$\rho_0(\boldsymbol{r}) = (m/4\pi\hbar^2 a)[\mu - V_{\mathrm{trap}}(\boldsymbol{r})]\,, \tag{88}$$

[for $\mu \geq V_{\mathrm{trap}}(\boldsymbol{r})$; $\rho_0(\boldsymbol{r}) = 0$ elsewhere], provided the number of atoms in the condensate is sufficiently large that the kinetic energy is negligible compared to the trap potential energy and interparticle interaction energy. In keeping with this approximation, one also neglects the kinetic energy pressure terms in Eqs. (85)–(87). Linearising Eqs. (85) and (86), and assuming for simplicity an isotropic harmonic oscillator potential, $V_{\mathrm{trap}}(\boldsymbol{r}) = \omega_0^2 r^2/2m$, one can derive the equation

$$\omega^2\delta\rho = -\tfrac{1}{2}\omega_0^2\nabla\cdot(R^2 - r^2)\nabla\delta\rho\,, \tag{89}$$

where $\delta\rho(\boldsymbol{r})\exp(-\mathrm{i}\omega t) = \rho(\boldsymbol{r},t) - \rho_0(\boldsymbol{r})$, and $R^2 = 2\mu/m\omega_0^2$ defines the boundary at which the density vanishes in the Thomas–Fermi model. Note that one can rewrite Eq. (89) in the form $\omega^2\delta\rho = -\nabla\cdot[c(r)^2\nabla\delta\rho]$, where $c(r) = [4\pi\hbar^2 a\rho_0(r)/m^2]^{1/2}$ is the *local speed of sound* (Bogoliubov, 1947; Lee et al., 1957).

The solutions to Eq. (89), in the interval $0 \leq r \leq R$, are given by

$$\delta\rho(\boldsymbol{r}) = P_l^{(2n)}(r/R)r^l Y_{lm}(\theta,\phi)\,, \tag{90}$$

where $\{n,l,m\}$ are quantum numbers classifying the normal modes of the condensate, with n the radial quantum number and l and m the quantum numbers for the total angular momentum and its axial projection, respectively. The functions $P_l^{(2n)}(x)$ are given by $P_l^{(2n)}(x) = 1 + \alpha_2 x^2 + \cdots + \alpha_{2n}x^{2n}$ and satisfy the orthogonality condition

$$\int_0^1 \mathrm{d}x\, P_l^{(2n)}(x)P_l^{(2n')}(x)x^{2l+2} = 0\,, \tag{91}$$

if $n \neq n'$. The coefficients α_{2k} satisfy the recurrence relation $\alpha_{2k+2} = -\alpha_{2k}(n-k) \times(2l+2k+3+2n)/(k+1)(2l+2k+3)$. Most importantly, the frequencies of the normal modes are given by the relatively simple form

$$\omega(n,l) = \omega_0(2n^2 + 2nl + 3n + l)^{1/2}\,, \tag{92}$$

which is to be compared with the result one obtains in the absence of interparticle interactions, $\omega_{\mathrm{HO}} = \omega_0(2n + l)$.

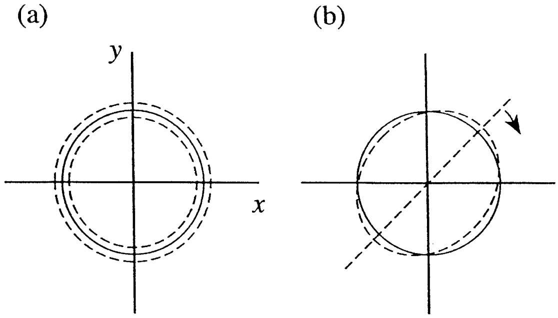

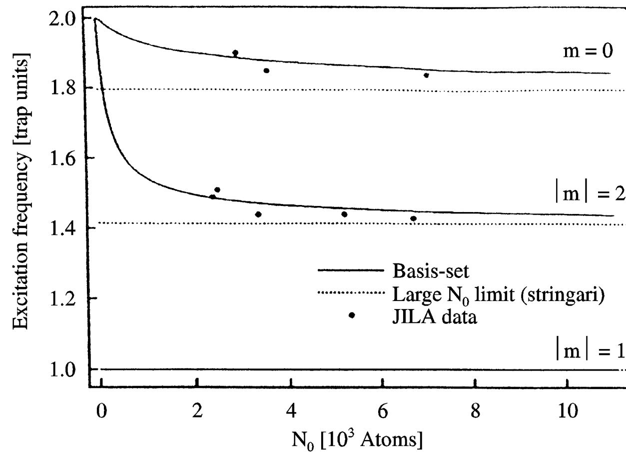

Fig. 15. Schematic of the (a) $m=0$ and (b) $m=2$ modes of excitation of an axially-symmetric trap (as in the JILA experiment). The solid lines represent the contours of the unperturbed condensate.

Fig. 16. Comparison of JILA excitation frequency data with mean-field theory predictions. From Edwards et al. (1996b).

The above results were also generalised by Stringari to allow for effects of kinetic energy pressure and for anisotropic trapping potentials (as exist in the experiments). When compared with the frequencies of the excitation modes observed in the experiments (at very low temperatures, with essentially pure condensate), the relatively simple analytic expressions derived as above give remarkably good agreement. For example, in the JILA experiment the $m=0$ (breathing) and $m=2$ (rotating ellipsoidal perturbation) modes,[10] depicted schematically in Fig. 15, were observed with frequencies $1.84\omega_\perp$ and $1.43\omega_\perp$, respectively, for a condensate of approximately $N=4500$ atoms, while the approximate (large-N) analytic results of Stringari, given by ($\lambda=\omega_z/\omega_\perp$)

$$\omega^2(m=0)=\omega_\perp^2\left(2+\tfrac{3}{2}\lambda^2-\tfrac{1}{2}\sqrt{9\lambda^4-16\lambda^2+16}\right), \tag{93}$$

$$\omega^2(|m|=2)=2\omega_\perp^2\,, \tag{94}$$

yield $1.8\omega_\perp$ and $1.4\omega_\perp$ (note that for a non-interacting condensate a frequency of $2\omega_\perp$ would be observed for both modes). A comparison of theory and experiment is shown in Fig. 16, where the frequencies of the $m=0$ and $m=2$ modes are shown as a function of effective interaction strength (i.e., number of condensate atoms). Theoretical curves are plotted for the mean-field numerical approach of Edwards et al. (1996b) and for the large-N limit of Stringari.

Alternative, and similarly successful, approaches to the analytical study of excitation frequencies have also been provided by Fetter (1996), who has employed variational condensate wave functions in the generalised Bogoliubov approach [see also Fetter and Rokhsar (1998), where the basic

[10] Because of the cylindrical symmetry of the trap, the modes can be labelled by the azimuthal angular quantum number m.

equivalence between this approach and the hydrodynamic approach outlined above is discussed], and by Pérez-García et al. (1996, 1997), who also employed a variational technique (using Gaussian trial wave functions) to analyse the time-dependent GP equation. Kagan et al. (1996) (see also Kagan et al., 1997a) and Castin and Dum (1996) have used scaling transformations to study the same equation in the context of collective excitations. This latter approach has been used by Dalfovo et al. (1997a) (but starting from the hydrodynamic equations) to consider the nonlinear regime of excitation and to examine such effects as mode coupling and harmonic generation, which have also been considered by Graham et al. (1998a).

Other analytical works modifying and generalising the approach and results of Stringari have been furnished by Wu and Griffin (1996), who have quantised the hydrodynamic model, and by Fliesser et al. (1997) and Öhberg et al. (1997), who have examined in more detail the derivation of approximate analytical expressions for the excitation energies. Meanwhile, Marinescu and Starace (1997) have derived approximate analytic results for the excitation spectrum in the weakly interacting, low-density limit (i.e., for small $N < 100$), where the Thomas–Fermi approximation breaks down.

To conclude this section, we note that an additional observation made by Jin et al. (1996a) and by Mewes et al. (1996b) was of the *decay* of the collective excitations in real time. In both experiments, this decay was evident even well below the critical temperature, such that thermal excitations should not have been significant. Theoretical proposals for the mechanism behind the decay of collective excitations of a trapped condensate at $T \approx 0$, and comparisons with experiments, have only recently appeared and we discuss them below.

3.2. Propagation of sound in a Bose–Einstein condensate

The propagation of sound in a magnetically trapped Bose–Einstein condensate has been studied experimentally by Andrews et al. (1997a), who used the optical dipole force of a focused off-resonant laser beam to excite localised density perturbations (i.e., much smaller than the size of the condensate) in their sodium condensate, which then propagate at the speed of sound. The large aspect ratio of their anisotropic trap results in elongated cigar-shaped condensates and by the technique of sequential nondestructive phase-contrast imaging (Andrews et al., 1996) they were able to directly observe this propagation along the long axis of the condensate (the axial direction). By adjusting the radial confinement of the condensate, the dependence of the speed of sound on the density could be studied; it was found to agree quite closely with the simple result

$$c = \sqrt{4\pi\hbar^2 a\rho_0(0)/m^2} \tag{95}$$

as derived earlier, but with $\rho_0(0)$ the maximum (central) density of the condensate.

As opposed to the earlier studies of collective excitations, the localised perturbations induced by the laser light correspond to a coherent superposition of many modes. The propagating wave packets were observed to disperse, as one might expect from either dephasing or damping of the modes. The actual variation of the density distribution should also come into play in certain limits and theoretical studies of such effects are underway (Zaremba, 1997; Kavoulakis and Pethick, 1997).

3.3. Decay of collective excitations

As illustrated above, good agreement exists between experiments and zero-temperature mean-field theory for the collective mode spectrum (i.e., excitation frequencies) of a trapped condensate. However, in addition to the mode frequencies, *decay* of the collective excitations has also been observed and measured in the experiments (Mewes et al., 1996b; Jin et al., 1996a,b). Theoretical studies have suggested several mechanisms that may be contributing to this decay.

3.3.1. Dissipative decay of excitations ($T > 0$)

For the initial excitation experiments, it is apparent that a finite noncondensate fraction (arising from a finite temperature) was present. As pointed out by Liu and Schieve (1997), and now elaborated upon by others (Liu, 1997; Pitaevskii and Stringari, 1997; Giorgini, 1997; Fedichev et al., 1998) (see also Plimak et al., 1996), interactions between the condensate excitation and the finite thermal (or normal) fraction are likely to have played a major role in the observed damping of the excitation. These interactions can involve, for example, the absorption of a quantum of (condensate) collective excitation by a thermal excitation to produce another thermal excitation of higher energy (so-called "Landau" damping).

Damping of collective excitations due to such interactions has been studied many years ago, although only for the case of *homogeneous* condensates; for long wavelength excitations (small k), damping rates for low (Hohenberg and Martin, 1965; Popov, 1972) and intermediate (Szépfalusy and Kondor, 1974) temperatures were derived in the forms

$$\gamma = \begin{cases} \dfrac{3\hbar k^5}{640\pi m\rho_0} + \dfrac{3\pi^3 k(k_B T)^4}{40 m\rho_0 c^4} & (T \ll T^*)\,, \\ \dfrac{(k_B T)ak}{\hbar} & (T^* \ll T \ll T_c)\,, \end{cases} \tag{96}$$

where $T^* = (4\pi a\hbar^2\rho_0)/(mk_B)$, with ρ_0 the density and $c = [4\pi a\hbar^2\rho_0/m^2]^{1/2}$ the speed of sound in the condensate. Using these simple expressions, and a modified version to cover the regime around T^*, Liu and Schieve (1997) and Liu (1997) obtain quite good agreement with both the JILA (Jin et al., 1996a,b) and MIT (Mewes et al., 1996b) experiments. Fedichev et al. (1998) have extended the theory to include the effect of the trapping potential (see also Giorgini, 1997) and also obtain reasonable agreement with experiment. Their results do, in addition, suggest that boundary effects should become important in certain regimes of excitation.

3.3.2. Nondissipative collapse of excitations ($T = 0$)

While it would appear that finite temperature effects have played the major role in the decay of the collective excitations observed in experiments thusfar, it is reasonable to assume that the same excitation experiments will be possible at effectively zero temperature (i.e., with pure condensates). Given such conditions, and assuming that the system can be regarded as being closed, a truly dissipative mechanism for decay should no longer exist.

However, following in the spirit of the work of Wright et al. (1996) on collapses and revivals of the condensate wave function (described in Section 2.8.3), Kuklov et al. (1997) have shown that particle number fluctuations in a finite condensate can in principle give rise to *collapses and revivals* of *collective excitations*. In particular, collapse, which mimics decay, can occur as a result of the dependence of the frequency of the collective mode on the particle number, which leads to an inhomogeneous broadening. Kuklov et al. (1997) use a model truncated to two modes, with the mode representing the condensate taken to be in a number eigenstate. It is then assumed that a phase relation between the condensate and an excited state is set up by the modulation of the trap, accompanied by a particle number uncertainty in the condensate proportional to the excited state amplitude.

Pitaevskii (1997) (see also Dalfovo et al., 1997a) has also developed a phenomenological model of collapse and revival of a collective mode focusing on fluctuations in the number of quanta of oscillation of the mode (rather than atom number fluctuations). An effective nonlinearity of the excited mode due to coupling to other modes gives rise to a dispersion of the collective mode frequency within the linear superposition of number states making up, for example, an initial coherent state.[11]

Using a full microscopic approach, Graham et al. (1998a) have analysed and compared both of the above mechanisms; for a spherically-symmetric trap of frequency ω_0, they find that the collapse time scales as

$$\omega_0 t_{\mathrm{coll}} \sim N^{9/5}(a/d_0)^{4/5}/(\Delta N) \tag{97}$$

when the collapse mechanism is particle number uncertainty, and

$$\omega_0 t_{\mathrm{coll}} \sim N^{7/5}(a/d_0)^{2/5}/(\Delta n_\mu) \tag{98}$$

when the collapse mechanism is excitation number uncertainty. Here, $d_0 = (\hbar/m\omega_0)^{1/2}$ and (Δn_μ) is the uncertainty in the number of quanta of oscillation in the excited mode μ; for an initial coherent excited state $(\Delta n_\mu) = \sqrt{E_\mu/\hbar\omega_\mu}$. Numerical estimates of the collapse times using parameters appropriate to the experiments generally give values larger than the experimentally observed damping times (Pitaevskii, 1997; Graham et al., 1998a) and it would seem that the finite temperature effects described in the previous section have been dominant in the experiments performed thusfar. However, the collapse times are sufficiently short (for example, compared to the condensate lifetime) that they should be observable, given that pure ($T = 0$) condensates can be realised. The scalings of the collapse times also suggest that it may be possible to distinguish one mechanism as the dominant cause of collapse.

It should also be noted that a significant enhancement of the nonlinear effects occurs if there exists a mode at or close to a resonance with the *second harmonic* (or higher harmonics) of the excited mode (Graham et al., 1998a; Dalfovo et al., 1997a; Ruprecht et al., 1996). For such a resonance, the transfer of energy from the fundamental mode to the harmonic looks similar, for short times, to a collapse of the fundamental mode.

3.4. Collective excitations of trapped double condensates

As noted in Section 2.7, the dynamics of double condensates are now of considerable interest, given the recent experiment of Myatt et al. (1997). Following on from the analytical work of Stringari presented above, Graham and Walls (1998) have analysed collective excitations of binary

[11] A careful numerical study by Smerzi and Fantoni (1997) of the Gross–Pitaevskii equation with a time-dependent potential, modelling the experiment of Jin et al. (1996a), has also explicitly demonstrated a relaxation mechanism due to coupling between different modes of oscillation. Kagan et al. (1997a) have also pointed to chaotic evolution arising from such coupling as a mechanism for relaxation.

mixtures of Bose–Einstein condensates (with positive scattering lengths and interaction parameters satisfying $U_1 > 0$, $U_2 > 0$, and $U_1 U_2 - U_{12}^2 > 0$) via linearisation of the coupled time-dependent GP equations [Goldstein and Meystre (1997) have used a similar approach to study excitations in a homogeneous two-component condensate].

In general, the spectrum of collective excitations of the total system depends on the details of the geometry of the interphase boundaries (Ho and Shenoy, 1996), and solutions of the coupled equations can only be obtained numerically. However, for the special case of a pure binary-phase condensate (i.e., no interphase boundaries exist) in a spherically symmetric trap confining the two condensates at frequencies ω_1 and ω_2,[12] the mode spectrum can be determined analytically in the long-wavelength and Thomas–Fermi approximations. Its dependence on the radial and angular momentum quantum numbers n and l is the same as in the case of a single-component mixture,

$$\omega_{\pm} = \omega_{\mathrm{b}\pm}\sqrt{2n^2 + 2nl + 3n + l}\,, \tag{99}$$

but the prefactor $\omega_{\mathrm{b}\pm}$ is no longer simply the trap frequency; instead, it is given by

$$\omega_{\mathrm{b}\pm}^2 = \frac{1}{2(a_1 a_2 - a_{12}^2)}\{\omega_1^2 a_2(a_1 - a_{12}) + \omega_2^2 a_1(a_2 - a_{12}) \pm \sqrt{\mathscr{P}}\}\,, \tag{100}$$

with

$$\mathscr{P} = [\omega_1^2 a_2(a_1 + a_{12}) - \omega_2^2 a_1(a_2 + a_{12})]^2 + 4a_{12}^2(a_2\omega_1^2 - a_{12}\omega_2^2)(a_1\omega_2^2 - a_{12}\omega_1^2)\,. \tag{101}$$

For $a_{12} = 0$, Eq. (100) reduces to the result of Section 3.1.2, $\omega_{\mathrm{b}\pm}^2 = \omega_{1,2}^2$, for each particle species. For $a_{12} > 0$ the coupling between the two components in the binary phase produces two branches with frequencies differing from the single-component results. Importantly, and in contrast to the single component case, these frequencies are dependent on the microscopic properties of the condensates through the various scattering lengths.

Using a variational technique with Gaussian wave functions, Busch et al. (1997) have also demonstrated this feature for the low energy excitation frequencies of the collective motion. They also allow for a displacement of the trap centers for the two condensates; a finite displacement gives rise to a lifting of the degeneracies in certain modes as the isotropy of the system is broken.

3.5. *Finite temperature excitations*

Extensions of the mean-field theory of Section 2.2 to take into account the non-condensate fraction [represented by $\tilde{\Psi}(\boldsymbol{r},t)$] arising due to a finite temperature or to interparticle interactions have been formulated and modify the treatment of elementary excitations outlined in the first part of the current section. In particular, using the decomposition (7), Griffin (1996) has derived coupled equations for the stationary condensate wave function $\psi(\boldsymbol{r})$ and the (non-condensate) operator $\tilde{\Psi}(\boldsymbol{r},t)$ in what is known as the Hartree–Fock–Bogoliubov approximation [see also Proukakis and Burnett (1996), and references therein; a discussion of the validity of the approach outlined below has also be given by these authors (Proukakis and Burnett, 1997; Proukakis et al., 1997)]. The first

[12] From the work of Ho and Shenoy (1996), the binary phase is possible where $\mu_2/\mu_1 = (\omega_2/\omega_1)^2$, with $\max(U_2/U_{12}, U_{12}/U_1) > (\omega_2/\omega_1)^2 > \min(U_2/U_{12}, U_{12}/U_1)$. To arrange this evidently requires that the ratios of the scattering lengths be known and that the ratios of particle numbers can be chosen appropriately.

of these equations takes the form

$$\left[-\frac{\hbar^2}{2m}\nabla^2+V_{\mathrm{trap}}(\boldsymbol{r})\right]\psi(\boldsymbol{r})+U_0[n(\boldsymbol{r})+2\tilde{n}(\boldsymbol{r})]\psi(\boldsymbol{r})+U_0\tilde{m}(\boldsymbol{r})\psi^*(\boldsymbol{r})=\mu\psi(\boldsymbol{r})\,, \tag{102}$$

where $n(\boldsymbol{r})=|\psi(\boldsymbol{r})|^2$ is the equilibrium condensate density and $\tilde{n}(\boldsymbol{r})=\langle\tilde{\Psi}^\dagger(\boldsymbol{r})\tilde{\Psi}(\boldsymbol{r})\rangle$ and $\tilde{m}(\boldsymbol{r})=\langle\tilde{\Psi}(\boldsymbol{r})\tilde{\Psi}(\boldsymbol{r})\rangle$ are the non-condensate density and "anomalous" density, respectively. The equation for $\tilde{\Psi}(\boldsymbol{r},t)$ is given by

$$\begin{aligned}\mathrm{i}\hbar\frac{\partial\tilde{\Psi}(\boldsymbol{r},t)}{\partial t}&=\left[-\frac{\hbar^2}{2m}\nabla^2+V_{\mathrm{trap}}(\boldsymbol{r})-\mu\right]\tilde{\Psi}(\boldsymbol{r},t)\\&\quad+2U_0[n(\boldsymbol{r})+\tilde{n}(\boldsymbol{r})]\tilde{\Psi}(\boldsymbol{r},t)+U_0[\psi(\boldsymbol{r})^2+\tilde{m}(\boldsymbol{r})]\tilde{\Psi}^\dagger(\boldsymbol{r},t)\,.\end{aligned} \tag{103}$$

The normalisation is chosen such that $\int\mathrm{d}^3r\,n(\boldsymbol{r})=N$ and $\int\mathrm{d}^3r\,\tilde{n}(\boldsymbol{r})=\tilde{N}$, where N and $\tilde{N}$ are the number of condensate and noncondensate atoms, respectively (the total number of atoms, $N_{\mathrm{tot}}=N+\tilde{N}$).

These equations have served as the starting point for recent studies of finite temperature effects by Giorgini et al. (1996, 1997a,b) and Hutchinson et al. (1997),[13] looking, e.g., at the condensate fraction as a function of temperature and at shifts in the critical temperature for condensation itself (from the ideal gas result in the thermodynamic limit) caused by a finite number of atoms and by interparticle interactions. In particular, using a semiclassical WKB approximation for the energies of the elementary excitations, Giorgini et al. (1996) find the following result for the shift in the critical temperature,

$$\frac{\delta T_{\mathrm{c}}}{T_{\mathrm{c}}^0}\simeq-0.73\left(\frac{\omega_{\mathrm{av}}}{\bar{\omega}}\right)N_{\mathrm{tot}}^{-1/3}-1.33\left(\frac{a}{d_{\mathrm{HO}}}\right)N_{\mathrm{tot}}^{1/6}\,, \tag{104}$$

with $\bar{\omega}=(\omega_x\omega_y\omega_z)^{1/3}$, $\omega_{\mathrm{av}}=(\omega_x+\omega_y+\omega_z)/3$, $d_{\mathrm{HO}}=(\hbar/m\bar{\omega})^{1/2}$, and $T_{\mathrm{c}}^0\simeq0.94(\hbar\bar{\omega}/k_{\mathrm{B}})N_{\mathrm{tot}}^{1/3}$. The first term in Eq. (104) is due to the finite number of particles in the trap (see, e.g., Grossmann and Holthaus, 1995a; Ketterle and van Druten, 1996b), while the second term is the result of interparticle interactions (i.e., the "mean-field" shift). This theoretical result for the shift in critical temperature appears to be in reasonable agreement with recent experiments (Ensher et al., 1996; Mewes et al., 1996a; Minguzzi et al., 1997).[14]

An alternative approach, outlined by Griffin (1996), and used by Hutchinson et al. (1997) and by Dodd et al. (1998), is to employ the Bogoliubov transformation,

$$\tilde{\Psi}(\boldsymbol{r},t)=\sum_\lambda\,[u_\lambda(\boldsymbol{r})\hat{\alpha}_\lambda\mathrm{e}^{-\mathrm{i}\omega_\lambda t}-v_\lambda^*(\boldsymbol{r})\hat{\alpha}_\lambda^\dagger\mathrm{e}^{\mathrm{i}\omega_\lambda t}]\,, \tag{105}$$

which leads to the eigenvalue equations,

$$\begin{aligned}&\{\mathscr{L}-(\mu+\hbar\omega_\lambda)+2U_0[n(\boldsymbol{r})+\tilde{n}(\boldsymbol{r})]\}u_\lambda(\boldsymbol{r})-U_0[\psi(\boldsymbol{r})^2+\tilde{m}(\boldsymbol{r})]v_\lambda(\boldsymbol{r})=0\,,\\&\{\mathscr{L}-(\mu-\hbar\omega_\lambda)+2U_0[n(\boldsymbol{r})+\tilde{n}(\boldsymbol{r})]\}v_\lambda(\boldsymbol{r})-U_0[\psi^*(\boldsymbol{r})^2+\tilde{m}^*(\boldsymbol{r})]u_\lambda(\boldsymbol{r})=0\,,\end{aligned} \tag{106}$$

[13] Actually, in both of these works, the anomalous density $\tilde{m}(\boldsymbol{r})$ is neglected in the so-called "Popov approximation" (Popov, 1987).

[14] Note that Krauth (1996) has also demonstrated the same basic trends in the critical temperature via detailed Monte Carlo calculations of a collection of bosons in a harmonic trap.

for the quasiparticle amplitudes $u_\lambda(\boldsymbol{r})$ and $v_\lambda(\boldsymbol{r})$, where $\mathscr{L} \equiv [-(\hbar^2/2m)\nabla^2 + V_{\rm trap}(\boldsymbol{r})]$. From Eq. (105), expressions for $\tilde{n}(\boldsymbol{r})$ and $\tilde{m}(\boldsymbol{r})$ in terms of self-consistent solutions of the eigenvalue equations follow in the forms

$$\tilde{n}(\boldsymbol{r}) = \sum_\lambda \{[|u_\lambda(\boldsymbol{r})|^2 + |v_\lambda(\boldsymbol{r})|^2] N_0(\omega_\lambda) + |v_\lambda(\boldsymbol{r})|^2\}\,, \tag{107}$$

$$\tilde{m}(\boldsymbol{r}) = -\sum_\lambda u_\lambda(\boldsymbol{r}) v_\lambda^*(\boldsymbol{r})[2N_0(\omega_\lambda) + 1]\,, \tag{108}$$

where $N_0(\omega_\lambda)$ is the Bose distribution for the quasiparticle excitations,

$$N_0(\omega_\lambda) = \frac{1}{\exp(\hbar\omega_\lambda/k_{\rm B}T) - 1}\,. \tag{109}$$

Note that the last term in Eq. (107) represents the noncondensate density in the limit $T \to 0$; i.e., a finite noncondensate fraction exists even at $T = 0$ due to interparticle interactions.

By solving the set of equations (102) and (106) in an iterative manner [and using Eqs. (107) and (108)], self-consistent solutions for the various quantities can be obtained. Hutchinson et al. (1997) have used this approach (in the Popov approximation) to examine the temperature dependence of the condensate and noncondensate density profiles of a gas of rubidium atoms ($N_{\rm tot} \sim 2000$) in a spherically symmetric harmonic trap. [Javanainen (1996a) has also computed the noncondensate fraction using Bogoliubov theory and numerical calculations, but only at $T = 0$.] At finite temperatures (approaching the critical temperature), they find a two-component structure consisting of a dense core of condensed atoms on top of a diffuse cloud of excited atoms with an extended tail.

For a sample of atoms with $N_{\rm tot} = 2000$, they also considered the variation of the lowest excitation frequencies with temperature, finding a relatively weak temperature dependence until the temperature approaches $T_{\rm c}$, where the lowest excitation frequencies approach those of a non-interacting gas. Dodd et al. (1998) have since followed the same numerical approach (also in the Popov approximation) to compare the theory with recent experiments, performed by Jin et al. (1997), probing the temperature dependence of the elementary excitation frequencies. In these experiments, with $N_{\rm tot} \simeq 6000$, the frequencies of the collective $m = 0$ and $m = 2$ condensate modes were in fact found to exhibit strong (and different, i.e., opposite) dependencies on temperature (although above the critical temperature for BEC they become degenerate at twice the trap frequency, as for a noninteracting cloud). The theoretical results of Dodd et al. (1998) are in good agreement with the experimental results for $T \leq 0.65T_{\rm c}$, but fail at higher temperatures. Interestingly, the Hartree–Fock–Bogoliubov model in the Popov approximation gives results for a finite temperature condensate that are essentially the same as those of a *zero-temperature condensate* with the *same number of condensate atoms*. The model treats the condensate excitations as taking place in a static thermal cloud and therefore neglects the possibility of coupling between thermal and condensate modes of oscillation.[15] This, as well as the neglect of the anomalous, or pair, terms [e.g., $\tilde{m}(\boldsymbol{r})$] in the Popov approximation [which may become important near the transition temperature – see Proukakis et al. (1997) and Bijlsma and Stoof (1997)], could be contributing to the discrepancy between theory and experiment.

---

[15] A more general theory allowing for such coupling has been outlined by Proukakis and Burnett (1996).

4. Light scattering from a Bose–Einstein condensate

Analysing the properties of light scattered from a sample of cold bosonic atoms can provide a means of detecting effects associated with the formation of a Bose–Einstein condensate. For example, a photon-scattering event for which the photon recoil takes an atom into an already-occupied momentum state will be enhanced in a Bose gas and, as we shall see, can lead to qualitatively new features in the spectrum of scattered light.

Studies of light scattering from degenerate atomic gases were initiated by Svistunov and Shlyapnikov (1990) and by Politzer (1991), who considered scattering of weak light from a low-temperature ($T \simeq 0$) condensate formed from a spatially homogeneous gas. For this configuration, band gaps exist in the condensate excitation spectrum giving rise to strong reflection of resonant light from the (sharp) boundary of the condensate. In the context of experiments, however, this situation is inappropriate as it corresponds formerly to the case of an infinitely large trap; in present BEC experiments with atomic gases, the size (d_0) of the ground state of the trap is of the order of tens of microns and the trap boundaries are not sharp.

A number of papers have since appeared dealing with light scattering from condensates confined in traps of a more realistic size and shape. A review of much of this work has been given by Lewenstein and You (1996a). As with that review, we summarise the research done thusfar by dividing the various studies into two primary categories: *coherent* and *incoherent* light scattering. The reason for this categorisation, as we shall see, is that *coherent* scattering probes the *density* of the system, whereas *incoherent* scattering probes *density–density correlations* (i.e., density fluctuations) of the system.

On the experimental side, Andrews et al. (1996) have already used dispersive light scattering to spatially image a trapped condensate. A systematic study of the properties of light scattered from a condensate should be possible in the near future.

4.1. Coherent light scattering

4.1.1. Spontaneous emission linewidth

The spontaneous emission linewidth of a Bose-condensed gas is obviously a quantity of basic interest. Javanainen (1994) considered this for the case of an optically thin condensate, with size d_0 of the order of λ (the optical wavelength), weakly excited by resonant continuous-wave light. In a simplified approach, he replaced the atomic field by a single harmonic oscillator describing collective excitations of the condensate. For this model, light scattering is predicted to occur predominantly in the *forward* direction and the scattering cross section (i.e., the number of scattered photons as a function of the laser frequency) has a Lorentzian line shape with a width, Γ, proportional to the collective spontaneous emission rate, i.e.,

$$\Gamma \sim N\gamma/(k_L d_0)^2 , \tag{110}$$

where γ is the single-atom free-space spontaneous emission linewidth, N is the number of atoms in the condensate, and $k_L = 2\pi/\lambda$. Hence, for a macroscopic condensate (N large) the optical resonance is extremely broad as a result of Bose-enhanced spontaneous emission into the condensate, which, due to momentum conservation, is also responsible for the predominantly forward scattering [into a solid angle of size $\sim 1/(k_L d_0)$ about the direction of the incident photons].

However, in a system of more significant optical thickness, as is most likely to be the case for a trap of size $d_0 \sim (1-20)\lambda$, the approach of Javanainen (1994) is less adequate, as shown by You et al. (1996, 1994). In particular, propagation effects start to play a role. You et al. showed that, although the large scale width of the spectrum remains the same as found by Javanainen, the spectrum becomes non-Lorentzian and exhibits a narrow peak at resonance with a width, of order γ, determined by single-atom dissipative and dephasing processes such as spontaneous emission to non-condensed states.

The approach of You et al. is based on a linearisation of the Heisenberg equations of motion for the radiation and atomic field operators, valid for the case in which the light scattering only weakly perturbs the equilibrium state of the condensate. The atomic amplitudes are linearised about the ground state and, on eliminating the atomic excited-state operators and averaging over the fluctuations of the radiation field and the atomic distribution in a decorrelation approximation,[16] they derive a scattering equation for the averaged photonic operator in the form

$$\langle \dot{\hat{a}}_{\boldsymbol{k}\mu}(t)\rangle = -\mathrm{i}ck\langle \hat{a}_{\boldsymbol{k}\mu}(t)\rangle - \sum_{\mu'}\int \mathrm{d}\boldsymbol{k}'\int_0^t \mathrm{d}t'\mathscr{K}(t-t';\boldsymbol{k},\mu,\boldsymbol{k}',\mu')\langle \hat{a}_{\boldsymbol{k}'\mu'}(t')\rangle\,. \tag{111}$$

The so-called *self-energy kernel*, $\mathscr{K}(t-t';\boldsymbol{k},\mu,\boldsymbol{k}',\mu')$, describes the amplitude for the absorption of a photon with momentum $\boldsymbol{k}'$ at time t', with the associated creation of a wave packet in the excited state trap potential, followed by free evolution of the wave packet until the time t' at which it returns to the ground state emitting a photon with momentum $\boldsymbol{k}$. The free evolution consists of quantum diffusion and drift (due to the momentum of the absorbed photon) of the wavepacket; sufficient drift and diffusion away from the center of the trap reduces the quantum statistical enhancement of the spontaneous emission rate into the condensate, hence reducing the probability of returning to the condensate upon emission. This, together with spontaneous emission out of the condensate (at rate γ), causes the kernel to decay on a characteristic timescale we denote as $1/\gamma'$. For the case in which multiple scattering is of importance, the cumulative effect of this broadening and drift of the excited atomic state wave packet is to produce a narrow feature in the spectrum near resonance, with a characteristic width γ'.

Finally, as shown by You et al. (1996), an approximate form for the kernel is

$$\mathscr{K}(\tau;\boldsymbol{k},\mu,\boldsymbol{k}',\mu') \;\propto\; \bar{\rho}(\boldsymbol{k}-\boldsymbol{k}')\exp[-\mathrm{i}(\omega_0 + k_{\mathrm{L}}^2/2M)\tau - \gamma'\tau]\,, \tag{112}$$

where

$$\bar{\rho}(\boldsymbol{k}) = \int \mathrm{d}^3 r\,\rho(\boldsymbol{r})\,\mathrm{e}^{-\mathrm{i}\boldsymbol{k}\cdot\boldsymbol{r}} \tag{113}$$

is the *form factor*, or Fourier transform of the equilibrium density profile. This demonstrates explicitly that coherent scattering [which is proportional to $\langle a_{\boldsymbol{k}\mu}(t)\rangle$] probes the density profile of the trapped atoms. Hence, quantum statistical effects only manifest themselves in coherent scattering to the extent that the density profiles for bosons and fermions are different at low temperatures and that the density profile changes in the condensation process.

[16] In fact, these approximations mean that the approach of You et al. (1996) is still limited to a regime of relatively low optical thickness.

4.1.2. Scattering of short laser pulses

Lewenstein and You (1993) and You et al. (1995) investigated the scattering of short but intense laser pulses from a trapped sample of cold bosonic atoms with $d_0 \sim 10\lambda$. They found that above the critical temperature, T_c, for BEC, coherent scattering is weak and restricted to a very narrow cone in the forward direction (due to phase matching conditions), while below T_c the number of scattered photons increases dramatically and coherent scattering occurs into a solid angle in the *forward* direction determined by the size of the condensate.

4.2. Incoherent light scattering

As shown above, coherent scattering provides a probe of the density of the system through the first-order correlation function of the scattered field. In contrast, incoherent scattering, which deals with higher-order correlation functions of the scattered field, offers a probe of higher-order correlations of the atomic density and therefore of explicit quantum statistical effects.

4.2.1. Far-off-resonant light scattering

In the limit of a large detuning of the incident light from the atomic resonance (at the least, comparable to the *collective linewidth*, Γ, of the condensate), multiple scattering of photons becomes increasingly improbable (i.e., the sample is optically thin). If, also, the size of the condensate is much larger than the wavelength of light, dipole shifts due to neighbouring atoms may be ignored compared to the collective linewidth, Γ, and the equations for light and for matter may be decoupled. Eliminating the atomic excited state operators from the dynamics, expressions can again be derived for the scattered light field in terms of atomic ground state operators. Javanainen (1995) and Javanainen and Ruostekoski (1995) have done this for the case of a homogeneous, noninteracting Bose gas; given that the motion of the atoms during the excited state lifetime is negligible, the scattered field is derived as (assuming detection at a large distance r in the direction $\boldsymbol{n}$)

$$\begin{aligned}\hat{\boldsymbol{E}}_{\mathrm{S}}^{(+)}(\boldsymbol{r},t) &= -\frac{\mathscr{D}^2\omega_{\mathrm{C}}^2[(\boldsymbol{n}\times\boldsymbol{E}_{\mathrm{C}}^{(+)})\times\boldsymbol{n}]}{4\pi\varepsilon_0\hbar r c^2\delta}\int \mathrm{d}^3r'\,\mathrm{e}^{-\mathrm{i}(\Delta\boldsymbol{k})\cdot\boldsymbol{r}'}\hat{\Psi}_g^\dagger(\boldsymbol{r}',t)\hat{\Psi}_g(\boldsymbol{r}',t)\\ &= \frac{\mathscr{D}^2\omega_{\mathrm{C}}^2[(\boldsymbol{n}\times\boldsymbol{E}_{\mathrm{C}}^{+})\times\boldsymbol{n}]}{4\pi\varepsilon_0\hbar r c^2\delta}\hat{\rho}(\Delta\boldsymbol{k},t)\,,\end{aligned}\tag{114}$$

where $\hat{\rho}(\Delta\boldsymbol{k},t)$ is called the density fluctuation operator. In these formulae, $\boldsymbol{E}_{\mathrm{C}}^{+}\,\mathrm{e}^{\mathrm{i}\boldsymbol{k}_{\mathrm{C}}\cdot\boldsymbol{r}}$ represents the incoming field of frequency ω_{C}, $\delta=\omega_{\mathrm{C}}-\omega_0$ is the detuning of the field from the atomic resonance, $\mathscr{D}$ is the atomic dipole matrix element, and $(\Delta\boldsymbol{k})=k\boldsymbol{n}-\boldsymbol{k}_{\mathrm{C}}$ denotes the change of the wave vector of light upon scattering.

The spectrum of the scattered light, calculated as the Fourier transform with respect to time of the two-time correlation function of the scattered field, follows as

$$\begin{aligned}G_{ij}(\Delta\boldsymbol{k},\Delta\omega,\boldsymbol{r}) &= \int \mathrm{d}t\,\mathrm{e}^{\mathrm{i}(\Delta\omega)t}\langle[\hat{\boldsymbol{E}}_{\mathrm{S}}^{(-)}(\boldsymbol{r},0)]_i[\hat{\boldsymbol{E}}_{\mathrm{S}}^{(+)}(\boldsymbol{r},t)]_j\rangle\\ &= K_{ij}(\boldsymbol{r})S(\Delta\boldsymbol{k},\Delta\omega)\,,\end{aligned}\tag{115}$$

where $K_{ij}(\boldsymbol{r})$ describes the scattered dipole radiation of one atom and $S(\Delta\boldsymbol{k},\Delta\omega)$ is the *dynamic structure function*, given by (see, e.g., Forster, 1975)

$$S(\Delta\boldsymbol{k},\Delta\omega) = \frac{1}{2\pi\hbar}\int \mathrm{d}t\, \mathrm{e}^{\mathrm{i}(\Delta\omega)t}\langle\hat{\rho}(\Delta\boldsymbol{k},0)\hat{\rho}^{\dagger}(\Delta\boldsymbol{k},t)\rangle$$

$$= \frac{1}{Z}\sum_{\mu,\mu'} \mathrm{e}^{-\beta E_{\mu}}|\langle\mu'|\hat{\rho}(\Delta\boldsymbol{k})|\mu\rangle|^{2}\delta(\hbar\Delta\omega + E_{\mu} - E_{\mu'})\,, \tag{116}$$

with $\Delta\omega = \omega - \omega_{\mathrm{C}}$ denoting the change in frequency of the emitted photon.[17] In the formula (116), $|\mu\rangle$ and E_{μ} are energy eigenstates and eigenvalues of the unperturbed system respectively. The expression (116) amounts to a transition probability calculated in perturbation theory, involving a summation over all possible final states and thermally averaged over initial states. The detailed balance condition $S(\Delta\boldsymbol{k},\Delta\omega) = \mathrm{e}^{-\beta\hbar\Delta\omega}S(\Delta\boldsymbol{k},-\Delta\omega)$ at finite temperature will automatically give rise to a symmetrically placed two-peak structure if $S(\Delta\boldsymbol{k},\Delta\omega)$ develops a sufficiently sharp peak at a non-zero frequency. The density fluctuation operator $\hat{\rho}(\Delta\boldsymbol{k})$, for $\Delta\boldsymbol{k} \neq 0$, can be expressed in terms of creation and annihilation operators as

$$\rho(\Delta\boldsymbol{k}) = \sqrt{fN}(\hat{a}_{\Delta k} + \hat{a}^{\dagger}_{-\Delta k}) + \sum_{\boldsymbol{q}\neq 0,-\Delta\boldsymbol{k}} \hat{a}^{\dagger}_{\boldsymbol{q}}\hat{a}_{\Delta\boldsymbol{k}+\boldsymbol{q}}\,. \tag{117}$$

Of course, for the case of a weakly interacting gas, these operators create or destroy Bogoliubov *quasiparticles.*

4.2.1.1. Degenerate ideal gas. We consider first the case of non-interacting bosons in free space. The scattering function is found to be

$$S(\Delta\boldsymbol{k},\Delta\omega) = \frac{fN}{\hbar}(1 + \langle n_{\Delta k}\rangle)[\delta(\Delta\omega + \omega_{\Delta k}) + \mathrm{e}^{-\beta\hbar\omega_{\Delta k}}\delta(\Delta\omega - \omega_{\Delta k})] + S_{\mathrm{b}}(\Delta\boldsymbol{k},\Delta\omega)\,, \tag{118}$$

where f is the fraction of atoms in the condensate and $S_{\mathrm{b}}(\Delta\boldsymbol{k},\Delta\omega)$ denotes a background given by

$$S_{\mathrm{b}}(\Delta\boldsymbol{k},\Delta\omega) = \frac{4}{\hbar}\sum_{\boldsymbol{q}\neq 0,-\Delta\boldsymbol{k}} (1 + \langle n_{\boldsymbol{q}}\rangle)(1 + \langle n_{\boldsymbol{q}+\Delta\boldsymbol{k}}\rangle)$$

$$\times\, \mathrm{e}^{-\beta\hbar\omega_{\boldsymbol{q}+\Delta\boldsymbol{k}}}\delta(\Delta\omega + \omega_{\boldsymbol{q}} - \omega_{\boldsymbol{q}+\Delta\boldsymbol{k}})\,, \tag{119}$$

with $\langle n_{\Delta k}\rangle = [\exp(\beta\hbar\omega_{\Delta k}) - 1]^{-1}$ and

$$\omega_{\Delta k} = \hbar|\Delta\boldsymbol{k}|^{2}/2m\,. \tag{120}$$

Fig. 17 displays the spectrum of light scattered from the Bose gas with various degrees of degeneracy, as determined by the fugacity $z\ (\leq 1)$;[18] a Maxwell–Boltzmann gas corresponds to the

[17] The proportionality of the spectrum to the density correlation function illustrates the fact that highly detuned light couples to the local number density of the sample.

[18] The fugacity z is determined from the equation $\rho\lambda_{D}^{3} = g_{3/2}(z)$, where ρ is the density, $\lambda_{\mathrm{D}} = (2\pi\hbar^{2}/Mk_{\mathrm{B}}T)^{1/2}$ and $g_{3/2}(z) = \sum_{k=1}^{\infty} z^{k}/k^{3/2}$.

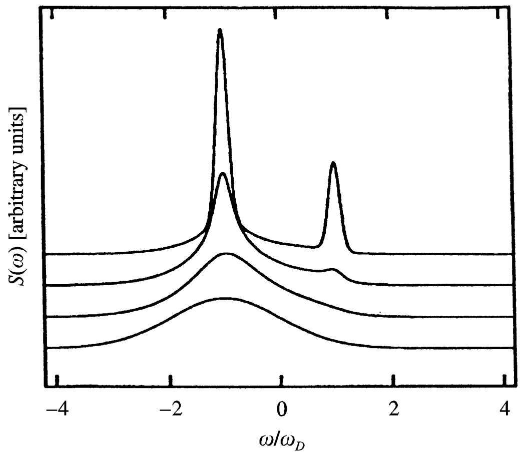

Fig. 17. Spectra of light scattered from a Bose gas with various degrees of degeneracy. Starting from the bottom curve, the fugacity and condensate fraction are $(z,f)=(0.1,0)$, $(0.9,0)$, $(1,0)$, and $(1,0.3)$. Vertical offsets have been added for ease of comparison and all of the spectra have been convoluted with a Gaussian with root-mean-square width $0.1\omega_D$. From Javanainen (1995).

limit $z\to 0$, whereas Bose–Einstein statistics prevail where $z=1$. Frequency is measured in units of the effective Doppler width, $\omega_D=(k_BT|\Delta\boldsymbol{k}|^2/M)^{1/2}$, for a temperature and scattering angle such that the effective recoil frequency $\omega_R=\hbar|\Delta\boldsymbol{k}|^2/2M=\omega_D$. As z is increased, the spectrum evolves from a Gaussian (reflecting the velocity distribution) to a structure with two distinct peaks at $\Delta\omega=\pm\omega_R$. With a condensate present ($f=0.3$ in the figure) the peak at $\Delta\omega=+\omega_R$ is most prevalent; this peak reflects the fact that scattering of an atom to an already-occupied state is favored by Bose–Einstein statistics and hence provides an explicit qualitative sign of boson degeneracy effects.

4.2.1.2. Weakly interacting gas. Graham and Walls (1996a) extended the analysis above to take into account weak interactions between atoms (treatable via the Bogoliubov approximation). The scattering function is modified to

$$S(\Delta\boldsymbol{k},\Delta\omega)=\frac{fN(1-\alpha_{\Delta k})}{\hbar(1+\alpha_{\Delta k})}(1+\langle n_{\Delta k}\rangle)[\delta(\Delta\omega+\omega_{\Delta k})+\mathrm{e}^{-\beta\hbar\omega_{\Delta k}}\delta(\Delta\omega-\omega_{\Delta k})]+S_b(\Delta\boldsymbol{k},\Delta\omega)\,, \tag{121}$$

with the background now given by

$$\begin{aligned}S_b(\Delta\boldsymbol{k},\Delta\omega)=\sum_{q\neq 0,-\Delta k}&\frac{(1+\langle n_q\rangle)(1+\langle n_{q+\Delta k}\rangle)(\alpha_q+\alpha_{q+\Delta k})^2}{2\hbar(1-\alpha_q^2)(1-\alpha_{q+\Delta k}^2)}\\&\times\left[2\left(\frac{1+\alpha_q\alpha_{q+\Delta k}}{\alpha_q+\alpha_{q+\Delta k}}\right)^2\mathrm{e}^{-\beta\hbar\omega_{q+\Delta k}}\delta(\Delta\omega+\omega_q-\omega_{q+\Delta k})\right.\\&\left.+\delta(\Delta\omega+\omega_q+\omega_{q+\Delta k})+\mathrm{e}^{-\beta\hbar(\omega_q+\omega_{q+\Delta k})}\delta(\Delta\omega-\omega_q-\omega_{q+\Delta k})\right],\end{aligned} \tag{122}$$

where $\langle n_{\Delta k}\rangle = [\exp(\beta\hbar\omega_{\Delta k}) - 1]^{-1}$, $\alpha_{\Delta k} = 1 + \eta^2|\Delta \boldsymbol{k}|^2 - \eta|\Delta \boldsymbol{k}|(2 + \eta^2|\Delta \boldsymbol{k}|^2)^{1/2}$, $\eta = (8\pi\rho a f)^{-1/2}$, and now (see Appendix A)

$$\omega_{\Delta k} = (\hbar|\Delta \boldsymbol{k}|/2m)(|\Delta \boldsymbol{k}|^2 + 16\pi\rho a f)^{1/2} . \tag{123}$$

Since the interactions are assumed to produce only a correction, the scattering spectrum is not changed qualitatively. However, for $|\Delta \boldsymbol{k}|^2 \gg 16\pi n a f$, Eq. (121) predicts a frequency shift $\omega_{\Delta k} - \omega_{\mathrm{R}} = (4\hbar/m)\pi n a f$ which is *constant*, i.e., given sufficient resolution, never becomes negligible. Therefore, given sufficient resolution in frequency, the important quantity naf can be determined from the position of the sharp line. For $T \to 0$ the double peak structure, required by detailed balance for finite T, disappears. Then $f \to 1 - (8/3)(na^3/\pi)^{1/2}$ and the spectrum (121) has a single sharp line at $\Delta\omega = -\omega_{\Delta k}$, arising from the excitation of single quasiparticles, and a broad background from the excitation of pairs of quasiparticles.

4.2.1.3. Weakly interacting gas in a harmonic trap. Far off-resonant light scattering from a weakly interacting condensate in a harmonic trap has been considered by Csordás et al. (1996), extending further still the work described above. Defining quasiparticle annihilation and creation operators, α_m, $\alpha_m^\dagger$, via the *space-dependent* Bogoliubov transformation (see, e.g., Fetter, 1996)

$$\hat{\psi}(\boldsymbol{r}) = \sum_m{}' [u_m(\boldsymbol{r})\hat{\alpha}_m - v_m^*(\boldsymbol{r})\hat{\alpha}_m^\dagger] + \phi_0(\boldsymbol{r}) , \tag{124}$$

where m denotes a complete set of single quasiparticle quantum numbers and $\phi_0(\boldsymbol{r})$ is the condensate wave function, Csordás et al. (1996) derive the scattering function as (see also Fetter and Rokhsar, 1997)

$$S(\Delta \boldsymbol{k}, \Delta\omega) = S_0(\Delta \boldsymbol{k})\delta(\hbar\Delta\omega) + \sum_m{}' S_m(\Delta \boldsymbol{k})[\delta(\hbar\Delta\omega + E_m) + \mathrm{e}^{-\beta E_m}\delta(\hbar\Delta\omega - E_m)] + S_{\mathrm{b}}(\Delta \boldsymbol{k}, \Delta\omega) , \tag{125}$$

with

$$S_0(\Delta \boldsymbol{k}) = \left| \int \mathrm{d}^3 r\, \mathrm{e}^{-\mathrm{i}(\Delta k)\cdot r} \left\{ |\phi_0|^2 + \sum_m{}' [n_m(|u_m|^2 + |v_m|^2) + |v_m|^2] \right\} \right|^2 , \tag{126}$$

$$S_m(\Delta \boldsymbol{k}) = (1 + n_m) \left| \int \mathrm{d}^3 r\, \mathrm{e}^{-\mathrm{i}(\Delta k)\cdot r} \phi_0^*(u_m - v_m) \right|^2 , \tag{127}$$

where the restricted sum $\sum'$ omits the ground state and $n_m = (\mathrm{e}^{\beta E_m} - 1)^{-1}$.

The first term in Eq. (125) describes elastic (coherent) scattering, which will be strong in the forward direction (i.e., for small $|\Delta \boldsymbol{k}|$), but will fall off sharply with increasing angle (i.e., for increasing $|\Delta \boldsymbol{k}|$). The second term is of most interest, describing scattering out of, or, at finite temperature, into the condensate with the creation or annihilation of a single quasiparticle, respectively. Finally, $S_{\mathrm{b}}(\Delta \boldsymbol{k}, \Delta\omega)$ describes a broad background associated with pairs of quasi-particles.

Csordás et al. (1996) derive an approximate analytical expression for the second term in Eq. (125), assuming that only scattering due to transitions between the condensate and highly excited states of the system is of importance (i.e., such that the momentum transfer in the scattering process is of the order of the photon momentum). Their results predict excitation of a band of levels with energies in the range $\hbar^2|\Delta\boldsymbol{k}|^2/2M < E < \hbar^2|\Delta\boldsymbol{k}|^2/2M + \mu$ and with angular momentum quantum numbers also in a restricted range. The repulsive interaction energy obviously provides the extra excitation energy beyond the recoil energy, while the transfer of angular momentum is limited by the finite size of the condensate.

4.2.2. Refractive index

Explicit signatures of quantum statistical effects have also been shown by Morice et al. (1995) to appear in the refractive index of a dilute Bose gas. Considering the propagation of a quasiresonant probe light field of frequency ω_L and initial form $E_\mathrm{L}\hat{\boldsymbol{e}}_x \mathrm{e}^{\mathrm{i}k_\mathrm{L}z}$ through such a sample (i.e., a Bose gas filling the half-space $z \geq 0$, with constant density ρ_0), they derive a dispersion relation to order two in the density, ρ_0, in the form

$$\frac{k^2}{k_\mathrm{L}^2} = 1 - \frac{(\mathscr{D}^2/\hbar\varepsilon_0)\rho_0}{\delta + \mathrm{i}\gamma}\,\frac{1}{1+C}\,, \tag{128}$$

where δ is the atom–laser detuning, $\mathscr{D}$ is the dipole moment for the atomic transition, and

$$C = \frac{\rho_0}{\mathrm{i}\delta - \gamma}\int \mathrm{d}^3r\,\varphi(\boldsymbol{r})\,\mathrm{e}^{-\mathrm{i}kz}\;\hat{\boldsymbol{e}}_x^*\cdot\mathsf{G}\cdot\hat{\boldsymbol{e}}_x + \;\rho_0\int \mathrm{d}^3r\,[1+\varphi(\boldsymbol{r})]\;\hat{\boldsymbol{e}}_x^*\cdot\left\{\frac{\mathrm{e}^{-\mathrm{i}kz}[\mathsf{G}/(\mathrm{i}\delta-\gamma)]^3 - [\mathsf{G}/(\mathrm{i}\delta-\gamma)]^2}{1-[\mathsf{G}/(\mathrm{i}\delta-\gamma)]^2}\right\}\cdot\hat{\boldsymbol{e}}_x\,, \tag{129}$$

with $\mathsf{G}(\boldsymbol{r})$ a 3×3 matrix given by

$$\mathsf{G}_{ij}(\boldsymbol{r}) = \mathrm{i}(\mathscr{D}^2/\hbar\varepsilon_0)\{[\partial/\partial r_i\,\partial/\partial r_j - \delta_{ij}\nabla^2]\mathrm{e}^{\mathrm{i}kr}/4\pi r - \delta_{ij}\delta(\boldsymbol{r})\}\,. \tag{130}$$

Quantum statistical corrections to the result for a dilute perfect classical gas arise through the two-body correlation function $\varphi(\boldsymbol{r})$, which is defined via

$$\rho_2(\boldsymbol{r}_1,\boldsymbol{r}_2) = \langle\hat{\psi}_\mathrm{g}^\dagger(\boldsymbol{r}_1)\hat{\psi}_\mathrm{g}^\dagger(\boldsymbol{r}_2)\hat{\psi}_\mathrm{g}(\boldsymbol{r}_2)\hat{\psi}_\mathrm{g}(\boldsymbol{r}_1)\rangle = \rho_0^2[1+\varphi(\boldsymbol{r}_1-\boldsymbol{r}_2)] \tag{131}$$

and depends on the bosonic nature of the atoms. These corrections are most pronounced around the critical point for BEC, as shown in Fig. 18, where the real and imaginary parts of the refractive index ($n' + \mathrm{i}n'' = k/k_\mathrm{L}$) are plotted as a function of temperature for a fixed density and detuning δ.

In their derivation, Morice et al. (1995) treat the center-of-mass motion of the atoms classically, enabling them to decouple the internal and external atomic dynamics. The dilute-gas assumption means that, with regards to multiple scattering of photons by the gas, they are able to restrict their attention to photon scattering processes by isolated atoms or between pairs of close atoms, and three-body correlations are neglected through the approximation $\rho_3(\boldsymbol{r}_1,\boldsymbol{r}_2,\boldsymbol{r}_3)/\rho_2(\boldsymbol{r}_1,\boldsymbol{r}_3) \simeq \rho_2(\boldsymbol{r}_1,\boldsymbol{r}_2)/\rho_1(\boldsymbol{r}_1)$.

Ruostekoski and Javanainen (1997a) have presented a fully quantum mechanical analysis of the response of a possibly dense gas to a weak light field; this generalises and expands upon the work of Morice et al. (1995). Their main result is an infinite hierarchy of equations of motion for atomic correlation functions that involve the atomic polarisation at one point in space and the density at

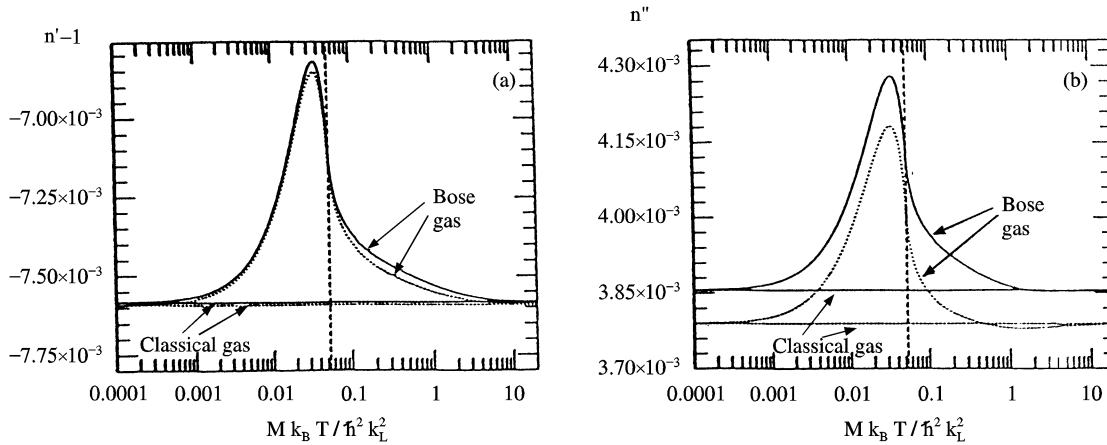

Fig. 18. Real part n' (a) and imaginary part n'' (b) of the refractive index as a function of the temperature for bosons and for classical particles, with $\delta = 2\gamma$ and $\rho_0 = k_L^3/16\pi^3$. The solid (dashed) lines give the results with all of the (the first two) terms of (Eq. (129)) included. The threshold for BEC is shown by the vertical dashed line. From Morice et al. (1995).

$\{0, 1, \dots\}$ points in space; the first two equations in the hierarchy correspond to the results of Morice et al. (1995). Noting that in the limit of low light intensity the atoms in fact behave like classical charged harmonic oscillators, and that an appropriate spatial distribution of such oscillators could share the correlation function hierarchy they derive, Ruostekoski and Javanainen (1997a) (see also Ruostekoski and Javanainen, 1997b) suggest that numerical simulation might offer a means of solving the hierarchy and examining more general regimes of the Bose gas.

4.3. Manipulation of the scattering length via light scattering

The very interesting possibility of manipulating the scattering length a of a trapped condensate using near-resonant light has been developed recently by Fedichev et al. (1996) (see also Bohn and Julienne, 1997). The idea is based upon inducing virtual transitions of a pair of interacting ground-state atoms to a bound electronically excited (p) level of the associated molecule. The resonant dipole interaction between atoms in the excited state is much stronger than in the ground state, meaning that the scattering amplitude can be significantly altered. In particular, for ^{7}Li they find that under suitable conditions the sign of the effective scattering length can in fact be *reversed*, producing repulsive rather than attractive interactions. This suggests the possibility of enhancing the stability of such a condensate and of a novel means of setting a condensate into an excited state of motion (via sudden changes in the scattering length). Alternatively, for other atomic species, the sign of the scattering length may be changed from positive to negative, inducing a sudden *collapse* of the condensate (Kagan et al., 1997b).

4.4. Nonlinear atom optics

The use of light waves to manipulate the matter wave properties of ultracold degenerate atomic samples has also been developed quite extensively in the context of so-called *nonlinear atom optics*.

In particular, Lenz et al. (1993, 1994) and Zhang et al. (Zhang, 1993; Zhang and Walls, 1994; Zhang et al., 1994) have shown that resonant dipole–dipole interactions (i.e., the exchange of photons) between excited and ground state atoms from an ultracold source, in which quantum statistical effects are important, can result in an effective manybody interaction in the form of a Kerr-type nonlinearity for atomic matter waves. For diffraction of an ultracold atomic beam by a standing-wave laser field this can lead, for example, to self-phase and cross-phase modulation of diffracted atomic waves. In certain configurations it is also possible for a laser beam to act as a nonlinear atomic waveguide which supports *atomic solitons.*

4.5. Interaction with quantised cavity radiation fields

An interesting progression from the study of condensates driven with laser light fields is to consider their interaction with few-photon (or possibly vacuum) radiation fields in a *cavity QED configuration*,[19] e.g., a trapped condensate interacting with a single quantised field mode of a microwave cavity. Marzlin and Audretsch (1997) have considered just such a situation in which the field is resonant with an internal atomic transition $|g\rangle \leftrightarrow |e\rangle$ (they neglect spontaneous emission and mechanical effects of the interaction). With all of the atoms initially in the excited internal state $|e\rangle$ and the field mode in the *vacuum* state, they find that the number of atoms in the excited state can exhibit periodic dips or fractional collapses and revivals as time progresses for the case that the initial external atomic state is a number state or a coherent state, respectively.

5. Broken gauge symmetry in pairs of condensates

5.1. Interference of two Bose–Einstein condensates and measurement-induced phase

The standard approach to a Bose–Einstein condensate assumes that it exhibits a well-defined *amplitude*, which unavoidably introduces the condensate *phase*. Is this phase just a formal construct, not relevant to any real measurement, or can one actually observe something in an experiment? Since one needs a phase reference to observe a phase, two options are available for investigation of the above question. One could compare the condensate phase to itself at a different time, thereby examining the condensate phase dynamics, or one could compare the phases of two distinct condensates. This second option has been studied, with very interesting results, by a number of groups (Javanainen and Yoo, 1996; Naraschewski et al., 1996; Cirac et al., 1996; Wallis et al., 1997; Hoston and You, 1996; Wong et al., 1996b; Graham et al., 1998b; Castin and Dalibard, 1997; Yoo et al., 1997; Röhrl et al., 1997). A physical configuration relevant to all of these works consists of a pair of statistically independent, physically separated condensates allowed to drop and, by virtue of their horizontal motion, overlap as they reach the surface of an atomic detector. The essential result of the analyses is that, even though no phase information is initially present (the initial condensates may, for example, be in number states), an interference pattern may be formed

[19] For a review of cavity quantum electrodynamics, see, e.g., Berman (1994).

and a relative phase established as a result of the measurement. This result may be regarded as a constructive example of spontaneous symmetry breaking. Every particular measurement produces a certain relative phase between the condensates; however, this phase is random, so that the symmetry of the system, being broken in a *single measurement*, is restored if an *ensemble of measurements* is considered.

Remarkably, the physical configuration we have just described and the predicted interference between two overlapping condensates have recently been realised in a beautiful experiment performed by Andrews et al. (1997b) at MIT.[20] In this experiment, mechanical instabilities introduced random noise that cloaked the "intrinsic" randomness described above, but improvements should allow controlled studies of the phase properties of condensates and of phenomena such as those described below.

5.1.1. Interference of two condensates initially in number states

To outline this effect, we follow the working of Javanainen and Yoo (1996) and consider two condensates made to overlap at the surface of an atom detector. The condensates each contain $N/2$ (noninteracting) atoms of momenta k_1 and k_2, respectively, and in the detection region the appropriate field operator is

$$\hat{\psi}(x) = (1/\sqrt{2})[\hat{a}_1 + \hat{a}_2 e^{i\phi(x)}] , \tag{132}$$

where $\phi(x) = (k_2 - k_1)x$ and $\hat{a}_1$ and $\hat{a}_2$ are the atom annihilation operators for the first and second condensate, respectively. For simplicity, the momenta are set to $\pm\pi$, so that $\phi(x) = 2\pi x$. The initial state vector is represented simply by

$$|\varphi(0)\rangle = |N/2, N/2\rangle . \tag{133}$$

Assuming *destructive* measurement of atomic position, whereby none of the atoms interacts with the detector twice, a direct analogy can be drawn with the theory of absorptive photodetection and the joint counting rate R^m for m atomic detections at positions $\{x_1, \dots, x_m\}$ and times $\{t_1, \dots, t_m\}$ can be defined as the normally ordered average

$$R^m(x_1, t_1, \dots, x_m, t_m) = K^m \langle \hat{\psi}^\dagger(x_1, t_1) \cdots \hat{\psi}^\dagger(x_m, t_m) \hat{\psi}(x_m, t_m) \cdots \hat{\psi}(x_1, t_1) \rangle . \tag{134}$$

Here, K^m is a constant that incorporates the sensitivity of the detectors, and $R^m = 0$ if $m > N$, i.e., no more than N detections can occur.

Further assuming that all atoms are in fact detected, the *joint probability density* for detecting m atoms at positions $\{x_1, \dots, x_m\}$ follows as

$$p^m(x_1, \dots, x_m) = \frac{(N-m)!}{N!} \langle \hat{\psi}^\dagger(x_1) \cdots \hat{\psi}^\dagger(x_m) \hat{\psi}(x_m) \cdots \hat{\psi}(x_1) \rangle . \tag{135}$$

The *conditional probability density*, which gives the probability of detecting an atom at the position x_m given $m-1$ previous detections at positions $\{x_1, \dots, x_{m-1}\}$, is defined as

$$p(x_m | x_1, \dots, x_{m-1}) = \frac{p^m(x_1, \dots, x_m)}{p^{m-1}(x_1, \dots, x_{m-1})} , \tag{136}$$

[20] Note that the theoretical work of Wallis et al. (1997) and Röhrl et al. (1997) on interference between a pair of condensates closely follows the MIT experimental configuration.

and offers a straightforward means of directly simulating a sequence of atom detections (Javanainen and Yoo, 1996; Wong et al., 1996b). This follows from the fact that, by virtue of the form for $p^m(x_1,\dots,x_m)$, the conditional probabilities can all be expressed in the simple form

$$p(x_m|x_1,\dots,x_{m-1}) = 1 + \beta\cos(2\pi x_m + \varphi)\,, \tag{137}$$

where β and φ are parameters that depend on $\{x_1,\dots,x_{m-1}\}$. The origin of this form can be seen from the action of each measurement on the previous result,

$$\langle\varphi_m|\hat{\psi}^\dagger(x)\hat{\psi}(x)|\varphi_m\rangle = (N-m) + 2A\cos[\theta - \phi(x)]\,, \tag{138}$$

with $A\mathrm{e}^{-\mathrm{i}\theta} = \langle\varphi_m|\hat{a}_1^\dagger\hat{a}_2|\varphi_m\rangle$.

So, to simulate an experiment, one begins with the distribution $p^1(x) = 1$, i.e., one chooses the first random number (the position of the first atom detection), x_1, from a uniform distribution in the interval $[0,1]$ (obviously, before any measurements are made, there is no information about the phase or visibility of the interference). After this "measurement", the state of the system is

$$|\varphi_1\rangle = \hat{\psi}(x_1)|\varphi_0\rangle = \sqrt{N/2}\,\{|(N/2)-1, N/2\rangle + |N/2,(N/2)-1\rangle\mathrm{e}^{\mathrm{i}\phi(x_1)}\}\,. \tag{139}$$

That is, one now has an entangled state containing phase information due to the fact that one does not know from which condensate the detected atom came. The corresponding conditional probability density for the second detection can be derived as

$$p(x|x_1) = \frac{p^2(x_1,x)}{p^1(x_1)} = \frac{1}{N-1}\,\frac{\langle\hat{\psi}^\dagger(x_1)\hat{\psi}^\dagger(x)\hat{\psi}(x)\hat{\psi}(x_1)\rangle}{\langle\hat{\psi}^\dagger(x_1)\hat{\psi}(x_1)\rangle} \tag{140}$$

$$= \frac{1}{2}\left\{1 + \frac{N}{2(N-1)}\cos[\phi(x) - \phi(x_1)]\right\}. \tag{141}$$

Hence, after just one measurement the visibility (for large N) is already close to $\frac{1}{2}$, with the phase of the interference pattern dependent on the first measurement x_1. The second position, x_2, is chosen from the distribution (141). The conditional probability $p(x|x_1)$ has, of course, the form (137), with β and φ taking simple analytic forms. However, expressions for β and φ become more complicated with increasing m, and in practice the approach one takes is to simply calculate $p(x|x_1,\dots,x_{m-1})$ numerically for two values of x [using the form (135) for $p^m(x_1,\dots,x_{m-1},x)$, and noting that $p^{m-1}(x_1,\dots,x_{m-1})$ is simply a number already determined by the simulation] and then, using these values, solve for β and φ. This then defines exactly the distribution from which to choose x_m.

The results of simulations making use of the above procedure are shown in Figs. 19–21. These figures also display results for cases in which collisions are included in the model; we discuss this in more detail below. Fig. 19a shows a histogram of 5000 atom detections from condensates initially containing $N/2 = 5000$ atoms each (neglecting collisions). From a fit of the data to a function of the form $1 + \beta\cos(2\pi x + \varphi)$, the visibility of the interference pattern, β, is calculated to be 1. The conditional probability distributions calculated before each detection contain what one can define as a *conditional visibility*. Following the value of this conditional visibility gives a quantitative measure of the buildup of the interference pattern as a function of the number of detections. The conditional visibility, averaged over many simulations, is shown as a function of the number of detections in Fig. 20 for $N = 200$. One clearly sees the sudden increase to a value of approximately 0.5 after the first detection, followed by a steady rise towards the value 1.0 (in the absence of

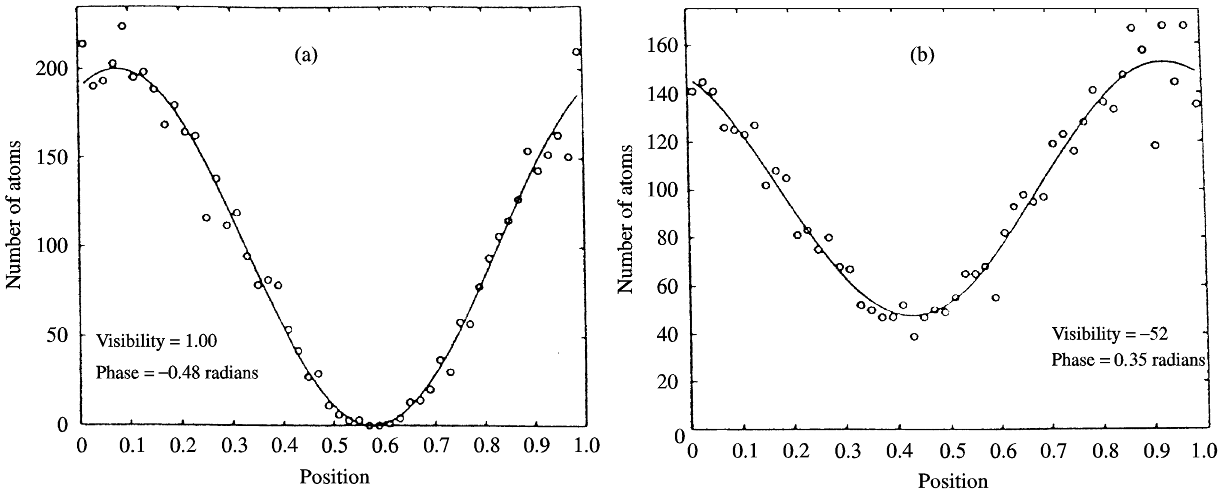

Fig. 19. (a) Histogram of 5000 simulated atomic detections for $N = 10\,000$ (circles). The solid curve is a least-squares fit using the function $1 + \beta\cos(2\pi x + \varphi)$. The free parameters are the visibility β and the phase φ. The detection positions are sorted into 50 equally spaced bins. (b) Histogram of 5000 position detections as in (a), but including the effects of collisions with $\kappa = \gamma$. From Wong et al. (1996b).

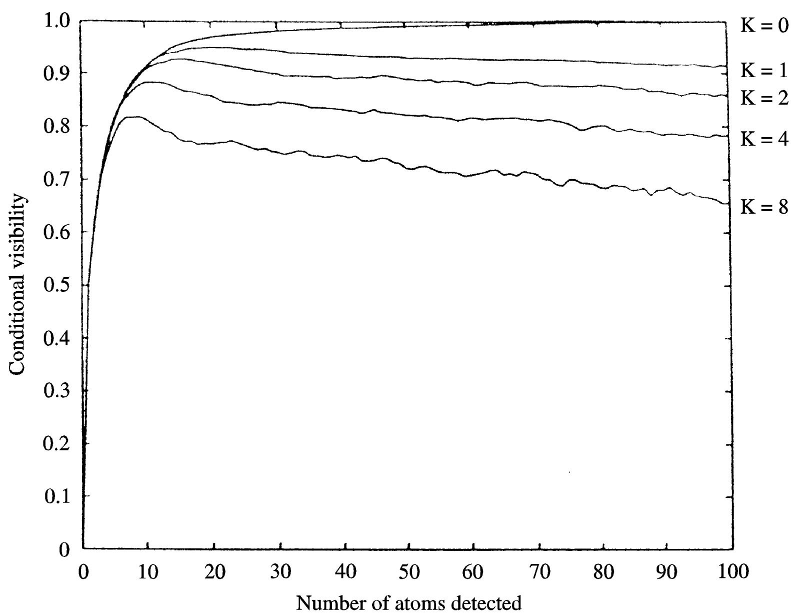

Fig. 20. Averaged conditional visibility as a function of the number of detected atoms for varying collision rates, κ. The visibility curves are averaged over 1000 simulations, each starting with $N = 200$. From Wong et al., 1996b.

collisions) as each further detection provides more information about the phase of the interference pattern.

One can also follow the evolution of the *conditional phase* contained within the conditional probability distribution. The final phase produced by each individual simulation is, of course,

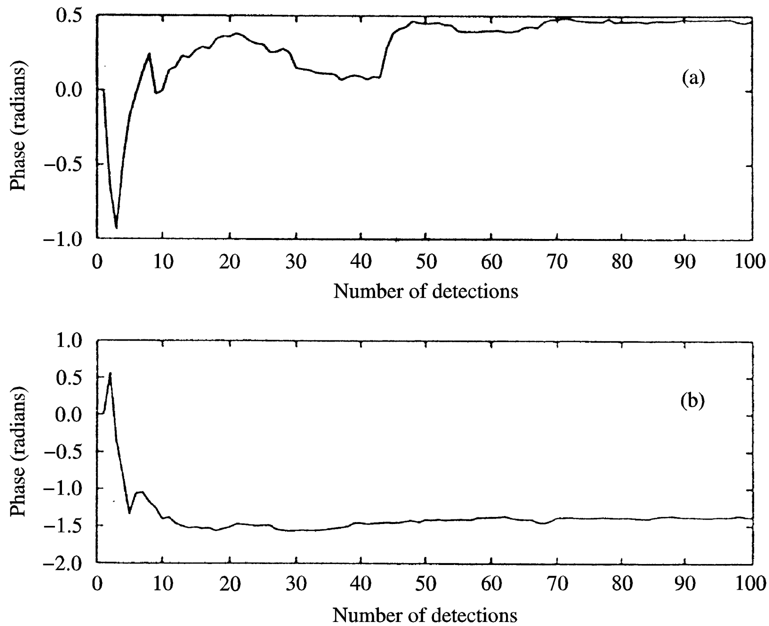

Fig. 21. Conditional phases for two simulations without collisions, with $N = 200$. From Wong et al. (1996b).

random; two sample simulations of the conditional phase are shown in Fig. 21. The trajectories are seen to stabilise about a particular value after approximately 50 detections (for $N = 200$).

These simulations emphasise the existence of an instantaneous, although random, phase as a *kinematical* property of bosonic systems with large occupation numbers, to be held distinct from the phase correlations in such systems, in space or time, that are determined by the system *dynamics*. In the conventional approach to the Bose liquid, where a symmetry breaking interaction is formally introduced, collisions lock the kinematical phase to the interaction and the distinction between the kinematical and dynamical phase properties is in large part wiped out.

Alternative models for simulating the formation of an interference pattern between two Bose–Einstein condensates have been developed based on coherent state (Cirac et al., 1996) or phase state (Castin and Dalibard, 1997) representations of the condensate state. These models concentrate explicitly on the evolution of the probability distribution of the relative phase, showing that this distribution evolves into a sharply peaked function with an increasing number of atom counts. They have also been used to study the buildup of the relative phase in the case where the two condensates are assumed to initially be in *mixed states* (Cirac et al., 1996; Graham et al., 1998b). For a Poissonian distribution of atom number the visibility approaches one for sufficiently many counts (given equal counting rates for the atoms from either condensate), while for a thermal distribution of atom number the visibility is a random variable, varying from run to run about an average value of $\pi/4$ (Graham et al., 1998b).

5.1.2. Interference of two condensates with collisions

The approach outlined above has been modified to include the effect of collisions by Wong et al. (1996b), who make use of the Monte Carlo wave function (MCWF) simulation method (see, e.g., Gardiner et al., 1992; Carmichael, 1993; Mølmer et al., 1993) to incorporate time evolution of the system wave function caused by inter-atom interactions.[21] This method calculates the times of the atom detections stochastically, with the evolution of the system in between these times determined by an effective Hamiltonian of the form

$$\hat{H}_{\rm eff} = \hbar\kappa[(\hat{a}_1^\dagger\hat{a}_1)^2 + (\hat{a}_2^\dagger\hat{a}_2)^2] - {\rm i}\hbar(\gamma/2)(\hat{a}_1^\dagger\hat{a}_1 + \hat{a}_2^\dagger\hat{a}_2)\,, \tag{142}$$

where γ and κ are the detection and collision rates, respectively, and it is assumed that only collisions between atoms from the same condensate need be modeled (i.e., collision terms of the form $\hat{a}_1^\dagger\hat{a}_1\hat{a}_2^\dagger\hat{a}_2$ are neglected). At the time of an atom detection, the position at which the atom is detected is chosen using the conditional probability method of the previous section. So, after m atom detections at positions $\{x_1,\dots,x_m\}$ and times $\{t_1,\dots,t_m\}$, the state vector of the system will be of the form

$$|\varphi_m\rangle = \hat{\psi}(x_m){\rm e}^{-{\rm i}\hat{H}_{\rm eff}(t_m-t_{m-1})/\hbar}\dots\hat{\psi}(x_1){\rm e}^{-{\rm i}\hat{H}_{\rm eff}t_1/\hbar}|\varphi_0\rangle\,. \tag{143}$$

To obtain some idea of the influence of collisions on the interference, one can inspect the expectation value

$$\langle\varphi_m|\hat{\mathscr{U}}^\dagger(t)\hat{\psi}^\dagger(x)\hat{\psi}(x)\hat{\mathscr{U}}(t)|\varphi_m\rangle, \tag{144}$$

where the evolution operator $\hat{\mathscr{U}}(t)$ is given by

$$\hat{\mathscr{U}}(t) = \exp\{-{\rm i}\kappa[(\hat{a}_1^\dagger\hat{a}_1)^2 + (\hat{a}_2^\dagger\hat{a}_2)^2]t\}\,, \tag{145}$$

and the state vector after m detections is

$$|\varphi_m\rangle = \sum_{k=0}^{m} c_k|N/2-m+k, N/2-k\rangle\,, \tag{146}$$

with $\sum|c_k|^2 = 1$. One can show that

$$\begin{aligned}&\langle\varphi_m|\hat{\mathscr{U}}^\dagger(t)\hat{\psi}^\dagger(x)\hat{\psi}(x)\hat{\mathscr{U}}(t)|\varphi_m\rangle\\ &\quad = N - m + \sum_{k=1}^{m}\mathscr{A}(k)\cos[\phi(x) + 2\kappa t(2k-m-1) + \Theta_k]\,,\end{aligned} \tag{147}$$

where the phase Θ_k is defined by $A{\rm e}^{{\rm i}\Theta_k} = c_k^* c_{k-1}$ and

$$\mathscr{A}(k) = 2A\sqrt{(N/2-k+1)(N/2-m+k)}\,. \tag{148}$$

The conditional probabilities are proportional to this expectation value; for non-zero collision rates ($\kappa \neq 0$), this value is a weighted sum over cosine functions with differing phase shifts, $4\kappa kt$. This leads to a dephasing of these functions in time and hence to a loss of coherence, or visibility; this effect obviously becomes more pronounced with increasing m. Examples of this effect are

[21] Note that the effects of interactions are also included in, for example, the work of Hoston and You (1996), Naraschewski et al. (1996), and Wallis et al. (1997), but these authors base their studies of the interference of interacting condensates on the time–dependent GP equation and insert an initial relative phase *by hand*.

shown in Fig. 19b and Fig. 20. With $\kappa=\gamma$, the visibility of the interference pattern in Fig. 19b is only $\frac{1}{2}$, while Fig. 20 shows the reduction in the averaged conditional visibility with increasing collisional rate, κ. Averages over many simulations also confirm that the variance in the conditional phase increases with increasing κ.

5.2. Collapses and revivals of the interference pattern visibility

As described earlier in Section 2.8.3, interparticle interactions are expected to give rise to collapses and revivals of the macroscopic wave function of a relatively small ($N\sim 10^3$–10^5) Bose–Einstein condensate. In the spirit of the present section, one can also examine this phenomenon in the context of the interference between a pair of condensates and indeed one finds that the visibility of the interference pattern also exhibits collapses and revivals (Wright et al., 1997; Castin and Dalibard, 1997; Wong et al., 1996a; Javanainen and Wilkens, 1997), offering an alternative means of detecting this effect.

To see this, consider, as above, that atoms are released from two condensates with momenta k_1 and k_2, respectively. Collisions within each condensate are described by the Hamiltonian (neglecting cross-collisions)

$$\hat{H}=\hbar\kappa[(\hat{a}_1^\dagger\hat{a}_1)^2+(\hat{a}_2^\dagger\hat{a}_2)^2]\,, \tag{149}$$

from which the intensity at the detector follows as

$$\begin{aligned} I(x,t) &= I_0\langle[\hat{a}_1^\dagger(t)e^{ik_1x}+\hat{a}_2^\dagger(t)e^{ik_2x}][\hat{a}_1(t)e^{-ik_1x}+\hat{a}_2(t)e^{-ik_2x}]\rangle \\ &= I_0\{\langle\hat{a}_1^\dagger\hat{a}_1\rangle+\langle\hat{a}_2^\dagger\hat{a}_2\rangle+\langle\hat{a}_1^\dagger\exp[2i(\hat{a}_1^\dagger\hat{a}_1-\hat{a}_2^\dagger\hat{a}_2)\kappa t]\hat{a}_2\rangle e^{-i\phi(x)}+\text{h.c.}\}\,, \end{aligned} \tag{150}$$

where $\phi(x)=(k_2-k_1)x$.

If one assumes that each condensate is initially in a coherent state of amplitude $|\alpha|$, with a relative phase ϕ between the two condensates, i.e., assuming that

$$|\varphi(t=0)\rangle=|\alpha\rangle|\alpha e^{-i\phi}\rangle\,, \tag{151}$$

then one obtains for the intensity

$$I(x,t)=\tfrac{1}{2}I_0|\alpha|^2\{1+\exp[2|\alpha|^2(\cos(2\kappa t)-1)]\cos[\phi(x)-\phi]\}\,. \tag{152}$$

From this expression, it is clear that the visibility of the interference pattern undergoes collapses and revivals with a period equal to π/κ.

Alternatively, one can consider an initial state formed by the quantum measurement scheme of the previous section; i.e., a state formed from two condensates initially in number states $|N/2\rangle$ after m atoms have been detected:

$$|\phi_m\rangle=\sum_{k=0}^{m}c_k|N/2-m+k,N/2-k\rangle\,, \tag{153}$$

with $\sum|c_k|^2=1$ and $\{c_k\}$ depending on the actual sequence of measurements. To a good approximation, this state yields an intensity of the form

$$I(x,t)=I_0\left\{N-m+\sum_{k=1}^{m}\mathscr{A}_k\cos[2(2k-m-1)\kappa t]\cos[\phi(x)-\phi]\right\}, \tag{154}$$

which, again, exhibits collapses and revivals, *but now with a period of* $\pi/(2\kappa)$. Hence, a factor of two difference occurs between the situation where broken symmetry is assumed from the outset and where it is not assumed. The origin of this difference in period follows from the exponential term appearing in Eq. (150); in particular, the number difference operator $\hat{a}_1^\dagger\hat{a}_1 - \hat{a}_2^\dagger\hat{a}_2$ is quantised in units of 2 when the total number is fixed and in units of 1 when it is not fixed, giving rise to factors $\exp(2\mathrm{i}N\kappa t)$ and $\exp(\mathrm{i}N\kappa t)$, respectively.

Hence, the validity of imposing broken gauge symmetry from the outset as a means of describing the quantum dynamics of Bose–Einstein condensates could, in principle, be tested by measuring the visibility of the interference pattern between two condensates as a function of time (Wong et al., 1996a). However, as discussed by Wong et al. (1996a), significant practical problems would face such a scheme as in the second case discussed above (with fixed atom number) the parity of the number m of detected atoms plays a significant role in that a change in this parity produces a phase shift π in the interference pattern. The loss of atoms by means other than the measurement process would introduce random phase shifts into the system with obviously detrimental effects.

5.3. *Pumping of twin-trap condensates*

Given that each condensate can contain only a finite number of atoms, the measurement schemes outlined above can obviously only operate for a finite length of time before exhausting the supply of atoms. Steel and Walls (1997) have recently developed a modified scheme that incorporates pumping of atoms into the condensates, thereby enabling them to realise a *steady-state* device. In principle, continuous output beams could be extracted from the two condensates with a well-defined relative phase established by the measurement process; this property could then be exploited in, for example, another interference experiment.

In their model, Steel and Walls (1997) assume pumping from thermal atom sources, or "baths", allowing for both two-way pumping, in which atoms are exchanged with the baths in both directions, and one-way pumping, in which atoms can only be transferred from the baths into the condensates but not vice versa. Their calculations are based on Monte Carlo wave-function simulations of a master equation of the form

$$\begin{aligned}\frac{\partial\rho}{\partial t} = \frac{\mathrm{i}}{\hbar}[\rho,\hat{H}] + \gamma\int_0^{2\pi}\mathrm{d}\phi\,\mathscr{D}[\hat{\psi}(\phi)]\rho + \chi_1^{\mathrm{out}}(N_1+1)\mathscr{D}[\hat{a}_1]\rho + \chi_1^{\mathrm{in}}N_1\mathscr{D}[\hat{a}_1^\dagger]\rho \\ + \chi_2^{\mathrm{out}}(N_2+1)\mathscr{D}[\hat{a}_2]\rho + \chi_2^{\mathrm{in}}N_2\mathscr{D}[\hat{a}_2^\dagger]\rho + \nu_1\mathscr{D}[\hat{a}_1]\rho + \nu_2\mathscr{D}[\hat{a}_2]\rho\,,\end{aligned} \tag{155}$$

where $\hat{H}$ is given by Eq. (149) (describing collisions), and

$$\mathscr{D}[\hat{c}]\rho = \hat{c}\rho\hat{c}^\dagger - \tfrac{1}{2}(\hat{c}^\dagger\hat{c}\rho + \rho\hat{c}^\dagger\hat{c})\,. \tag{156}$$

A schematic of the pumped twin-trap system is shown in Fig. 22. The parameters χ_1 and χ_2 are rate coefficients for pumping from the thermal baths, and N_1 and N_2 describe the populations, or strengths, of these baths. For one-way pumping one has $\chi_i^{\mathrm{in}} \neq 0$ and $\chi_i^{\mathrm{out}} = 0$,[22] while for two-way

[22] One-way pumping would correspond, for example, to the case in which excited-state atoms enter the condensate via spontaneous emission to the ground state. Provided the medium is optically thin, the emitted photon is lost and excitation out of the ground state is impossible.

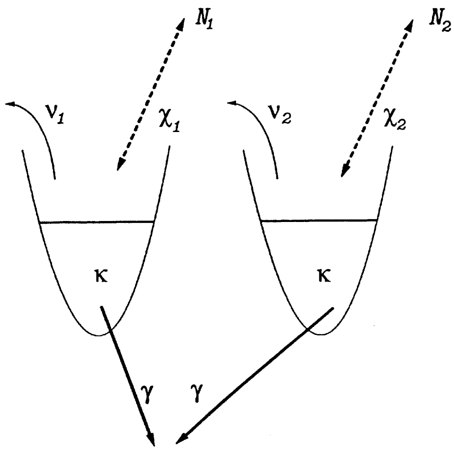

Fig. 22. Schematic of the pumped twin-trap system. From Steel and Walls (1997).

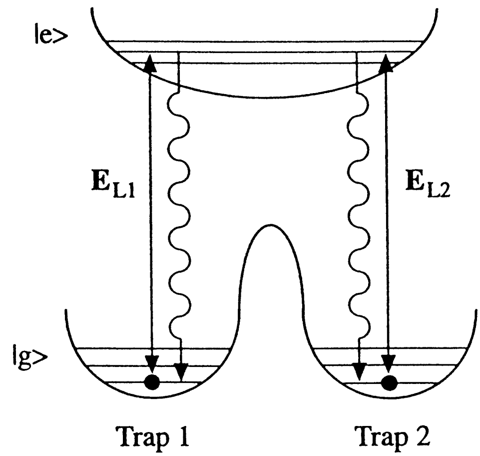

Fig. 23. Ground and excited state trap potentials for light-scattering detection of the relative phase as in the scheme of Imamoḡlu and Kennedy (1997).

pumping both $\chi_i^{\rm in}$ and $\chi_i^{\rm out}$ are nonzero. The field operator, $\hat{\psi}(\phi) = \hat{a}_1 + \hat{a}_2 e^{-i\phi}$, with $\phi = 2\pi x$, describes the detection of an atom at position x. Finally, separate "leaks" from each condensate at rates ν_1 and ν_2 into empty modes (the "output beams") are accounted for by the final two terms of Eq. (155).

With parameters chosen to maintain a mean number of atoms, n, in each condensate, fluctuations in the visibility for thermal pumping are found to be significant and often of order one. The timescale for these fluctuations is much longer for one-way pumping than for two-way pumping. For the one-way case, on average one atom is added to the system for each atom detected and so all of the atoms are replaced once every γt. For the two-way case, n atoms are exchanged with the baths for each atom detected, and so in the time γt all the atoms are replaced n times over and hence one expects a correspondingly shorter time scale for the fluctuations. Obviously, if the exchange of atoms with the baths occurs faster than an entangled state of a particular phase can be constructed (via atom detections), then one expects the average visibility to be reduced.

While the work outlined above does not explicitly identify the pumping mechanism, Savage et al. (1997b) have proposed an optical method for supplying atoms to a pair of condensates based on laser-driven Raman transitions between non-condensate and condensate fractions. We will discuss this further in the following section on light scattering from double condensates.

5.4. Detection of broken gauge symmetry via light scattering

Given that gauge symmetry has been broken and that macroscopic wave functions with well-defined phases exist for a pair of Bose–Einstein condensates, schemes to probe these wave functions using light scattering have been proposed by Imamoḡlu and Kennedy (1997), Javanainen (1996b), and Ruostekoski and Walls (1997a). A scheme simply involving spontaneous emission from initially excited atoms incident upon a pair of condensates has also been put forward by Savage et al. (1997a).

5.4.1. *Condensates in the same internal atomic state*

The scheme of Imamoḡlu and Kennedy (1997) involves *two independent condensates* confined in *spatially separated* potential wells (with separation $\boldsymbol{d}$). The two condensates are sufficiently well separated that they can be accessed independently, but are close enough together that laser-excited atoms, moving in a wider potential, have enough time to travel from the region of one (ground-state) potential well to the other (see Fig. 23). Weak monochromatic light fields $\boldsymbol{E}_{\mathrm{L1}}$ and $\boldsymbol{E}_{\mathrm{L2}}$ (which do not overlap in space) resonantly excite atoms in the two wells to a single quasi-metastable excited state. Using Heisenberg equations of motion for the atomic field operators and eliminating the excited state, Imamoḡlu and Kennedy (1997) derive an expression for the scattered light field in terms of ground-state atomic field operators $\hat{\Psi}_{\mathrm{g1}}(r,t)$ and $\hat{\Psi}_{\mathrm{g2}}(r,t)$. They then consider two particular schemes for detecting broken gauge symmetry:

5.4.1.1. Excitation of trap 1 only. Assuming that laser 1 is used to excite trap 1 only, and that only photons from trap 2 are collected, the relevant scattered field is of the form

$$\hat{\boldsymbol{E}}^{(+)}_{\mathrm{sc},2}(\boldsymbol{r},t) = \int \mathrm{d}^3 r' \int \mathrm{d}^3 r'' \sum_q \boldsymbol{A}_q(\boldsymbol{r}, \boldsymbol{r}' + \boldsymbol{d}/2, \boldsymbol{r}'' - \boldsymbol{d}/2) \cdot \hat{\boldsymbol{E}}^{(+)}_{\mathrm{L1}}(\boldsymbol{r}'' - \boldsymbol{d}/2)$$
$$\times \hat{\Psi}^{\dagger}_{\mathrm{g2}}(\boldsymbol{r}' + \boldsymbol{d}/2, t) \hat{\Psi}_{\mathrm{g1}}(\boldsymbol{r}'' - \boldsymbol{d}/2, t)\,, \tag{157}$$

where the tensor $\boldsymbol{A}_q(\boldsymbol{r}, \boldsymbol{r}', \boldsymbol{r}'')$ contains the light propagation kernel, atomic dipole moment, and excited state trap wave functions, over which the sum is taken. From the form (157), it follows that the mean scattered field will vanish unless broken symmetry is present in both traps ($\langle \hat{\Psi}_{\mathrm{g}i}(\boldsymbol{r},t) \rangle \neq 0$, $i = 1, 2$) and when the mean field is non-zero it will depend on the relative phase between the two condensates.

5.4.1.2. Excitation of both traps. Assuming now that both traps are excited, but that again only the photons scattered from trap 2 are detected, the scattered field is given by

$$\hat{\boldsymbol{E}}^{(+)}_{\mathrm{sc},2}(\boldsymbol{r},t) = \int \mathrm{d}^3 r' \int \mathrm{d}^3 r'' \hat{\Psi}^{\dagger}_{\mathrm{g2}}(\boldsymbol{r}' + \boldsymbol{d}/2, t)$$
$$\times \Bigg[\sum_q \boldsymbol{A}_q(\boldsymbol{r}, \boldsymbol{r}' + \boldsymbol{d}/2, \boldsymbol{r}'' - \boldsymbol{d}/2) \cdot \hat{\boldsymbol{E}}^{(+)}_{\mathrm{L1}}(\boldsymbol{r}'' - \boldsymbol{d}/2) \hat{\Psi}_{\mathrm{g1}}(\boldsymbol{r}'' - \boldsymbol{d}/2, t)$$
$$+ \sum_q \boldsymbol{A}_q(\boldsymbol{r}, \boldsymbol{r}' + \boldsymbol{d}/2, \boldsymbol{r}'' + \boldsymbol{d}/2) \cdot \hat{\boldsymbol{E}}^{(+)}_{\mathrm{L2}}(\boldsymbol{r}'' + \boldsymbol{d}/2) \hat{\Psi}_{\mathrm{g2}}(\boldsymbol{r}'' + \boldsymbol{d}/2, t) \Bigg]. \tag{158}$$

Again, the scattered field will be non-zero only when $\langle \hat{\Psi}_{\mathrm{g1}}(\boldsymbol{r},t) \rangle \neq 0$ and $\langle \hat{\Psi}_{\mathrm{g2}}(\boldsymbol{r},t) \rangle \neq 0$, but now there is also the interesting possibility of being able to adjust the amplitude and phases of the classical laser fields so that the two terms inside the brackets exactly cancel each other, giving zero mean field. The appropriate settings for the laser fields will of course depend once again on the relative phase between the two condensates.

5.4.2. Condensates in different internal atomic states

An alternative scheme employing the same methods would be one in which two condensates in different internal ground states are confined in the *same* trapping potential. One or two coherent laser fields would drive Raman transitions between the two condensates and signatures of broken gauge symmetry would be coherent light generation by spontaneous Raman scattering (first method) or complete elimination of Raman and Rayleigh scattering (second method). Javanainen (1996b) has also shown that if two phase-coherent laser beams drive Raman transitions in such a configuration, then amplification of one of the Raman beams immediately following the turn-on of the light is an unambiguous sign of broken symmetry.

Ruostekoski and Walls (1997a) have computed the spectrum of scattered light, in the spirit of Section 4.2.1, for this kind of Raman configuration. They find that the relative heights of the peaks appearing in the characteristic two-peaked scattering spectrum are sensitive to the phase difference between the macroscopic wave functions of the two condensates, as illustrated in Fig. 24. The reason for this is discussed in the following section, where pumping of double condensates using the same underlying mechanism is considered.

In a further application of this configuration, Savage et al. (1997a) have studied the rate of optical spontaneous emission into two ground state condensates (from a common excited internal state). Given that the two possible final states are indistinguishable (i.e., one does not know into which condensate the atom has gone), interference terms in the transition probability result in a transition rate that depends on the relative phase of the two condensates. The relative phase can therefore be detected from, for example, the total emitted power.

5.5. Pumping of double condensates via light scattering

In the above-mentioned work of Ruostekoski and Walls (1997a) on the spectrum of light scattered from a pair of condensates, it was found that for certain values of the relative phase between the condensates scattering of atoms out of the condensates could be suppressed while scattering into the condensates was enhanced. This shows up as the reduction (increase) in the height of the peak at $\omega/\omega_R = -1$ $(+1)$ in Fig. 24 for $\Delta\varphi = \pi$ and $\pi/2$. In fact, for $\Delta\varphi = \pi$, they showed that scattering out of the condensates is completely suppressed (note that the peak that remains at $\omega/\omega_R = -1$ is a consequence of scattering between noncondensate atoms). The origin of this effect is destructive quantum interference between the amplitudes for transitions from each condensate into the noncondensate fraction.[23]

Making use of this effect, Savage et al. (1997b) have proposed Raman light scattering as a mechanism for pumping atoms into a pair of Bose–Einstein condensates, with obvious relevance to the realisation of a continuous-wave atom laser. They show that for reasonable parameters a significant condensate growth rate should be achievable, although issues such as repopulation of the noncondensate fraction and diffusion of the condensate phase due to atomic interactions could be limiting factors.

[23] This suppression of atom scattering out of the condensates is analogous to the suppression of absorption associated with optical lasing without inversion (Harris, 1989; Scully and Zhu, 1989).

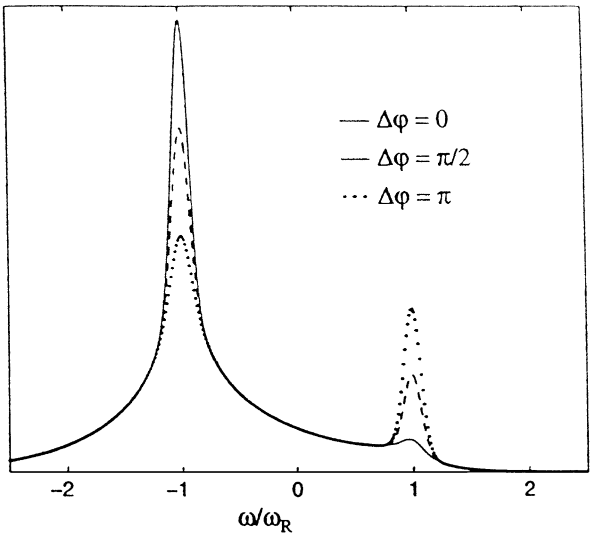

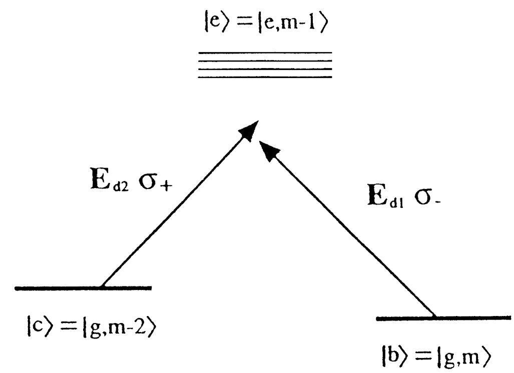

Fig. 24. Spectrum of light scattered from a Bose gas occupying two ground internal atomic states for various values of the relative phase $\Delta\varphi$. The condensate fraction is 0.8 for both internal states. The spectrum is convoluted in each case with a Gaussian of variance $0.01\omega_R$. From Ruostekoski and Walls (1997a).

Fig. 25. Atomic level scheme for the phase establishment scheme of Ruostekoski and Walls (1997b).

5.6. Establishment of relative phase via light scattering

Whereas the light scattering schemes discussed above assume broken gauge symmetry from the outset, it has been shown in a recent work by Ruostekoski and Walls (1997b) that a related light scattering scheme can be used to establish a relative phase (where initially no phase information need exist) between two condensates in the same manner as the atom detection schemes described earlier. The obvious interest of this scheme is that it is *non-destructive*, i.e., it uses the detection of scattered photons to establish the phase while conserving the total number of atoms in the two condensates.

In the scheme, it is assumed that the condensates are confined in the same trap (i.e., spatial overlap of the condensate wave functions is assumed to be significant) and occupy two different Zeeman sublevels that are optically coupled through a common excited state by two low-intensity off-resonant light beams (Fig. 25).[24] Considering only the coherent spontaneous scattering between the condensates (stimulated by a large number of atoms in the condensates), the emitted photons of interest propagate in a narrow cone in the forward direction. With a number of further assumptions and approximations (large detunings, Born approximation, neglect of dipole–dipole interactions and multiple scattering; refer to Section 4), Ruostekoski and Walls derive a master equation for the reduced density matrix of the system, from which they are able to formulate

[24] This coupling can be likened to the tunnelling of Cooper pairs in a Josephson junction.

a Monte Carlo wave-function simulation model (see, e.g., Gardiner et al., 1992; Carmichael, 1993; Mølmer et al., 1993) in which the quantum jumps are associated with photon detections. They show that the relative phase between the two condensates (initially in number states) may be established by a sequence of photon detections and that the conditional probability for the detection of spontaneously scattered photons as a function of time depends strongly on the relative phase thus established. (As pointed out by the authors, the dependence of the conditional probability on the relative phase may also provide a means of distinguishing between initial number states or coherent states of the condensates.) The phase establishment is made possible in this scheme by the uncertainty in the initial state of the atoms when they are excited by the driving light fields.

6. Quantum dynamics of a Bose–Einstein condensate in a double-well potential

6.1. Coherent quantum tunnelling

The double-well potential provides a simple and yet physically relevant example for studies of quantum tunnelling in mesoscopic systems. In the context of BEC in an atomic vapour, it is possible to conceive of experimental configurations in which a condensate is trapped in just such a potential. In fact, in the BEC experiments of Davis et al. (1995) and Andrews et al. (1997b), double-well trapping potentials were formed using an off-resonant optical dipole force to perturb a magnetic-rf trap. Hence, it is natural to ask if behavior analogous or similar to that observed, for example, in Josephson junctions can arise in the context of trapped atomic Bose–Einstein condensates. Numerous authors have addressed this issue and found that this is indeed the case (Javanainen, 1986, 1991; Grossmann and Holthaus, 1995b; Dalfovo et al., 1996; Jack et al., 1996; Milburn et al., 1997; Smerzi et al., 1997; Raghavan et al., 1997; Zapata et al., 1997); below, we outline the simplified and transparent two-state analysis and results of Milburn et al. (1997), who were particularly concerned with the influence of particle interactions on the Josephson-type effect.

Consider the case of a symmetric double-well potential, $V(\boldsymbol{r})$, with minima at $\pm\boldsymbol{r}_0$. We assume that the two lowest energy states of the system are closely spaced and well separated from the higher energy levels (Fig. 26); this enables us to use a simple two-state model. Defining $u_0(\boldsymbol{r})$ as the ground state of a *single* isolated potential well, with energy E_0, then if the position uncertainty in this ground state is much less than the separation, $2\boldsymbol{r}_0$, of the minima of the double-well potential, the energy eigenstates of $V(\boldsymbol{r})$ may be approximated by

$$\psi_1(\boldsymbol{r}) \simeq (1/\sqrt{2})[u_0(\boldsymbol{r}-\boldsymbol{r}_0) - u_0(\boldsymbol{r}+\boldsymbol{r}_0)] , \tag{159}$$

$$\psi_2(\boldsymbol{r}) \simeq (1/\sqrt{2})[u_0(\boldsymbol{r}-\boldsymbol{r}_0) + u_0(\boldsymbol{r}+\boldsymbol{r}_0)] , \tag{160}$$

with eigenvalues $E_1 \simeq E_0 - \mathscr{R}$ and $E_2 \simeq E_0 + \mathscr{R}$ where

$$\mathscr{R} = \int d^3r\, u_0(\boldsymbol{r}+\boldsymbol{r}_0)\mathscr{H}(\boldsymbol{r})\, u_0(\boldsymbol{r}-\boldsymbol{r}_0) , \tag{161}$$

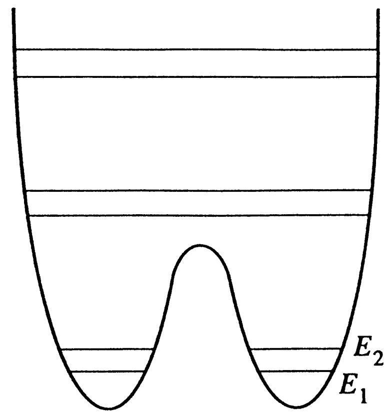

Fig. 26. Schematic of double-well potential with lowest energy levels.

and $\mathscr{H}(\boldsymbol{r})$ is the single-particle Hamiltonian. The tunnelling frequency between the two minima is given by

$$\Omega = 2\mathscr{R}/\hbar\,. \tag{162}$$

In the two-state approximation, one expands the atomic field operators in terms of the localised single-particle states and the annihilation and creation operators,

$$\hat{c}_1 = \int \mathrm{d}^3 r\, u_0^*(\boldsymbol{r} - \boldsymbol{r}_0)\hat{\Psi}(\boldsymbol{r}, 0)\,, \tag{163}$$

$$\hat{c}_2 = \int \mathrm{d}^3 r\, u_0^*(\boldsymbol{r} + \boldsymbol{r}_0)\hat{\Psi}(\boldsymbol{r}, 0)\,, \tag{164}$$

such that $[\hat{c}_i, \hat{c}_j^\dagger] = \delta_{ij}$. To lowest order in the overlap between the single-well modes, the many-body Hamiltonian can be written in term of the operators $\hat{c}_1$ and $\hat{c}_2$ as

$$\hat{H} = E_0(\hat{c}_1^\dagger \hat{c}_1 + \hat{c}_2^\dagger \hat{c}_2) + \tfrac{1}{2}\hbar\Omega(\hat{c}_1 \hat{c}_2^\dagger + \hat{c}_1^\dagger \hat{c}_2) + \hbar\kappa[(\hat{c}_1^\dagger)^2 \hat{c}_1^2 + (\hat{c}_2^\dagger)^2 \hat{c}_2^2]\,, \tag{165}$$

where $\kappa = (U_0/2\hbar)\int \mathrm{d}^3 r\, |u_0(\boldsymbol{r})|^4$. Note that this result neglects interactions between particles in different wells.

The two-mode approximation requires that the many-body interactions only slightly modify the ground state properties of the individual potentials. In practice, this limits the model to a small number of atoms (of the order of hundreds) compared to current BEC experiments. Nevertheless, condensate tunnelling can still be strongly modified by atom–atom interactions.

Heisenberg equations of motion for c_1 and c_2 take the forms (in a frame rotating at frequency $E_0/\hbar$)

$$\frac{d\hat{c}_1}{dt} = -\tfrac{1}{2}i\Omega\hat{c}_2 - 2i\kappa\hat{c}_1^\dagger\hat{c}_1^2 , \tag{166}$$

$$\frac{d\hat{c}_2}{dt} = -\tfrac{1}{2}i\Omega\hat{c}_1 - 2i\kappa\hat{c}_2^\dagger\hat{c}_2^2 . \tag{167}$$

Adopting a semiclassical mean-field analysis, in which one factorises products in these equations and introduces the amplitudes $b_i = \langle\hat{c}_i\rangle/\sqrt{N}$, the following coupled-mode equations can be derived:

$$\frac{db_1}{dt} = -\tfrac{1}{2}i\Omega b_2 - 2i\kappa N|b_1|^2 b_1 , \tag{168}$$

$$\frac{db_2}{dt} = -\tfrac{1}{2}i\Omega b_1 - 2i\kappa N|b_2|^2 b_2 . \tag{169}$$

These equations have an exact solution; for the case that all N atoms are initially localised in well 1, i.e., $N_1(0) = N|b_1(0)|^2 = N$, one finds

$$N_1(t) = \tfrac{1}{2}N[1 + \mathrm{cn}(\Omega t|N^2/N_c^2)] , \tag{170}$$

where $\mathrm{cn}(\phi|m)$ is a Jacobi elliptic function, and N_c is the critical number of atoms given by

$$N_c = \Omega/\kappa . \tag{171}$$

For $N \ll N_c$, $\mathrm{cn} \to \cos$ and the solution exhibits periodic oscillations with frequency Ω, precisely like those in Josephson junctions. As the number of atoms increases, the oscillation period increases until, at $N = N_c$, it becomes infinite. For $N > N_c$, the oscillations are inhibited; the interaction energy now exceeds the energy level splitting and one finds a self-trapping effect in which a population imbalance is maintained between the two potential wells.

Within the two-level approximation, an analysis of the full quantum problem is also tractable (numerically) (Milburn et al., 1997), allowing an assessment of the effect of quantum fluctuations. For N not too large, the solution of the quantum problem predicts a *collapse* of the oscillation due to intrinsic quantum fluctuations in the initial condition, and then a *revival* of the oscillation at a later time due to the discrete spectrum of the many-body Hamiltonian (cf. Section 2.8.3). Increasing N while keeping κN fixed increases the collapse and revival times, and improves the semiclassical approximation.

6.2. Quantum phase between tunnelling Bose–Einstein condensates

In the earlier section on interference between Bose–Einstein condensates, we saw how atom detections from overlapping condensates can establish a relative phase where, initially, no phase information existed; in particular, where the condensates were initially in number states. A similar effect has been demonstrated in the context of tunnelling condensates in a double-well potential by Jack et al. (1996). More specifically, assuming the same system and model as above, but neglecting atom interactions, the expectation value of the atom number in well 1 is easily derived as

$$\langle \hat{c}_1^\dagger(t)\hat{c}_1(t)\rangle = \tfrac{1}{2}N[1 + \alpha\cos(\Omega t) + \beta\sin(\phi)\sin(\Omega t)]\,, \tag{172}$$

where $N = \langle \hat{c}_1^\dagger\hat{c}_1 + \hat{c}_2^\dagger\hat{c}_2\rangle$ is the total number of atoms, $\alpha = \langle \hat{c}_1^\dagger\hat{c}_1 - \hat{c}_2^\dagger\hat{c}_2\rangle$, and $\beta e^{i\phi} = 2\langle \hat{c}_1^\dagger\hat{c}_2\rangle/N$. If the condensates are initially in number states with equal populations, then $\alpha = \beta e^{i\phi} = 0$ and population oscillations do not occur. However, by virtue of spontaneous symmetry breaking induced by measurements of the atom number in one of the wells, it is possible for a relative phase between the condensates to be established ($\beta e^{i\phi} \neq 0$) and for population oscillations to be observed.

In their model, based on wave-function simulations, Jack et al. (1996) assume that atoms are destructively detected in one of the wells at a rate γ. Given that this rate is much smaller than the tunnelling rate Ω, they observe oscillations in the number of atom detections, with the quantity $\beta\sin(\phi)$ converging to a well-defined (non-zero) value after a sufficient number of detections ($\beta \to 1$). As before, however, the phase difference ϕ varies from one run of detections to the next. As the amplitude of the oscillation is actually given by $\sin(\phi)$, this amounts to a random *amplitude* for each experimental run.

7. The atom laser

7.1. What is an "atom laser"?

Experimental success with the preparation of Bose-condensed samples of alkali gases has spurred on theoretical investigations into so-called "atom lasers", or, in other words, coherent atomic beam generators (Anderson and Holland, 1996). The macroscopic occupation of a single trap mode achieved in BEC experiments clearly has similarities with conventional laser systems and it has been a natural progression to look for modified configurations in which a quantised atomic field mode can exhibit properties analogous to those of the resonant mode in an above-threshold laser oscillator; that is, configurations in which the atomic field mode has a *large coherent amplitude*, or something approximating it.

Such a configuration should, of course, satisfy a number of basic criteria in order to be called an atom laser. Wiseman (1997) has defined and carefully elucidated such a set of criteria, which can be summarised as follows. In particular, with regards to the output from the device, the atomic field should (i) be highly directional, (ii) be monochromatic, (iii) have a well-defined phase, and (iv) have a well-defined intensity. The first condition is somewhat obvious and enables one to define a direction of propagation and directions of diffraction. The condition for monochromaticity (or mono-energeticity) can be given in terms of the power spectrum,

$$P(\omega) = (2\pi\bar{I})^{-1}\int d\tau\, e^{-i\omega\tau}\langle b^\dagger(t+\tau)b(t)\rangle \sim (2\pi)^{-1}\frac{\gamma}{(\omega-\bar{\omega})^2 + (\gamma/2)^2}\,, \tag{173}$$

of the atomic field mode, $b(t)$, with $\bar{I} = \langle b^\dagger b\rangle$ the intensity, or output flux of bosons. This spectrum might typically take a Lorentzian form with a spectral width γ, as shown above. The output can be regarded as monochromatic if this width is sufficiently small, $\gamma \ll \bar{\omega}$, amounting to a long first-order coherence time, $\tau_{coh} = \gamma^{-1}$. The coherence time, τ_{coh}, gives the time over which the phase of the field is approximately constant. Any meaningful measurement of phase must therefore be performed within $\tau_{\rm coh}$ and for an accurate measurement one requires many quanta in this interval, i.e., one requires that $\bar{I}\tau_{\rm coh} \gg 1$, or $\bar{I} \gg \gamma$, corresponding to high intensity. Finally, the condition of well-defined intensity amounts to the condition of higher-order coherence of the field, distinguishing it from, for example, a filtered thermal field. Defining $I(t) = b^\dagger(t)b(t)$, the intensity noise spectrum is given by

$$S(\omega) = \bar{I}^{-1}\int \mathrm{d}\tau\, \mathrm{e}^{-\mathrm{i}\omega\tau}\langle I(t+\tau)I(t) - \bar{I}^2\rangle\,, \tag{174}$$

which for a filtered thermal field might have the form $S(\omega) = 1 + \bar{I}^2/(\gamma^2 + \omega^2)$, whereas for a true laser one has $S(\omega) = 1 + \mathcal{O}(1)$, corresponding to a shot-noise-limited source obeying Poissonian statistics.

Note that the density of an "intense coherent" atomic beam should be, roughly speaking, that of a Bose-condensed gas. Indeed, considering for simplicity a one-dimensional case,

$$\delta E_{\rm kinetic} = \delta p^2/2M = p\delta p/M = v\delta p = v\hbar/l_{\rm dB}\,, \tag{175}$$

$$I = nv = v/l\,, \tag{176}$$

where $l_{\rm dB}$ and l are, respectively, the de Broglie wavelength and the average inter-atomic distance. For an "intense coherent" beam,

$$\frac{I}{\gamma} = l_{\rm dB}/l \gg 1\,. \tag{177}$$

This is exactly the condition for Bose-condensation, yet the atom laser output need not be condensed (i.e., concentrated mainly in a particular momentum state) since it need not be in thermal equilibrium.

7.2. Proposed models

A number of atom laser schemes have now been proposed and the basic operating principles involved in the majority of these schemes are depicted schematically in Fig. 27. Typically, a (cold) thermal source of atoms supplies atoms to an upper-lying mode (or modes) of an atom trap; this mode is coupled to the ground state mode of the trap via a particular cooling mechanism. The ground state mode corresponds to the "laser mode", where it is hoped that a macroscopic population can be built up and coupled to the outside world, via some kind of loss mechanism, to produce the laser output. The cooling mechanisms proposed for coupling the upper states to the ground state provide something of a dividing line between the various proposals in that they can be divided into two distinct classes – optical cooling (Wiseman and Collett, 1995; Spreeuw et al., 1995; Olshanii et al., 1995; Moy and Savage, 1997; Moy et al., 1997) and evaporative cooling (Wiseman et al., 1996; Holland et al., 1996; Guzmán et al., 1996; Moore and Meystre, 1997). In the optical cooling schemes, spontaneous emission from an excited internal atomic state (which does not "see" the trap, or at least not very strongly) takes the atom into a lower, trapped, internal state. The rate at which this occurs is, of course, subject to Bose enhancement by the presence of atoms already in the lower state. The evaporative cooling schemes make use of binary collisions between atoms to

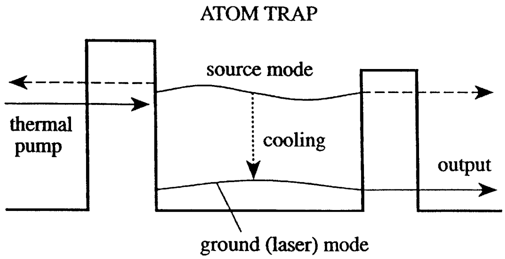

Fig. 27. Schematic of a generic atom-laser model.

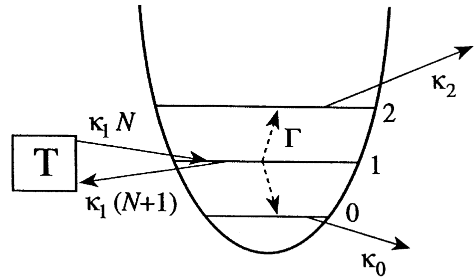

Fig. 28. Schematic of the evaporative-cooling atom-laser model of Wiseman et al. (1996). Arrows represent irreversible processes by which atoms enter and leave the trap, and are redistributed within the trap.

transfer population into the ground state. In particular, two atoms in the source mode collide, scattering one atom into the lasing mode (once again, a process enhanced by a large population in the laser mode) and the other into a higher energy mode. In keeping with evaporative cooling, the higher energy atom is rapidly removed from the system, producing the necessary irreversibility in the pumping process.

Finally, we note that related schemes have been discussed for media other than dilute atomic gases. In particular, matter-wave amplification has also been considered in the context of molecular dissociation (Bordē, 1995) and of exciton lasers (Imamoḡlu and Ram, 1996).

7.3. *An atom laser based on evaporative cooling*

Holland et al. (1996) and Wiseman et al. (1996) have studied an atom laser scheme based on a very rudimentary three-level model of evaporative cooling, as depicted in Fig. 28.[25] The three levels, or atomic energy eigenstates, are referred to as the ground, source, and excited modes, with energies E_0, E_1, and E_2 respectively ($E_0 < E_1 < E_2$). In the approach of Wiseman et al. (1996), the source mode is coupled to a broadband thermal beam, or reservoir, of atoms, with a flux per unit bandwidth of N. A collision between two atoms in this mode may cool one atom to the ground mode, while the other atom is heated into the excited mode. The ground and excited modes are coupled to vacuum reservoirs to facilitate outputs from these modes; for the excited state, the loss rate into the reservoir is large and simulates the rapid evaporation of high-energy atoms from the system, while for the ground state the reservoir coupling provides the output channel for the atom laser. While this model constitutes a gross simplification of the true many-level system in a realistic trap, it is expected to contain the essential features of steady-state evaporative cooling and to provide at least qualitatively correct results.

[25] Note that Quadt et al. (1996) have also studied a similar model, but in the context of a dynamical model for Bose–Einstein condensation.

In a second quantised formalism, for which each mode has an associated annihilation operator $\hat{a}_i$ ($i=0,1,2$), a master equation for the system density matrix, W, can be written in the form

$$\dot{W} = -\mathrm{i}[\hat{H}_0 + \hat{H}_{\mathrm{col}}, W] + \sum_{i=0}^{2} \kappa_i \mathscr{D}[\hat{a}_i]W + \kappa_1 N(\mathscr{D}[\hat{a}_1] + \mathscr{D}[\hat{a}_1^\dagger])W , \tag{178}$$

where

$$\mathscr{D}[\hat{c}]W = \hat{c}W\hat{c}^\dagger - \tfrac{1}{2}(\hat{c}^\dagger\hat{c}W + W\hat{c}^\dagger\hat{c}) \tag{179}$$

and the free and collisional Hamiltonians are, respectively,

$$\hat{H}_0 = \sum_{i=0}^{2} E_i \hat{a}_i^\dagger \hat{a}_i , \tag{180}$$

$$\hat{H}_{\mathrm{col}} = \sum_{i \le j, k \le l} V_{ijkl} \hat{a}_i^\dagger \hat{a}_j^\dagger \hat{a}_k \hat{a}_l . \tag{181}$$

The coefficients κ_i give the characteristic damping or loss rates of the modes.

Assuming that the collision amplitudes V_{ijkl} are small compared to the energy separations of the modes, it is possible to simplify the collision Hamiltonian by retaining only energy-conserving terms (rotating-wave approximation). Under the further assumption that κ_2 is much larger than all other decay rates, one can adiabatically eliminate the excited mode from the dynamics to yield the following master equation for the reduced density operator, $\rho = \mathrm{Tr}_{\mathrm{mode}\,2}[W]$:

$$\dot{\rho} = \mathrm{i}[\hat{V}, \rho] + \sum_{i=0}^{1} \kappa_i \mathscr{D}[\hat{a}_i]\rho + \kappa_1 N(\mathscr{D}[\hat{a}_1] + \mathscr{D}[\hat{a}_1^\dagger])\rho + \Gamma \mathscr{D}[\hat{a}_0^\dagger \hat{a}_1^2]\rho , \tag{182}$$

where

$$\Gamma = \frac{\kappa_2 |V_{0211}|^2}{(\kappa_2/2)^2 + \Delta^2} , \tag{183}$$

$$\hat{V} = V_{0000} \hat{a}_0^{\dagger 2} \hat{a}_0^2 + V_{0101} \hat{a}_0^\dagger \hat{a}_1^\dagger \hat{a}_0 \hat{a}_1 + V_{1111} \hat{a}_1^{\dagger 2} \hat{a}_1^2 + v \hat{a}_0^\dagger \hat{a}_1^{\dagger 2} \hat{a}_0 \hat{a}_1^2 , \tag{184}$$

with $\Delta = E_2 + E_0 - 2E_1$ and $v = (\Delta/\kappa_2)\Gamma$. The quantity Γ is the "spontaneous" rate of binary collisions in the source mode (1) that result in one atom entering the "lasing" mode (0) and the other escaping the trap from the (eliminated) excited mode (2).

7.3.1. Weak collision regime

Wiseman et al. (1996) distinguish two regimes of particular interest: the weak collision regime, for which $\Gamma \ll \kappa_0$, and the strong collision regime, for which $\Gamma \gg \kappa_0$. In the weak collision regime, a strong pump ($N \gg 1$) is required to produce a large population in the laser mode. In the lasing regime, therefore, the populations in both modes 0 and 1 will be large and the assumption of well-defined amplitudes for these modes seems reasonable. Hence, a P function representation can be used for the pump and lasing modes and an associated Fokker–Planck equation derived from which population and fluctuation properties can be calculated.

Considering the populations in a semiclassical analysis (i.e., ignoring fluctuations), and setting $n_0 + 1 \approx n_0$ (this corresponds to ignoring the "spontaneous" collisional transitions $1 \to 0$ in comparison with "stimulated" transitions due to Bose enhancement), one obtains the coupled equations

$$\dot{n}_0 = (\Gamma n_1^2 - \kappa_0)n_0\,, \tag{185}$$

$$\dot{n}_1 = -2\Gamma n_0 n_1^2 - \kappa_1 n_1 + \kappa_1 N\,. \tag{186}$$

The stationary solutions to these equations exhibit a threshold at

$$v = N - \sqrt{\kappa_0/\Gamma} = 0\,. \tag{187}$$

Below threshold ($v < 0$), the stationary solutions are

$$\bar{n}_0 = 0, \quad \bar{n}_1 = N\,, \tag{188}$$

while above threshold ($v > 0$)

$$\bar{n}_0 = \tfrac{1}{2}(\kappa_1/\kappa_0)v = \tfrac{1}{2}(\kappa_1/\kappa_0)(N - \sqrt{\kappa_0/\Gamma}), \quad \bar{n}_1 = \sqrt{\kappa_0/\Gamma}\,. \tag{189}$$

Well above threshold, $v \geq \bar{n}_1$, and so in order for the population of the lasing mode to be much greater than that of the source mode one requires $\kappa_1 \gg \kappa_0$.

Assuming that atoms leaking from the lasing mode are detectable (with unit efficiency) outside the trap, the fluctuation properties of the laser could be investigated by measuring the correlations between arrivals of atoms. The mean output intensity, in atoms per unit time, is simply (above threshold)

$$\bar{I} = \kappa_0 \bar{n}_0 = \tfrac{1}{2}\kappa_1 v\,. \tag{190}$$

Normalised to the shot noise level of one, the intensity fluctuation spectrum is found to be

$$S(\omega) = 1 + \frac{N}{\sigma}\left(\frac{\kappa_0}{\kappa_1}\right)^2 \frac{4\sigma^2\kappa_1^4}{4\sigma^2\kappa_1^4 + \omega^2\kappa_1^2(1+\sigma^2) + \omega^4}\,, \tag{191}$$

where σ is a normalised threshold parameter,

$$\sigma = \frac{N - \sqrt{\kappa_0/\Gamma}}{\sqrt{\kappa_0/\Gamma}}\,. \tag{192}$$

This spectrum is non-Lorentzian and its bandwidth is determined by κ_1, not κ_0. This is because the origin of the fluctuations in the output atom flux is the thermal fluctuations in the number of atoms in the source mode. From the above expression, one also sees that the intensity fluctuations are above shot noise; just above threshold ($\sigma \ll 1$), the noise fluctuations are extremely large, as expected. Far above threshold, the excess noise at low frequencies is of order unity (since $\kappa_0 \ll \kappa_1$ but $N \gg 1$), which, although worse than for an ideal laser (which is shot-noise limited far above threshold), is much less than for a thermal field, for which the noise would be of order $(\bar{n}_0)^2 \gg 1$.

Far above threshold, phase fluctuations dominate intensity fluctuations and so, writing the coherent field amplitude in the form $\alpha_0 = \sqrt{n_0}\,e^{i\phi}$, the appropriate expression for the power spectrum takes the form

$$P(\omega) = \frac{\kappa_0}{2\pi}\int d\tau\, e^{-i\omega\tau}\langle \alpha_0^*(t+\tau)\alpha_0(t)\rangle \simeq \frac{\kappa_0\bar{n}_0}{2\pi}\int d\tau\, e^{-i\omega\tau}\langle e^{i\phi(t+\tau)-i\phi(t)}\rangle\,. \tag{193}$$

An approximate stochastic differential equation for the phase $\phi(t)$ can be derived, via the Fokker–Planck equation, as

$$\dot{\phi} = \sqrt{l}\,\eta(t) + \sqrt{(\kappa_0/2\bar{n}_0)}\varepsilon(t)\,, \tag{194}$$

where the first term is due to collisions while the second is due to gain; $\eta(t)$ and $\varepsilon(t)$ are independent white noise sources and the parameter l is given by

$$l = \frac{2V_{0000}^2 N^2}{\kappa_1(1+\sigma)}\,. \tag{195}$$

It can be shown that, typically, $l \gg \kappa_0/(2\bar{n}_0)$, and in the power spectrum,

$$P(\omega) = \frac{\bar{I}}{\pi}\frac{(l/2)^2}{(l/2)^2 + (\omega)^2}\,, \tag{196}$$

l gives the linewidth. Hence, the linewidth is obviously much greater than in an ideal laser above threshold ($\kappa_0/(2\bar{n}_0)$), and is in fact greater than the bare linewidth of the mode, κ_0. In spite of this, the phase diffusion rate l may still be slow in the sense of being much less than the total loss rate of atoms from the ground mode of the trap, i.e., it may still satisfy the inequality $\bar{I} \gg l$, and hence the system as a whole, according to the criteria specified earlier, can be regarded as an atom laser.

7.3.2. Strong collision regime

In the case of strong collisions, $\Gamma \gg \kappa_0$, it is found that the intensity is well-defined and subject to Poissonian fluctuations above threshold. However, the phase diffusion rate may be greater than the output flux of atoms, i.e., $l \gg \bar{I}$, and hence, in this regime, the device would not be regarded as an atom laser.

7.4. An atom laser based on optical cooling

A relatively simple and quite general model of an atom laser based on optical cooling has been described by Olshanii et al. (1995) and we outline this model here. Atoms in an internal state a are injected into the atom laser system at a rate R_a with initial momenta of the order of or smaller than $\hbar k$. They decay via spontaneous emission into the internal state b and are then trapped by an external potential forming a three-dimensional "box" of volume V. The density of states in momentum space for this volume is $V/(2\pi\hbar)^3$, and, allowing for the photon recoil associated with spontaneous emission, the momenta of atoms in state b must lie within a sphere of radius $p_0 = 2\hbar k$. Hence, the number of levels $|b,\boldsymbol{p}\rangle$ that can be reached by the incoming atoms is

$$N_{\text{lev}} = \frac{V}{(2\pi\hbar)^3}\frac{4\pi p_0^3}{3} = \frac{32\pi}{3}\frac{V}{\lambda^3}\,, \tag{197}$$

where $\lambda = 2\pi/k$. The situation considered by Olshanii et al. (1995), and that we follow here, assumes the limit $V \gg \lambda^3$ [note that Spreeuw et al. (1995) have considered a similar atom laser scheme but operating in the opposite limit].

A rate equation for the mean occupation number $n_b(\boldsymbol{p})$ of a given state $|b,\boldsymbol{p}\rangle$ can be written in the form

$$\dot{n}_b(\boldsymbol{p}) = -\gamma_b(\boldsymbol{p})n_b(\boldsymbol{p}) + \frac{\gamma_a}{N_{\text{lev}}}N_a[1 + n_b(\boldsymbol{p})] - \frac{\sigma c}{V}N_v n_b(\boldsymbol{p})\,. \tag{198}$$

The first term describes the loss of atoms from the cavity and a loss rate of the form

$$\gamma_b(\boldsymbol{p}) = \gamma_{b0} + \alpha\,|\boldsymbol{p}|^2/p_0^2 \tag{199}$$

can be assumed, modelling, e.g. (light-induced) velocity selective excitation from b to another untrapped state.

The second term in Eq. (198) describes the populating of state $|b,\boldsymbol{p}\rangle$ due to the decay

$$a \to b + \text{photon}\,, \tag{200}$$

where N_a is the number of atoms in state a and, for simplicity, it is assumed that the decay rates into each of the N_{lev} accessible levels have the same value γ_a/N_{lev} [in a more precise treatment, these rates would depend on the Franck–Condon factors describing the overlap of the initial atomic wave function in state a with the trap wave functions for the states $|b,\boldsymbol{p}\rangle$; see, e.g., Spreeuw et al. (1995) and Moy et al. (1997)]. The factor $[1 + n_b(\boldsymbol{p})]$ accounts for both spontaneous and stimulated emission into the state $|b,\boldsymbol{p}\rangle$.

The third term in Eq. (198) accounts for reabsorption of emitted photons, producing the transition

$$b + \text{photon} \to a\,. \tag{201}$$

In this term, σ is the absorption cross-section of a photon and N_v denotes the number of photons present in the volume V. Equations of motion for N_v and for the number of atoms N_a in state a are given by

$$\dot{N}_a = R_a - \gamma_a N_a(1 + N_b/N_{\text{lev}}) + \frac{\sigma c}{V}N_v N_b\,, \tag{202}$$

$$\dot{N}_v = -\gamma_v N_v + \gamma_a N_a(1 + N_b/N_{\text{lev}}) - \frac{\sigma c}{V}N_v N_b\,, \tag{203}$$

where $N_b = \sum_p n_b(\boldsymbol{p})$ and $\gamma_v^{-1} \sim V^{1/3}/c$ denotes the time of flight of a photon across the box of volume V.

From the equations of motion for $n_b(\boldsymbol{p})$, N_a, and N_v, a steady state solution for $n_b(\boldsymbol{p})$ can be derived in the form

$$n_b(\boldsymbol{p}) = \frac{1 + fu}{\left(\dfrac{1+f}{r_a}\right)\gamma_b(\boldsymbol{p}) - 1 + u}\,, \tag{204}$$

where $f = N_b/N_{\text{lev}}$, $r_a = R_a/N_{\text{lev}}$ (feeding rate per mode), and $u = (\sigma c N_{\text{lev}})/(\gamma_v V)$. To obtain a macroscopic population of the state $|b,\boldsymbol{p} = 0\rangle$, a necessary condition is $u < 1$, so that the denominator in Eq. (204) can in principle approach zero and hence $n_b(\boldsymbol{p} = 0)$ can become very large. This condition

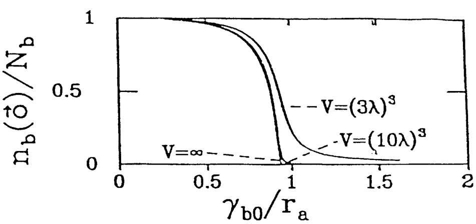

Fig. 29. Population $n_b(\boldsymbol{p}=0)$ as a function of γ_{b0}/r_a for various volumes V and for $\alpha = 40r_a$. From Olshanii et al. (1995).

amounts to the requirement that loss of atoms from the state $|b, \boldsymbol{p}=0\rangle$ due to photon reabsorption is outweighed by gain in the lasing system.

Given that $u < 1$, the population $n_b(\boldsymbol{p}=0)$ exhibits a threshold as a function of the feeding rate r_a. Examples are shown in Fig. 29 for the case in which $u = 0$ and for several values of the volume V. In the context of a possible experimental configuration, Olshanii et al. (1995) suggest the use of two hyperfine ground states of an alkali atom for the states a and b, with atoms in state a prepared in a magneto-optical trap and pumped into the state b via a Raman process. For the confining potential in state b, one could use a magnetic trap or far-off-resonance dipole trap. Unfortunately, the analysis outlined above does not examine the temporal statistics of the output beam of the atom laser, and so, in particular, it is not yet clear what control over phase fluctuations is possible and whether or not all of the proposed criteria for lasing can be simultaneously satisfied.

7.5. Output couplers for Bose–Einstein condensates

Output coupling obviously constitutes a vital element of an atom laser. The models outlined above have not addressed specifics of the output coupling in any great detail, simply assuming the existence of a loss mechanism from the lasing mode. Ballagh et al. (1997) have analysed a specific scheme for output coupling from a magnetically trapped Bose–Einstein condensate involving the coherent coupling of different internal states of the condensed atoms (e.g., different ground hyperfine levels), say $|1\rangle$ and $|2\rangle$, which "see" different trapping potentials. For example, atoms in state $|1\rangle$ are confined by the magnetic field, while atoms in state $|2\rangle$ are not. Hence, given a trapped condensate of atoms in state $|1\rangle$, a coherent output beam may be formed by coherently transferring atomic population, via a radiofrequency or microwave field, to the state $|2\rangle$; atoms transferred to this state then typically "fall out" of the trapping region. Using a mean field approach, based on numerical solutions of the Gross–Pitaevskii equation (modified to incorporate the external driving field), Ballagh et al. examined various parameter regimes for the external electromagnetic field. Depending on the strength or detuning of the field, the densities of the two fractions ($|1\rangle$ and $|2\rangle$) can show interesting spatial dependencies as a result of spatial variations in the pumping rate caused by the trapping potential and by the (repulsive) collisional self- and exchange interactions. This suggests useful ways of combining trap geometry with the external electromagnetic field parameters to control the orientation and shape of the output beam.

On the experimental side, Mewes et al. (1997) have demonstrated precisely such an output coupler for Bose-condensed sodium atoms, although in a regime where the pumping rates from state $|1\rangle$ to state $|2\rangle$ are essentially uniform in space across the condensate. Using short resonant pulses of radiofrequency radiation, 0–100% of the atomic population could be transferred in a controllable manner to the output state;[26] atoms in the output state simply fall from the condensate under the action of gravity, giving the output a distinct direction. In this way, output pulses of coherent atoms are generated and the configuration can therefore be looked upon as the realisation of a "pulsed atom laser." As mentioned in the introduction, this demonstration of coherent output coupling has now been complimented by the experimental confirmation of the coherence of the output pulses, via the observation of matter-wave interference fringes from overlapping condensates (Andrews et al., 1997b).

Returning to theoretical investigations, Zhang and Walls (1998) have now modelled the above experiment in some detail, also using modified (multicomponent) versions of the Gross–Pitaevskii equation, and obtain good agreement for, in particular, the density distribution of the output atom pulses. Naraschewski et al. (1997) have also analysed a similar configuration to that described above but assuming a very weak output coupling and a constant amplitude of the condensate wave function (i.e., they assume that some form of repumping process is continuously refilling the condensate), such that they can consider continuous-wave operation of their system (a modification of this work taking into account condensate depletion, i.e., without repumping, has been given by Steck et al., 1997). They find that the outgoing matter wave can be highly monoenergetic; this is in contrast with the case of strong output coupling, as in the (pulsed) configurations of Ballagh et al. (1997) and Mewes et al. (1997) where the output spectrum reflects the (much broader) momentum spread of the initial trapped condensate wave function. Similar results have been obtained by Hope (1997) and Moy and Savage (1997), who have also modelled output coupling from a trapped condensate via light-induced transitions to an untrapped state [note that these authors develop a theoretical approach that generalises the optical input–output formalism (Gardiner and Collett, 1985)].

7.6. Higher-order coherence of Bose–Einstein condensates

The above-mentioned interference experiment of Andrews et al. (1997b) confirmed that their condensates possess *first-order* coherence. Evidence for *higher-order* coherence, strengthening the analogy between condensates and optical laser photons, has also been provided through careful interpretation of some fundamental condensate properties, in particular, of the loss rate of atoms from the condensate via three-body recombination (Burt et al., 1997) and of the mean field energy of the condensate (Ketterle and Miesner, 1997).

As pointed out by Kagan et al. (1985) (see also Kagan et al., 1996), the atom loss rate due to three-body recombination is directly related to the probability of finding three atoms close to each other and can therefore act as a probe of the third-order correlation function

$$g^{(3)}(\boldsymbol{r},\boldsymbol{r},\boldsymbol{r}) = \frac{\langle \hat{\Psi}^\dagger(\boldsymbol{r})\hat{\Psi}^\dagger(\boldsymbol{r})\hat{\Psi}^\dagger(\boldsymbol{r})\hat{\Psi}(\boldsymbol{r})\hat{\Psi}(\boldsymbol{r})\hat{\Psi}(\boldsymbol{r})\rangle}{n(\boldsymbol{r})^3}, \tag{205}$$

[26] For a percentage between 0 and 100%, the state produced is a *coherent superposition* of trapped and untrapped condensates; the scheme thus acts as a *coherent beam splitter* for matter waves.

where $n(\mathbf{r}) = \langle \hat{\Psi}^\dagger(\mathbf{r})\hat{\Psi}(\mathbf{r}) \rangle$ is the atomic density. Importantly, the value of this function differs between condensates and thermal clouds by a factor of $3! = 6$; in particular, the value of $g^{(3)}(\mathbf{r},\mathbf{r},\mathbf{r})$ for a thermal cloud is a factor of six larger than that for a condensate, implying an atom loss rate due to three-body recombination six times larger. The ratio of the noncondensate to the condensate rate constants for this loss process was found by Burt et al. (1997) to be 7.4 ± 2.0, confirming the presence of at least third-order coherence in their condensates.

Similarly, Ketterle and Miesner (1997) have pointed out that the mean-field energy of a condensate, $\langle U \rangle$, provides a direct measure of the second-order correlation function,

$$g^{(2)}(\mathbf{r},\mathbf{r}) = \frac{\langle \hat{\Psi}^\dagger(\mathbf{r})\hat{\Psi}^\dagger(\mathbf{r})\hat{\Psi}(\mathbf{r})\hat{\Psi}(\mathbf{r}) \rangle}{n(\mathbf{r})^2}, \tag{206}$$

through the relationship

$$\langle U \rangle = \left(\frac{2\pi\hbar^2 a}{m}\right) g^{(2)}(0) \int d^3r [n(\mathbf{r})]^2 , \tag{207}$$

where $g^{(2)}(0) \equiv g^{(2)}(\mathbf{r},\mathbf{r})$, assuming that $g^{(2)}(\mathbf{r},\mathbf{r}')$ depends only on $\mathbf{r}-\mathbf{r}'$. Re-analysing condensate data from earlier experiments, they obtain values of $g^{(2)}(0)$ close to 1, as expected for a condensate and differing from that of a thermal cloud, for which $g^{(2)}(0) = 2$. The reduced value of $g^{(2)}(0)$ for a condensate reflects reduced density fluctuations, in direct analogy with the reduced intensity fluctuations of a (photon) laser in comparison with a thermal light source (see, e.g., Walls and Milburn, 1994).

8. Conclusions

In this review, we have endeavoured to provide a broad overview of the various avenues of theoretical research being pursued in the context of trapped dilute-gas Bose–Einstein condensates. At the same time, we have tried to incorporate reasonably detailed descriptions and explanations of some of the more interesting condensate properties and behaviour revealed thusfar, including, where possible, the comparisons that have been made between theory and experiment. The level of agreement between theory and experiment has to date been quite impressive, although some experimental results are already pointing to the need for more careful theoretical investigation in certain regimes; e.g., excitations at finite temperatures and in the nonlinear regime. Of course, much of the theoretical work detailed here does not yet have an experimental counterpart and might well represent a huge experimental challenge. As we complete writing this review, however, we have learned of yet another remarkable experiment in which alkali-gas condensates have been realised in an all-optical dipole trap following the transfer of atoms from a magnetic trap (Stamper-Kurn et al., 1997). Without constraints (for trapping) on the internal atomic hyperfine sublevel, this configuration should enhance the outlook for a number of the proposals described earlier, for example, those involving double condensate configurations, and certain output-coupling and atom-laser schemes.

As we are sure the reader will agree, the landmark alkali-gas BEC experiments of 1995 have opened up a rich assortment of fascinating new possibilities for theoretical and experimental investigation, addressing both fundamental issues in physics, such as broken gauge symmetry, and practical applications, such as the atom laser. The next few years are likely to witness many more significant developments in this field as further experiments are established, testing theoretical predictions and revealing new and possibly unexpected phenomena. We hope that the present review can serve as a useful progress report in this dynamic new regime of many-body quantum physics research.

Acknowledgements

The authors gratefully acknowledge discussions with E. Bolda, K. Burnett, M. Collett, J. Dunningham, R. Graham, M. Holland, R. Hulet, M. Jack, B. Kennedy, W. Ketterle, M.-O. Mewes, G. Milburn, M. Olsen, L. Plimak, J. Ruostekoski, C. Savage, M. Steel, H. Wiseman, T. Wong, and E. Wright. This work was supported by the Marsden Fund of the Royal Society of New Zealand.

Appendix A. Bose–Einstein condensation in a weakly interacting gas: Bogoliubov theory

Here we give an outline of the derivation of the elementary excitation spectrum of a weakly interacting, homogeneous Bose gas. This derivation is due to Bogoliubov (1947), whose treatment provided the first significant microscopic theory of such a system. Useful references are the books of Huang (1963), March et al. (1967), and Lifshitz and Pitaevskii (1980). In second quantised form, the standard model for a system of weakly interacting particles is described by a Hamiltonian of the form

$$\hat{H} = \hat{H}_0 + \hat{H}_{\mathrm{I}} \tag{A.1}$$

with

$$\hat{H}_0 = \sum_{\boldsymbol{p}} E_{\boldsymbol{p}} \hat{a}^\dagger_{\boldsymbol{p}} \hat{a}_{\boldsymbol{p}} \tag{A.2}$$

$$\hat{H}_{\mathrm{I}} = \frac{1}{2} \sum_{\boldsymbol{p}_1 \boldsymbol{p}_2 \boldsymbol{p}_3 \boldsymbol{p}_4} U_{\boldsymbol{p}_1 \boldsymbol{p}_2 \boldsymbol{p}_3 \boldsymbol{p}_4} \hat{a}^\dagger_{\boldsymbol{p}_1} \hat{a}^\dagger_{\boldsymbol{p}_2} \hat{a}_{\boldsymbol{p}_3} \hat{a}_{\boldsymbol{p}_4} , \tag{A.3}$$

where $E_{\boldsymbol{p}} = \boldsymbol{p}^2/2m$ is the energy in the absence of interactions and $\hat{a}^\dagger_{\boldsymbol{p}}$ ($\hat{a}_{\boldsymbol{p}}$) is the boson creation (annihilation) operator for a particle with momentum $\boldsymbol{p}$. The interaction Hamiltonian, $\hat{H}_{\mathrm{I}}$, describes collisions between particles, i.e., two particles with initial momenta $\boldsymbol{p}_3$ and $\boldsymbol{p}_4$ collide and are scattered into states with momenta $\boldsymbol{p}_1$ and $\boldsymbol{p}_2$. It is common to assume that momentum is conserved in the collision and that the interaction occurs over a very short range, in which case one can make the substitution

$$U_{\boldsymbol{p}_1 \boldsymbol{p}_2 \boldsymbol{p}_3 \boldsymbol{p}_4} \to \frac{U_0}{V} \delta_{\boldsymbol{p}_1 + \boldsymbol{p}_2, \boldsymbol{p}_3 + \boldsymbol{p}_4} , \tag{A.4}$$

where U_0 is a constant and V is the volume of the system.

A.1. Elimination of the condensate mode

We now assume that the condensate is macroscopically occupied, i.e., a large number of particles are in the state with $\boldsymbol{p}=0$. More specifically, if N_{tot} is the total number of particles and N is the *mean* number of particles in the condensate, then N is of order N_{tot}, while the population of any nonzero momentum state is at most of order one. The Bogoliubov theory for determining the excitation spectrum of the condensate assumes that the operators $\hat{a}_0$ and $\hat{a}_0^\dagger$ can be regarded as large c-numbers of magnitude $\sqrt{N}$, and that only terms of order higher than 2 in $\hat{a}_0$ and $\hat{a}_0^\dagger$ need to be retained in the Hamiltonian. So, in particular, one writes

$$\hat{H}_{\mathrm{I}} \simeq \frac{U_0}{2V}\hat{a}_0^\dagger\hat{a}_0^\dagger\hat{a}_0\hat{a}_0 + \frac{U_0}{2V}\sum_{p\neq 0}(2\hat{a}_p^\dagger\hat{a}_p\hat{a}_0^\dagger\hat{a}_0 + 2\hat{a}_{-p}^\dagger\hat{a}_{-p}\hat{a}_0^\dagger\hat{a}_0 + \hat{a}_p^\dagger\hat{a}_{-p}^\dagger\hat{a}_0\hat{a}_0 + \hat{a}_p\hat{a}_{-p}\hat{a}_0^\dagger\hat{a}_0^\dagger)\,. \tag{A.5}$$

Now, defining the number operator

$$\hat{N} = \hat{a}_0^\dagger\hat{a}_0 + \frac{1}{2}\sum_{p\neq 0}(\hat{a}_p^\dagger\hat{a}_p + \hat{a}_{-p}^\dagger\hat{a}_{-p})\,, \tag{A.6}$$

we can write

$$\hat{N}^2 \simeq (\hat{a}_0^\dagger\hat{a}_0)^2 + \sum_{p\neq 0}(\hat{a}_p^\dagger\hat{a}_p\hat{a}_0^\dagger\hat{a}_0 + \hat{a}_{-p}^\dagger\hat{a}_{-p}\hat{a}_0^\dagger\hat{a}_0) \tag{A.7}$$

$$= \hat{a}_0^\dagger\hat{a}_0^\dagger\hat{a}_0\hat{a}_0 + \hat{a}_0^\dagger\hat{a}_0 + \sum_{p\neq 0}(\hat{a}_p^\dagger\hat{a}_p\hat{a}_0^\dagger\hat{a}_0 + \hat{a}_{-p}^\dagger\hat{a}_{-p}\hat{a}_0^\dagger\hat{a}_0)\,. \tag{A.8}$$

One uses this expression to substitute for $\hat{a}_0^\dagger\hat{a}_0^\dagger\hat{a}_0\hat{a}_0$ in Eq. (A.5), yielding

$$\hat{H}_{\mathrm{I}} = \frac{U_0}{2V}(\hat{N}^2 - \hat{a}_0^\dagger\hat{a}_0) + \frac{U_0}{2V}\sum_{p\neq 0}(\hat{a}_p^\dagger\hat{a}_p\hat{a}_0^\dagger\hat{a}_0 + \hat{a}_{-p}^\dagger\hat{a}_{-p}\hat{a}_0^\dagger\hat{a}_0 + \hat{a}_p^\dagger\hat{a}_{-p}^\dagger\hat{a}_0\hat{a}_0 + \hat{a}_p\hat{a}_{-p}\hat{a}_0^\dagger\hat{a}_0^\dagger)\,. \tag{A.9}$$

With the assumption $N \simeq N_{\mathrm{tot}}$ and the c-number substitutions $(\hat{N}^2 - \hat{a}_0^\dagger\hat{a}_0) \to N(N-1)$ and $\hat{a}_0^\dagger\hat{a}_0 \to N$, the total Hamiltonian thus becomes

$$H = \frac{U_0N(N-1)}{2V} + \frac{1}{2}\sum_{p\neq 0}\left[\left(\frac{\boldsymbol{p}^2}{2m} + \frac{U_0N}{V}\right)(\hat{a}_p^\dagger\hat{a}_p + \hat{a}_{-p}^\dagger\hat{a}_{-p}) + \frac{U_0N}{V}(\hat{a}_p^\dagger\hat{a}_{-p}^\dagger + \hat{a}_p\hat{a}_{-p})\right]. \tag{A.10}$$

A.2. Bogoliubov transformation

The Hamiltonian Eq. (A.10) can be diagonalised via the *Bogoliubov transformation*, whereby new creation and annihilation operators $\hat{A}_p^\dagger$ and $\hat{A}_p$ are defined through

$$\hat{a}_p = c_p\hat{A}_p + s_p\hat{A}_{-p}^\dagger \tag{A.11}$$

$$\hat{a}_p^\dagger = c_p\hat{A}_p^\dagger + s_p\hat{A}_{-p} \tag{A.12}$$

with c_p, s_p real numbers satisfying $c_p^2 - s_p^2 = 1$. With a suitable choice of c_p and s_p, the coefficients of the terms $\hat{A}_p \hat{A}_{-p}$ and $\hat{A}_p^\dagger \hat{A}_{-p}^\dagger$ can be made to vanish in the transformed Hamiltonian to yield

$$\hat{H} = E_0 + \sum_{p \neq 0} \mathcal{E}_p \hat{A}_p^\dagger \hat{A}_p \tag{A.13}$$

with

$$E_0 = \frac{U_0 N(N-1)}{V} + \frac{1}{2} \sum_{p \neq 0} \left(\mathcal{E}_p - \frac{\boldsymbol{p}^2}{2m} - \frac{U_0 N}{V} \right), \tag{A.14}$$

$$\mathcal{E}_p = \sqrt{\left(\frac{\boldsymbol{p}^2}{2m} + \frac{U_0 N}{V} \right)^2 - \left(\frac{U_0 N}{V} \right)^2}. \tag{A.15}$$

The modified energy spectrum now has a non-zero minimum energy E_0 and an elementary excitation spectrum given by $\mathcal{E}_p$. At sufficiently low energies, such that the dominant particle–particle interaction is s-wave scattering, the interaction strength U_0 takes the form

$$U_0 = \frac{4\pi\hbar^2 a}{m}, \tag{A.16}$$

where a is the s-wave scattering length. The elementary excitation spectrum can thus be rewritten as

$$\mathcal{E}_p = \frac{|\boldsymbol{p}|}{2m} \sqrt{\boldsymbol{p}^2 + 16\pi\hbar^2 a\rho}, \tag{A.17}$$

where $\rho = N/V$ is the particle density. Writing $|\boldsymbol{p}| = \hbar k$, $\mathcal{E}_k$ has the following limits:

$$\mathcal{E}_k \simeq \begin{cases} \sqrt{4\pi a\rho}\,\hbar^2 k/m, & \text{for } k \to 0, \\ \hbar^2 k^2/2m, & \text{for } k \to \infty. \end{cases} \tag{A.18}$$

The long-wavelength expression ($k \to 0$) corresponds to that of a sound wave, or phonon, with velocity $c = \sqrt{4\pi a\rho}\,\hbar/m$, while the opposite limit simply yields the free-particle spectrum.

Note that the above results are derived with the assumption that virtually all of the particles are in the ground state. Hence, it is to be expected that the expression for $\mathcal{E}_p$ given above is valid only for the first few excited states. With a more general treatment, for which a finite fraction $(1-f)$ of the particles is assumed to be in excited states (although with no single excited state macroscopically occupied), Huang (1963) shows that Eq. (A.17) should be modified to

$$\mathcal{E}_p = \frac{|\boldsymbol{p}|}{2m} \sqrt{\boldsymbol{p}^2 + 16\pi\hbar^2 a\rho f}. \tag{A.19}$$

Finally, extensions of the Bogliubov method to the case of spatially inhomogeneous condensates can be found, e.g., in Fetter (1996) and Lewenstein and You (1996b). Note that Gardiner (1997) has also provided a generalisation of the Bogoliubov method that applies to an *exact* number N of condensate particles (i.e., is particle-number-conserving).

References

Anderson, M.H., Ensher, J.R., Matthews, M.R., Wieman, C.E., Cornell, E.A., 1995. Science 269, 198.

Anderson, M.H., Holland, M., 1996. Opt. Photon. News 7 (4).

Anderson, P.W., 1984. Basic Notions of Condensed Matter Physics. Addison-Wesley, Reading, MA.

Andrews, M.R., Kurn, D.M., Miesner, H.-J., Durfee, D.S., Townsend, C.G., Inouye, S., Ketterle, W., 1997a. Phys. Rev. Lett. 79, 553.

Andrews, M.R., Mewes, M.-O., Druten, N.J., Durfee, D.S., Kurn, D.M., Ketterle, W., 1996. Science 273, 84.

Andrews, M.R., Townsend, C.G., Miesner, H.-J., Durfee, D.S., Kurn, D.M., Ketterle, W., 1997b. Science 275, 637.

Anglin, J., 1997. Phys. Rev. Lett. 79, 6.

Arimondo, E., Phillips, W.D., Strumia, F. (Eds.), 1991. Laser Manipulation of Atoms and Ions, Proc. Int. School of Physics "Enrico Fermi", Course CXVIII, Varenna. North-Holland, Amsterdam.

Arndt, M., Ben Dahan, M., Guéry-Odelin, D., Reynolds, M.W., Dalibard, J., 1997. Phys. Rev. Lett. 79, 625.

Bagnato, V., D.E. Pritchard, D. Kleppner, 1987, Phys. Rev. A 35, 4354.

Ballagh, R.J., Burnett, K., Scott, T.F., 1997. Phys. Rev. Lett. 78, 1607.

Barnett, S.M., Burnett, K., Vaccaro, J., 1996. J. Res. Natl. Inst. Stand. Technol. 101, 593.

Baym, G., Pethick, C.J., 1996. Phys. Rev. Lett. 76, 6.

Bergeman, T., 1997. Phys. Rev. A 55, 3658.

Berman, P. (Ed.), 1994. Cavity Quantum Electrodynamics, Academic Press, San Diego.

Bijlsma, M., Stoof, H.T.C., 1997. Phys. Rev. A 55, 498.

Bogoliubov, N., 1947. J. Phys. USSR 11, 23.

Bohn, J.L., Julienne, P.S., 1997. Phys. Rev. A 56, 1486.

Bolda, E.L., Tan, S.M., Walls, D.F., 1997. Phys. Rev. Lett. 79, 4719.

Bolda, E.L., Walls, D.F., 1997. Report No. cond-mat/9708189, unpublished.

Bordē, Ch. J. 1995. Phys. Lett. A 204, 217.

Bose, S.N., 1924. Z. Phys. 26, 178.

Bradley, C.C., Sackett, C.A., Hulet, R.G., 1997a. Phys. Rev. Lett. 78, 985.

Bradley, C.C., Sackett, C.A., Hulet, R.G., 1997b. Phys. Rev. A 55, 3951.

Bradley, C.C., Sackett, C.A., Tollett, J.J., Hulet, R.G., 1995. Phys. Rev. Lett. 75, 1687.

Burke Jr., J.P., Bohn, J.L., Esry, B.D., Greene, C.H., 1997. Phys. Rev. A 55, R2511.

Burnett, K., 1996. Contemp. Phys. 37, 1.

Burt, E.A., Ghrist, R.W., Myatt, C.J., Holland, M.J., Cornell, E.A., Wieman, C.E., 1997. Phys. Rev. Lett. 79, 337.

Busch, Th., Cirac, J.I., Pérez-García, V.M., Zoller, P., 1997. Phys. Rev. A 56, 2978.

Carmichael, H.J., 1993. An Open Systems Approach to Quantum Optics, Lecture Notes in Physics, vol. 18, Springer, Berlin.

Castin, Y., Dalibard, J., 1997. Phys. Rev. A 55, 4330.

Castin, Y., Dum, R., 1996. Phys. Rev. Lett. 77, 5315.

Cirac, J.I., Gardiner, C.W., Naraschewski, M., Zoller, P., 1996. Phys. Rev. A 54, R3714.

Cornell, E., 1996. J. Res. Natl. Inst. Stand. Technol. 101, 419.

Csordás, A., Graham, R., Szépfalusy, P., 1996. Phys. Rev. A 54, R2543.

Dalfovo, F., Minniti, C., Pitaevskii, L., 1997a. Phys. Rev. A 56, 4855.

Dalfovo, F., Minniti, C., Stringari, S., Pitaevskii, L., 1997b. Phys. Lett. A 227, 259.

Dalfovo, F., Pitaevskii, L., Stringari, S., 1996. Phys. Rev. A 54, 4213.

Dalfovo, F., Stringari, S., 1996. Phys. Rev. A 53, 2477.

Davis, K.B., Mewes, M.-O., Andrews, M.R., van Druten, N.J., Durfee, D.S., Kurn, D.M., Ketterle, W., 1995. Phys. Rev. Lett. 75, 3969.

de Groot, S.R., Hooyman, G.J. ten Seldam, C.A. 1950. Proc. R. Soc. London Ser. A 203, 266.

Dodd, R.J., Burnett, K., Edwards, M., Clark, C.W., 1997. Phys. Rev. A 56, 587.

Dodd, R.J., Edwards, M., Clark, C.W., Burnett, K., 1998. Phys. Rev. A 57, R32.

Dodd, R.J., Edwards, M., Williams, C.J., Clark, C.W., Holland, M.J., Ruprecht, P.A., Burnett, K., 1996. Phys. Rev. A 54, 661.

Dum, R., Cirac, J.I., Lewenstein, M., Zoller, P., 1997. Report No. cond-mat/9710238, unpublished.

Dunningham, J.A., 1997. MSc. Thesis, University of Auckland, unpublished.

Dunningham, J.A., Collett, M.J., Walls, D.F., 1997. "Quantum state of a trapped Bose–Einstein condensate," preprint.
Eberly, J.H., Narozhny, N.B., Sanchez-Mondragon, J.J., 1980. Phys. Rev. Lett. 44, 1323.
Edwards, M., Burnett, K., 1995. Phys. Rev. A 51, 1382.
Edwards, M. Dodd, R.J., Clark, C.W., Ruprecht, P.A., Burnett, K., 1996a. Phys. Rev. A 53, R1950.
Edwards, M., Ruprecht, P.A., Burnett, K., Dodd, R.J., Clark, C.W., 1996b. Phys. Rev. Lett. 77, 1671.
Einstein, A., 1925. Sitzber. Kgl. Preuss. Akad. Wiss. 1925, 3.
Ensher, J.R., Jin, D.S., Matthews, M.R., Wieman, C.E., Cornell, E.A., 1996. Phys. Rev. Lett. 77, 4984.
Esry, B.D., 1997. Phys. Rev. A 55, 1147.
Esry, B.D., Greene, C.H., Burke Jr., J.P., Bohn, J.L., 1997. Phys. Rev. Lett. 78, 3594.
Fedichev, P.O., Kagan, Yu., Shlyapnikov, V., Walraven, J.T.M., 1996. Phys. Rev. Lett. 77, 2913.
Fedichev, P.O., Shlyapnikov, G.V., Walraven, J.T.M., 1998. Phys. Rev. Lett. 80, 2269.
Fetter, A.L., 1972. Ann. Phys. (N.Y.) 70, 67.
Fetter, A.L., 1996. Phys. Rev. A 53, 4245.
Fetter, A.L., D. Rokhsar, 1998. Phys. Rev. A 57, 1191.
Fliesser, M., Csordás, A., Szépfalusy, P., Graham, R., 1997. Phys. Rev. A 56, R2533.
Forster, D., 1975. Hydrodynamic Fluctuations, Broken Symmetry, and Correlation Functions. W.A. Benjamin, New York.
Gardiner, C.W., 1991. Quantum Noise, Springer, Berlin.
Gardiner, C.W., 1997. Phys. Rev. A 56, 1414.
Gardiner, C.W., Collett, M.J., 1985. Phys. Rev. A 31, 3761.
Gardiner, C.W., Parkins, A.S., Zoller, P., 1992. Phys. Rev. A 46, 4363.
Gardiner, C.W., Zoller, P., 1997. Phys. Rev. A 55, 2902.
Gardiner, C.W., Zoller, P., Ballagh, R.J., Davis, M.J., 1997. Phys. Rev. Lett. 79, 1793.
Giorgini, S., 1997. Report No. cond-mat/9709259, unpublished.
Giorgini, S., Pitaevskii, L.P., Stringari, S., 1996. Phys. Rev. A 54, R4633.
Giorgini, S., Pitaevskii, L.P., Stringari, S., 1997a. Phys. Rev. Lett. 78, 3987.
Giorgini, S., Pitaevskii, L.P., Stringari, S., 1997b. Report No. cond-mat/9704014, J. Low Temp. Phys., to appear.
Goldstein, E.V., Meystre, P., 1997. Phys. Rev. A 55, 2935.
Graham, R., Walls, D.F., 1996. Phys. Rev. Lett. 76, 1774.
Graham, R., Walls, D.F., 1998. Phys. Rev. A 57, 484.
Graham, R., Walls, D.F., Collett, M.J., Fliesser, M., Wright, E.M., 1998a. Phys. Rev. A 57, 503.
Graham, R., Wong, T., Collett, M.J., Tan, S.M., Walls, D.F., 1998b. Phys. Rev. A 57, 493.
Griffin, A., 1993. Excitations in a Bose-Condensed Liquid. Cambridge University Press, Cambridge.
Griffin, A., 1996. Phys. Rev. B 53, 9341.
Griffin, A., Snoke, D., Stringari, S. (Eds.), 1995. Bose–Einstein Condensation. Cambridge University Press, Cambridge.
Grossmann, S., Holthaus, M., 1995a. Phys. Lett. 208, 188.
Grossmann, S., Holthaus, M., 1995b. Z. Naturforsch. Teil A 50, 323.
Guzmán, A.M., Moore, M., Meystre, P., 1996. Phys. Rev. A 53, 977.
Harris, S.E., 1989. Phys. Rev. Lett. 62, 1033.
Hijmans, T.W., Kagan, Y., Shlyapnikov, G.V., Walraven, J.T.M., 1993. Phys. Rev. B 48, 12886.
Ho, T.L., Shenoy, V.B., 1996. Phys. Rev. Lett. 77, 3276.
Hohenberg, P.C., Martin, P.C., 1965. Ann. Phys. (N.Y.) 34, 291.
Holland, M., Burnett, K., Gardiner, C.W., Cirac, J.I., Zoller, P., 1996. Phys. Rev. A 54, R1757.
Holland, M., Cooper, J., 1996. Phys. Rev. A 53, R1954.
Holland, M.J., Jin, D.S., Chiofalo, M.L., Cooper, J., 1997. Phys. Rev. Lett. 78, 3801.
Holland, M., Williams, J., Cooper, J., 1997. Phys. Rev. A 55, 3670.
Hope, J.J., 1997. Phys. Rev. A 55, R2531.
Hoston, W., You, L., 1996. Phys. Rev. A 53, 4254.
Houbiers, M., Stoof, H.T.C., 1996. Phys. Rev. A 54, 5055.
Huang, K., 1963. Statistical Mechanics. Wiley, New York.
Hutchinson, D.A.W., Zaremba, E., Griffin, A., 1997. Phys. Rev. Lett. 78, 1842.
Imamoḡlu, A., Kennedy, T.A.B., 1997. Phys. Rev. A 55, R849.

Imamoḡlu, A., Lewenstein, M., You, L., 1997. Phys. Rev. Lett. 78, 2511.
Imamoḡlu, A., Ram, R.J., 1996. Phys. Lett. A 214, 193.
Jack, M.W., Collett, M.J., Walls, D.F., 1996. Phys. Rev. A 54, R4625.
Jaksch, D., Gardiner, C.W., Zoller, P., 1997. Phys. Rev. A 56, 575.
Javanainen, J., 1986. Phys. Rev. Lett. 57, 3164.
Javanainen, J., 1991. Phys. Lett. A 161, 207.
Javanainen, J., 1994. Phys. Rev. Lett. 72, 2375.
Javanainen, J., 1995. Phys. Rev. Lett. 75, 1927.
Javanainen, J., 1996a. Phys. Rev. A 54, R3722.
Javanainen, J., 1996b. Phys. Rev. A 54, R4629.
Javanainen, J., Wilkens, M., 1997. Phys. Rev. Lett. 78, 4675.
Javanainen, J., Yoo, S.M., 1996. Phys. Rev. Lett. 76, 161.
Javanainen, J., Ruostekoski, J., 1995. Phys. Rev. A 52, 3033.
Jin, D.S., Ensher, J.R., Matthews, M.R., Wieman, C.E., Cornell, E.A., 1996a. Phys. Rev. Lett. 77, 420.
Jin, D.S., Ensher, J.R., Matthews, M.R.., Wieman C.E., Cornell, E.A., 1996b. Czech. J. Phys. 46 (Suppl.), S6.
Jin, D.S., Matthews, M.R., Ensher, J.R., Wieman, C.E., Cornell, E.A., 1997. Phys. Rev. Lett. 78, 764.
Julienne, P.S., Mies, F.H., Tiesinga, E., Williams, C.J., 1997. Phys. Rev. Lett. 78, 1880.
Julienne, P.S., Smith, A.M., Burnett, K., 1993. Adv. At. Mol. Opt. Phys. 30, 141.
Kagan, Y., Shlyapnikov, G.V., Walraven, J.T.M., 1996. Phys. Rev. Lett. 76, 2670.
Kagan, Y., Surkov, E.L., Shlyapnikov, G.V., 1996. Phys. Rev. A 54, R1753.
Kagan, Y., Surkov, E.L., Shlyapnikov, G.V., 1997a. Phys. Rev. A 55, R18.
Kagan, Yu., Surkov, E.L., Shlyapnikov, G.V., 1997b. Phys. Rev. Lett. 79, 2604.
Kagan, Yu., Svistunov, B.V., 1997. Phys. Rev. Lett. 79, 3331.
Kagan, Yu., Svistunov, B.V., Shlyapnikov, G.V., 1985. JETP Lett. 42, 209.
Kavoulakis, G.M., Pethick, C.J., 1997. Report No. cond-mat/9711224, unpublished.
Ketterle, W., van Druten, N.J., 1996a. In: Bederson, B., Walther, H. (Eds.), Advances in Atomic, Molecular, and Optical Physics, vol. 37, Academic Press, San Diego.
Ketterle, W., van Druten, N.J., 1996b. Phys. Rev. A 54, 656.
Ketterle, W., Miesner, H.-J., 1997. Phys. Rev. A 56, 3291.
Kokkelmans, S.J.J.M.F., Boesten, H.M.J.M., Verhaar, B.J., 1997. Phys. Rev. A 55, R1589.
Krauth, W., 1996. Phys. Rev. Lett. 77, 3695.
Kuklov, A.B., Chencinski, N., Levine, A.M., Schreiber, W.M., Birman, J.L., 1997. Phys. Rev. A 55, R3307.
Lee, T.D., Huang, K., Yang, C.N., 1957. Phys. Rev. 106, 1135.
Lenz, G., Meystre, P., Wright, E.M., 1993. Phys. Rev. Lett. 71, 3271.
Lenz, G., Meystre, P., Wright, E.M., 1994. Phys. Rev. A 50, 1681.
Leonhardt, U., Paul, H., 1995. Prog. Quant. Electron. 19, 89.
Lewenstein, M., You, L., 1993. Phys. Rev. Lett. 71, 1339.
Lewenstein, M., You, L., 1996a. In: Bederson, B., Walther, H. (Eds.), Advances in Atomic, Molecular, and Optical Physics, vol. 36, Academic Press, San Diego.
Lewenstein, M., You, L., 1996b. Phys. Rev. Lett. 77, 3489.
Lifshitz, E.M., Pitaevskii, L.P., 1980. Statistical Physics, Part II. Pergamon, Oxford.
Liu, W.V., 1997. Phys. Rev. Lett. 79, 4056.
Liu, W.V., Schieve, W.C., 1997. Report No. cond-mat/9702122, unpublished.
Lundh, E., Pethick, C.J., Smith, H., 1997. Phys. Rev. A 55, 2126.
Mancini, S., Tombesi, P., 1997. Europhys. Lett. 40.
March, N.H., Young, W.H., Sampanthar, S., 1967. The Many-Body Problem in Quantum Mechanics. Cambridge University Press, Cambridge.
Marinescu, M., Starace, A.F., 1997. Phys. Rev. A 56, 570.
Marzlin, K.-P., Audretsch, J., 1997. Report No. cond-mat/9708001, unpublished.
Marzlin, K.-P., Zhang, W., Wright, E.M., 1997. Report No. cond-mat/9708198, unpublished.
Mewes, M.-O., Andrews, M.R., van Druten, N.J., Kurn, D.M., Durfee, D.S., Ketterle, W., 1996a. Phys. Rev. Lett. 77, 416.

Mewes, M.-O., Andrews, M.R., van Druten, N.J., Kurn, D.M., Durfee, D.S., Townsend, C.G., Ketterle, W., 1996b. Phys. Rev. Lett. 77, 988.

Mewes, M.-O., Andrews, M.R., Kurn, D.M., Durfee, D.S., Townsend, C.G., Ketterle, W., 1997. Phys. Rev. Lett. 78, 582.

Milburn, G.J., Corney, J., Wright, E., Walls, D.F., 1997. Phys. Rev. A 55, 4318.

Minguzzi, A., Conti, S., Tosi, M.P., 1997. J. Phys.: Condens. Matter 9, L33.

Moerdijk, A.J., Boesten, H.M.J.M., Verhaar, B.J., 1996. Phys. Rev. A 52, 916.

Mølmer, K., 1997. Phys. Rev. A 55, 3195.

Mølmer, K., Castin, Y., Dalibard, J., 1993. J. Opt. Soc. Am. B 10, 524.

Moore, M.G., Meystre, P., 1997. Phys. Rev. A 56, 2989.

Morice, O., Castin, Y., Dalibard, J., 1995. Phys. Rev. A 51, 3896.

Moy, G.M., Hope, J.J., Savage, C.M., 1997. Phys. Rev. A 55, 3631.

Moy, G.M., Savage, C.M., 1997. Phys. Rev. A 56, R1087.

Myatt, C.J., Burt, E.A., Ghrist, R.W., Cornell, E.A., Wieman, C.E., 1997. Phys. Rev. Lett. 78, 586.

Naraschewski, M., Schenzle, A., Wallis, H., 1997. Phys. Rev. A 56, 603.

Naraschewski, M., Wallis, H., Schenzle, A., Cirac, J.I., Zoller, P., 1996. Phys. Rev. A 54, 2185.

Öhberg, P., Surkov, E.L., Tittonen, I., Stenholm, S., Wilkens, M., Shlyapnikov, G.V., 1997. Phys. Rev. A 56, R3346.

Olsen, M.K., Plimak, L.I., Drummond, P.D., Graham, R., Tan, S.M., Collett, M.J., Walls, D.F., 1997. Dynamical noise in Bose–Einstein condensates. Preprint.

Olshanii, M., Castin, Y., Dalibard, J., 1995. In: Inguscio, M., Allegrini, M., Sasso, A. (Eds.), Proc. 12th International Conference on Laser Spectroscopy, World Scientific, Singapore.

Pérez-García, V.M., Michinel, H., Cirac, J.I., Lewenstein, M., Zoller, P., 1996. Phys. Rev. Lett. 77, 5320.

Pérez-García, V.M., Michinel, H., Cirac, J.I., Lewenstein, M., Zoller, P., 1997. Phys. Rev. A 56, 1424.

Pitaevskii, L.P., 1997. Phys. Lett. A 229, 406.

Pitaevskii, L.P., Stringari, S., 1997. Phys. Lett. A 235, 398.

Plimak, L., Collett, M.J., Walls, D.F., 1996. Report No. cond-mat/9612086, unpublished.

Politzer, H.D., 1991. Phys. Rev. A 43, 6444.

Popov, V.N., 1972. Theor. Math. Phys. 11, 478.

Popov, V.N., 1987. Functional Integrals and Collective Excitations. Cambridge University Press, Cambridge, Ch. 6.

Proukakis, N.P., Burnett, K., 1996. J. Res. Natl. Inst. Stand. Technol. 101, 457.

Proukakis, N.P., Burnett, K., 1997. Phil. Trans. R. Soc. Lond. A 355, in press.

Proukakis, N.P., Burnett, K., Stoof, H.T.C., 1997. Preprint.

Quadt, R., Wiseman, H.M., Walls, D.F., 1996. Phys. Lett. A 219, 19.

Raghavan, S., Smerzi, A., Fantoni, S., Shenoy, S.R., 1997. Report No. cond-mat/9706220, unpublished.

Röhrl, A., Naraschewski, M., Schenzle, A., Wallis, H., 1997. Phys. Rev. Lett. 78, 4143.

Rokhsar, D.S., 1997. Phys. Rev. Lett. 79, 2164.

Ruostekoski, J., Javanainen, J., 1997a. Phys. Rev. A 55, 513.

Ruostekoski, J., Javanainen, J., 1997b. Phys. Rev. A 56, 2056.

Ruostekoski, J., Walls, D.F., 1997a. Phys. Rev. A 55, 3625.

Ruostekoski, J., Walls, D.F., 1997b. Phys. Rev. A 56, 2996.

Ruprecht, P.A., Edwards, M., Burnett, K., Clark, C.W., 1996. Phys. Rev. A 54, 4178.

Ruprecht, P.A., Holland, M.J., Burnett, K., Edwards, M., 1995. Phys. Rev. A 51, 4704.

Savage, C.M., Ruostekoski, J., Walls, D.F., 1997a. Phys. Rev. A 56, 2046.

Savage, C.M., Ruostekoski, J., Walls, D.F., 1997b. Pumping two dilute gas Bose–Einstein condensates with Raman light scattering. Preprint.

Scully, M.O., Zhu, S.Y., 1989. Phys. Rev. Lett. 62, 2813.

Shi, H., Zheng, W.-M., 1997. Phys. Rev. A 55, 2930.

Shuryak, E.V., 1996. Phys. Rev. A 54, 3151.

Singh, K.G., Rokhsar, D.S., 1996. Phys. Rev. Lett. 77, 1667.

Smerzi, A., Fantoni, S., 1997. Phys. Rev. Lett. 78, 3589.

Smerzi, A., Fantoni, S., Giovanazzi, S., Shenoy, S.R., 1997. Report No. cond-mat/9706221, unpublished.

Spreeuw, R.J.C., Pfau, T., Janicke, U., Wilkens, M., 1995. Europhys. Lett. 32, 469.

Stamper-Kurn, D.M., Andrews, M.R., Chikkatur, A.P., Inouye, S., Miesner, H.-J., Stenger, J., Ketterle, W., 1997. Report No. cond-mat/9711273, unpublished.
Steck, H., Naraschewski, M., Wallis, H., 1997. Phys. Rev. Lett., in press.
Steel, M.J., Walls, D.F., 1997. Phys. Rev. A 56, 3832.
Stoof, H.T.C., 1997a. J. Stat. Phys. 87, 1353.
Stoof, H.T.C., 1997b. Phys. Rev. Lett. 78, 768.
Stringari, S., 1996. Phys. Rev. Lett. 77, 2360.
Svistunov, B., Shlyapnikov, G., 1990. Sov. Phys. JETP 70, 460; Sov. Phys. JETP 71, 71.
Szépfalusy, P., Kondor, I., 1974. Ann. Phys. (N.Y.) 82, 1.
Timmermans, E., Tommasini, P., Huang, K., 1997. Phys. Rev. A 55, 3645.
Verhaar, B.J., 1995. In: Wineland, D.J., Wieman, C.E., Smith, S.J. (Eds.), Atomic Physics 14, AIP, New York.
Wallis, H., Röhrl, A., Naraschewski, M., Schenzle, A., 1997. Phys. Rev. A 55, 2109.
Walls, D.F., Milburn, G.J., 1994. Quantum Optics. Springer, Berlin, Ch. 1.
Walraven, J.T.M., 1996. In: Oppo, G.-L., Barnett, S.M., Riis, E., Wilkinson, M. (Eds.), Quantum Dynamics of Simple Systems, Institute of Physics, Bristol.
Walser, R., 1997. Phys. Rev. Lett. 79, 4724.
Walsworth, R., You, L., 1997. Phys. Rev. A 56, 555.
Wiseman, H.M., 1997. Phys. Rev. A 56, 2068.
Wiseman, H.M., Collett, M.J., 1995. Phys. Lett. A 202, 246.
Wiseman, H.M., Martins, A., Walls, D.F., 1996. Quantum Semiclass. Opt. 8, 737.
Wong, T., Collett, M.J., Tan, S.M., Walls, D.F., Wright, E.M., 1996a. Unpublished.
Wong, T., Collett, M.J., Walls, D.F., 1996b. Phys. Rev. A 54, R3718.
Wright, E.M., Walls, D.F., Garrison, J.C., 1996. Phys. Rev. Lett. 77, 2158.
Wright, E.M., Wong, T., Collett, M.J., Tan, S.M., Walls, D.F., 1997. Phys. Rev. A 56, 591.
Wu, W.-C., Griffin, A., 1996. Phys. Rev. A 54, 4204.
Yoo, S.M., Ruostekoski, J., Javanainen, J., 1997. J. Mod. Opt. 44, 1763.
You, L., Hoston, W., Lewenstein, M., 1997. Phys. Rev. A 55, R1581.
You, L., Lewenstein, M., Cooper, J., 1994. Phys. Rev. A 50, R3565.
You, L., Lewenstein, M., Cooper, J., 1995. Phys. Rev. A 51, 4712.
You, L., Lewenstein, M., Glauber, R.J., Cooper, J., 1996. Phys. Rev. A 53, 329.
Zapata, I., Sols, F., Leggett, A.J., 1997. Report No. cond-mat/9707143, unpublished.
Zaremba, E., 1997. Report No. cond-mat/9708237, unpublished.
Zhang, W., 1993. Phys. Lett. A 176, 225.
Zhang, W., Walls, D.F., 1994. Phys. Rev. A 49, 3799.
Zhang, W. Walls, D.F., 1998. Phys. Rev. A 57, 1248.
Zhang, W., Walls, D.F., Sanders, B.C., 1994. Phys. Rev. Lett. 72, 60.